

UNI  
BASEL

# Biophysical Characterization of Reactions Associated with Reverse Cholesterol Transport

INAUGURALDISSERTATION

zur

Erlangung der Würde eines Doktors der Philosophie  
vorgelegt der Philosophisch-Naturwissenschaftlichen Fakultät  
der Universität Basel

von

Fabian Zehender

aus

Freiburg, Deutschland

Basel, 2012



Genehmigt von der Philosophisch-Naturwissenschaftlichen Fakultät auf Antrag von

Prof. Dr. Joachim Seelig

Prof. Dr. Anna Seelig

Prof. Dr. Jörg Huwylar

Basel, den 21. Februar 2012

---

Prof. Dr. Martin Spiess (Dekan)



---

<b>1. Summery and Rationale</b> .....	<b>7</b>
<b>2. Thermodynamics of protein self-association and unfolding. The case of Apolipoprotein A-I <sup>†</sup></b> .....	<b>11</b>
<b>Published Article</b> .....	<b>12</b>
<b>Appendix: Dynamic light scattering and analytical ultracentrifugation with Apo A-1</b> .....	<b>61</b>
Dynamic light scattering (DLS) .....	61
Analytical ultracentrifugation .....	64
<b>3. Lipid binding of Apo A-1 mimetic peptides</b> .....	<b>75</b>
<b>Introduction</b> .....	<b>75</b>
<b>Materials and Methods</b> .....	<b>79</b>
Materials .....	79
Methods .....	79
<b>Results</b> .....	<b>83</b>
Association behavior of peptides 4F and P .....	83
Binding of peptides 4F and P to lipid membranes .....	92
<b>References</b> .....	<b>122</b>
<b>Appendix</b> .....	<b>127</b>
<b>4. Towards understanding of the allocritee specificity of the lipid floppase ABCA1</b> .....	<b>133</b>
<b>Preliminary manuscript</b> .....	<b>134</b>
<b>5. Acknowledgements</b> .....	<b>171</b>
<b>6. Curriculum vitae</b> .....	<b>173</b>
<b>7. Declaration</b> .....	<b>175</b>



## 1. Summery and Rationale

This thesis aimed at improving our understanding of reactions relevant in the reverse cholesterol transport (RCT). RCT facilitates cholesterol homeostasis and is the most important pathway involved in cardiovascular disease. For this purpose three different projects were chosen. Thermodynamics of protein self-association and unfolding was characterized in detail at the example of Apolipoprotein A-1 (Apo A-1). Lipid binding was characterized by means of small peptides that mimic Apo A-1 function. The third project gained insight about the molecular mechanisms of ABCA1`s allocritee flopping. Apo A-1 is the main protein constituent of high density lipoprotein (HDL) and is together with ABCA1 a key player of the RCT.

### *Apolipoprotein A-1*

Protein self-association and unfolding are two processes whose understanding is of utmost importance for the development of biological phamaceuticals as oligomerisation may alter functional properties of proteins. Apo A-1 is a perfect candidate for these investigations as it undergoes a concentration dependent self-association process and has high physiological relevance. Even though Apo A-1 is a highly investigated macromolecule, self-association was not investigated in such a comprehensive approach. Additionally, we used highly purified recombinant human Apo A-1, which was generously provided by H.-J. Schönfeld. For analyzing thermodynamics of self-association and thermal unfolding we introduced new theoretical and experimental methods

## 1. Summery and Rationale

---

Self-association data was obtained by a combination of high sensitivity micro calorimetry and analytical ultracentrifugation. The dissociation reaction of highly concentrated and thus oligomeric Apo A-1 was followed by injection into buffer in an isothermal titration calorimeter (ITC). Dilution of the sample moved the chemical equilibrium towards monomers. Complementary, this equilibrium was analyzed by data obtained from analytical ultracentrifugation in a sedimentation equilibrium mode. If any, self-association was described in former studies as equilibrium between distinct species, for example between monomers and dimers. We introduced a cooperative self-association model that describes the equilibrium of the protein between each possible oligomer in a concentration dependent manner. Furthermore, we introduced a “binding partition function” that represents the sum of all concentrations found in the system. Together with a dissociation degree of the protein we found a link between thermodynamic data and theory of self-association. The binding partition function describes the statistical properties of the system in thermodynamic equilibrium. Hence, it is independent of the theoretical model that is utilized to describe the reaction.

Thermal unfolding of Apo A-1 was followed by circular dichroism spectroscopy (CD) and differential scanning calorimetry (DSC). We found that melting of Apo A-1 caused a transition of  $\alpha$ -helix to  $\beta$ -sheet and random coiled secondary structure and appeared to be highly reversibly up to 75 °C. Thermal unfolding of Apo A-1 and in general of proteins is analyzed almost exclusively with an all-or-none model. As a powerful alternative for highly  $\alpha$ -helical proteins such as Apo A-1, we introduced the cooperative Zimm-Bragg theory. Zimm-Bragg theory is commonly used for thermal unfolding of peptides, but fits well to our data and to data of other proteins obtained from literature.



### *Apo A-1 mimetic peptides*

Apo A-1 was proposed as drug against cardiovascular disease. However, Apo A-1 mimetic peptides are more promising as they have to be administered in much lower dosage and are produced more easily. Understanding their lipid binding properties is essential for the estimation of *in vivo* effects as well as for formulation and dosage of possible drugs with these peptides. Apo A-1 structure is featured by several amphipathic class A motif  $\alpha$ -helices. Even though it is the main protein component of HDL, thermodynamic characterization of its lipid binding has not been achieved in detail. As a model of Apo A-1 we used two peptides (4F and P), which are featured by class A amphipathic  $\alpha$ -helical sequences. 4F showed Apo A-1 mimetic properties in animal models and clinical studies. We used isothermal titration calorimetry to determine thermodynamic parameters of binding to POPC lipid vesicles. In order to understand this reaction several other experimental methods were used. Static and dynamic light scattering illustrated the ability of the peptides to rupture unilamellar vesicles and form micellar-like particles. In contrast, many other peptides such as cell penetrating peptides (CPPs) only partition into the membrane. This finding is in agreement with a 1:1 lipid-to-peptide stoichiometry yielded from ITC data analyzed with a model of  $n$  identical binding sites. This behavior might have high physiological relevance as possible rupture of cell membranes is unwanted. Circular dichroism experiments yielded insight into structural transitions as part of the driving force of lipid binding. Associated with lipid binding is a transition of the peptide from  $\beta$ -sheet and random coiled to  $\alpha$ -helical secondary structure. Tryptophan fluorescence measurements complemented the studies indicating binding to lipids as well. Thermodynamic calculation proved the structural transition of  $\beta$ -sheet and random coiled to  $\alpha$ -helix as well as hydrophobic interactions as driving forces of the reaction.

## 1. Summary and Rationale

---

Further, we studied binding of the peptide 4F to cholesterol by means of ITC. Our results suggested affinity of 4F towards cholesterol but with lower affinity compared to POPC. This might explain the formation of HDL like particles, mainly consisting of phosphocholine lipids. These particles, in turn, could bind to cholesterol with high affinity.

### *ABCA1*

ABCA1 is an ATP binding cassette transporter that flops excess lipids of a cell to the outer membrane leaflet, where it can be picked up by Apo A-1 or HDL particles. Research in the field of ABCA1 is mainly focused on studies in cell culture and in animal models and is therefore rather indirect. Cholesterol efflux by ABCA1 was assumed to be controlled by the copy number of the transporter. The possibility of a direct modulation of the transporter activity by allocrites like in P-glycoprotein (Pgp) as well as the proposed allocrite specificity was rarely investigated in previous studies. Here, we measured the ATPase activity of inside-out vesicles prepared from *ABCA1* transfected Human Embryonic Kidney 293 cells by means of a spectroscopic phosphate release assay. Aluminum fluorides were found as strong inhibitor of the nucleotide binding sites (NBD) of ABCA1 in contrast to vanadate. Furthermore, a screening for putative allocrites interacting with the transmembrane domains (TMDs) was performed with numerous compounds. Therewith we found that all compounds with a pegylated chain, a heterocyclic group and a hydrocarbon tail indicated activation of the ABCA1 ATPase.

Manuscript accepted for Biochemistry

## **2. Thermodynamics of protein self-association and unfolding.**

### **The case of Apolipoprotein A-I <sup>†</sup>**

F. Zehender<sup>1</sup>, A. Ziegler<sup>1</sup>, H.-J. Schönfeld<sup>2</sup>, and J. Seelig<sup>1\*</sup>

<sup>1</sup>Biozentrum, University of Basel, Div. of Biophysical Chemistry, Klingelbergstrasse  
50/70, CH-4056 Basel, Switzerland

and

<sup>2</sup>F. Hoffman-La Roche Ltd., Pharmaceutical Research, CH-4070 Basel, Switzerland

\* To whom correspondence should be addressed:

Tel. +41-61-267 2190, Fax. +41-61-267 2189, e-mail: joachim.seelig@unibas.ch

<sup>†</sup> Supported by the Swiss National Science Foundation grant # 31003A-129701

### Published Article

#### Abstract

Protein self-association and protein unfolding are two temperature-dependent processes whose understanding is of utmost importance for the development of biological pharmaceuticals since protein association may stabilize or destabilize protein structure and function. Here we present new theoretical and experimental methods to analyze the thermodynamics of self-association and unfolding. We used isothermal dilution calorimetry and analytical ultracentrifugation to measure protein self-association and introduced binding partition functions to analyze the cooperative association equilibria. In a second type of experiment we monitored thermal protein unfolding with differential scanning calorimetry and circular dichroism spectroscopy and used the Zimm-Bragg theory to analyze the unfolding process. For  $\alpha$ -helical proteins the cooperative Zimm-Bragg theory appears to be a powerful alternative to the classical two-state model. As a model protein we chose highly purified human recombinant apolipoprotein A-I. Self-association of Apo A-1 showed a maximum at 21 °C with an association constant  $K_a = 5.6 \times 10^5 \text{ M}^{-1}$ , a cooperativity parameter  $\sigma = 0.003$ , and a maximum association number  $N = 8$ . The association enthalpy was linearly dependent on temperature and changed from endothermic at low temperatures to exothermic above 21 °C with a molar heat capacity  $\Delta C_p^0 = -2.76 \text{ kJ/molK}$ . Above 45 °C the association could no longer be measured because of the onset of unfolding. Unfolding occurred between 45 °C and 65 °C and was reversible and independent of protein concentration up to 160  $\mu\text{M}$ . The midpoint of unfolding as measured by DSC

was  $T_0 = 52\text{-}53\text{ }^\circ\text{C}$ , the enthalpy of unfolding  $\Delta H_N^U = 420\text{ kJ/mol}$ . The molar heat capacity increased by  $\Delta_N^U C_p = 5.0 \pm 0.5\text{ kJ/molK}$  upon unfolding corresponding to a loss of 80 to 85 helical segments, as was confirmed by CD spectroscopy. Unfolding was highly cooperative with a nucleation parameter  $\sigma = 4.4 \times 10^{-5}$ .

## Introduction

In situ, biological molecules are confronted with a spectrum of structures, concentrations, ions, etc., a situation thermodynamically distinct from dilute solutions in vitro. Macromolecular crowding may lead to non-specific homo- or hetero-association and an understanding of functional mechanisms requires quantitative analysis of protein association equilibria. The thermodynamic treatment of coupled reactions with many intermediates is a complex process, as temperature changes influence both the association equilibrium and protein stability. Here we consider protein association and protein unfolding as two independent cooperative processes. The protein association/dissociation equilibrium is described as a multi-state process using binding partition functions. Protein unfolding is analyzed with the nearest-neighbor Zimm-Bragg theory and compared to the classical two-state  $N \rightleftharpoons U$  model. We apply these theoretical models to experimental data obtained with Apolipoprotein A-I (Apo A-I).

Apo A-I, a 28.2 kDa protein, reduces cardiovascular risks by promoting the reverse transport and metabolism of cholesterol. Its structural and functional properties with and without lipid have been intensively investigated (for reviews see [40] and [41]). X-ray diffraction and CD spectroscopy demonstrate that Apo A-I contains long stretches of  $\alpha$ -helical structure [42-47].  $\alpha$ -Helix is enhanced after lipid binding [48]. Analysis of the thermodynamics of lipid binding reveal that the association number [49]

## 2. Thermodynamics of protein self-association and unfolding

---

and lipid-to-protein ratio [50] markedly influence the shape of reconstituted particles suggestive of functional differences. The association equilibrium of lipid-free Apo A-I is however an area of ambiguity with diverging reports on its association number and association mechanism (for a recent survey see [51]).

We investigated the above mentioned variability with highly purified recombinant human Apo A-I. The monomer-oligomer equilibrium was investigated with high sensitivity titration calorimetry (ITC). By diluting concentrated Apo A-I solutions in the calorimeter cell it was possible to determine the association enthalpy,  $\Delta H_a^0$ , association constant,  $K_a$ , and association number,  $n$ , of oligomer formation as a function of temperature. Sedimentation equilibrium runs in the analytical ultracentrifuge (AUC) provided an independent approach to elucidate the association constant and stoichiometry. We propose a cooperative association model and develop analytical expressions for the degree of dissociation and molar heat capacity change upon oligomer dissociation.

CD spectra were recorded as a function of protein concentration and temperature to monitor structural changes. Differential scanning calorimetry was used to quantify the thermodynamics of protein unfolding. Taking into account changes in molar heat capacity upon unfolding and using the cooperative Zimm-Bragg model for  $\alpha$ -helix-coil transitions it was possible to correlate structural changes observed by CD spectroscopy with thermodynamic DSC data. Apo A-I unfolding was found to thermodynamically override Apo A-I association.

## Materials and Methods

*Proteins.* A detailed protocol for medium scale preparation of recombinant human Apo A-I will be published in different context (Schönfeld et al., manuscript in preparation). Briefly, a fusion protein construct involving a hexahis purification tag, an ubiquitin sequence, a granzyme B cleavage site (IEPD|GG) and the human Apo A-I sequence (N- to C-terminus) was recombinantly expressed in E.coli.

After opening of cells by French press treatment the recombinant fusion protein was bound to a Ni-NTA column and then washed with alternating cycles of two buffers, one containing 8 M urea and the other containing 60% isopropanol to remove bacterial endotoxins. The fusion protein was eluted using EDTA, cleaved with Granzyme B and the hexahis tag containing N-terminus was removed from the mixture by a second NiNTA affinity step. Recombinant protein that did not bind to NiNTA contained the authentic human Apo A-I sequence with two additional glycines at the N-terminus. The Apo A-I protein was further purified by anion exchange chromatography and then extensively dialyzed against PBS. Purified Apo A-I contained no significant amounts of aggregates as analyzed by SEC with on-line static light scattering and no detectable endotoxins as measured by limulus assay. Purified recombinant Apo A-I sequence differed from human wild-type Apo A-I sequence by two additional N-terminal glycine residues. Electrospray mass spectrometry revealed a molecular mass of 28192.3 Da (theoretical value for wt Apo A-I + 2 Gly is 28192.7 Da). Comparison by size exclusion chromatography (data not shown) and analytical ultracentrifugation (Figure 3C) did not reveal any higher order structure differences between recombinant Apo A-I and Apo A-I purified from human plasma, a generous gift from Dr. Tim Tetaz, Roche Basel.

## 2. Thermodynamics of protein self-association and unfolding

---

*Circular dichroism (CD) spectroscopy.* CD spectra were obtained with a CD spectrometer Model 62 ADS (AVIV, Lakewood, N.J.) in the wavelength range of 190 nm - 260 nm using a total acquisition time of 25 min per spectrum. Measurements were made with protein concentrations of 0.1 mg/mL and 0.5 mg/mL in 100 mM NaF, 10 mM sodium phosphate, pH 7.4. Quartz cuvettes with path lengths of  $d = 1$  mm and 0.2 mm were used and a baseline with pure buffer was recorded for each cuvette and subtracted from the protein spectra. The CD-spectra were simulated with the non-commercial software CDpro [52] based on reference spectra of 56 proteins (data set # 10) and also with an Excel program based on a linear combination of reference spectra [53]. The melting behavior of Apo A-I was studied in the range of 25 - 85 °C.

*High sensitivity isothermal titration calorimetry (ITC).* ITC was performed using either the ITC-200 or the VP titration calorimeter from Microcal (Northampton, MA). The cell volumes were 200  $\mu$ L and 1.4 mL, respectively, and the injection volume varied between 2  $\mu$ L and 10  $\mu$ L. Solutions were degassed under vacuum for about 10 min. The calorimeter cell contained buffer and the protein solution (80  $\mu$ M or 160  $\mu$ M) was in the injection syringe. The injection of small amounts of a concentrated Apo A-I solution into buffer led to the dissociation of Apo A-I complexes. The heat flow induced by protein dissociation is recorded and analyzed by the software provided with the instrument. The quantitative interpretation of the Apo A-I dissociation isotherm in terms of thermodynamic parameters was not part of the commercial software and is discussed below. All measurements were made in PBS buffer (137 mM NaCl, 10 mM sodium phosphate, pH 7.4, 0.02% NaN<sub>3</sub>).



## 2. Thermodynamics of protein self-association and unfolding

---

*Differential scanning calorimetry (DSC).* DSC scans were made with a VP-DSC (Microcal, Northampton, MA). Protein solutions were degassed and the reference cell contained only buffer. The heating rate was 1 °C/min. DSC scans were made in PBS buffer, pH 7.4, with 0.02% NaN<sub>3</sub>. Further evaluation of the DSC curves was performed as described in the Results section.

*Analytical ultracentrifugation (AUC).* A Beckman XL-I ultracentrifuge (Beckman Coulter, Indianapolis, IN) with UV- and Interference detection systems was used. Protein solutions were measured in PBS buffer at concentrations from 0.5 to 2 mg/mL with 0.02% NaN<sub>3</sub>. Sedimentation velocity (SV) and sedimentation equilibrium (SE) measurements were done at 20 °C. Depending on protein concentration, the center piece length was 1.4, 3, or 12 mm. Rotational speeds in SE runs were between 5 and 18 krpm. Using a liquid column height of ~5 mm equilibria were reached within ca. 68 h, as verified by comparison with subsequent radial scans.

## Theory

*Analysis of calorimetric protein unfolding experiments.* The calorimetric enthalpy of the unfolding process  $N \rightleftharpoons U$  is temperature-dependent and can be calculated by

$$\Delta_N^U H(T) = f_U(T) \cdot [\Delta H^0 + \Delta_N^U C_p (T - T_0)] \quad (1)$$

$f_U = (1 - f_N)$  is the fraction of unfolded protein ( $0 \leq f_U \leq 1$ ),  $\Delta H^0$  is the unfolding enthalpy,  $\Delta_N^U C_p$  is the difference in the molar heat capacity between the native and the unfolded protein, and  $T_0$  is a reference temperature, usually the midpoint of the unfolding curve. The heat capacity change measured in the DSC calorimeter is given by

## 2. Thermodynamics of protein self-association and unfolding

---

$$\Delta_N^U C_p(T) = f_U(T) \cdot \Delta_N^U C_p + \left[ \Delta H^0 + \Delta_N^U C_p (T - T_0) \right] \frac{df_U(T)}{dT} \quad (2)$$

In the following we use two models to calculate the extent of unfolding  $f_U$ .

The classical model for protein unfolding is the  $N \rightleftharpoons U$  two-state model. The fraction of unfolded protein is related to the temperature-dependent equilibrium constant

$K_N^U(T) = [U]/[N]$  according to

$$f_U(T) = \frac{K_N^U(T)}{1 + K_N^U(T)} \quad (3)$$

At the midpoint  $T_0$  of the transition, enthalpy and entropy are equal. The free energy change of unfolding,  $\Delta_N^U G(T)$ , can be written

$$\Delta_N^U G(T) = \Delta H^0 \left( 1 - \frac{T}{T_0} \right) + \Delta_N^U C_p \left( T - T_0 + \ln \frac{T}{T_0} \right) \quad (4)$$

The temperature-dependence of the equilibrium constant is given by

$$K_N^U(T) = e^{\frac{-\Delta_N^U G(T)}{RT}} \quad (5)$$

The three independent parameters which need to be determined are  $\Delta H^0$ ,  $\Delta_N^U C_p$ , and  $T_0$ . The temperature  $T_0$  designates the midpoint of the  $N \rightleftharpoons U$  transition where  $\Delta_N^U G(T_0) = 0$  and  $K_N^U(T_0) = 1$ .  $\Delta H^0$  is the van't Hoff enthalpy of the transition and must be distinguished from the calorimetric enthalpy  $\Delta H_{cal}$  which is measured by the DSC instrument. In an ideal fit of the  $N \rightleftharpoons U$  model the two quantities are identical. However, if  $\Delta H^0$  and  $\Delta H_{cal}$  are different, the deviation of  $\Delta H^0/\Delta H_{cal}$  from unity is

considered to be indicative of intermediates in the transition. The calorimetric curve is then approximated by a superposition of several  $N \rightleftharpoons U$  transitions.

The  $N \rightleftharpoons U$  model does not completely reveal the molecular aspects of protein unfolding. However, many proteins - such as Apo A-I - have a high  $\alpha$ -helix content and a specific molecular process of unfolding is the cooperative "melting" of the  $\alpha$ -helix. We therefore propose an alternative description of Apo A-I unfolding in terms of the *cooperative  $\alpha$ -helix  $\rightleftharpoons$  random coil transition* and we will extend this model to include  $\beta$ -structure formation. The degree of unfolding,  $f_U(T)$ , is calculated with the Zimm-Bragg matrix method [54] and combined with equations (1) and (2). The Zimm-Bragg model considers the  $\alpha$ -helix  $\rightleftharpoons$  random coil transition as the cooperative disruption of  $n$  hydrogen bonds. It is an enthalpy-driven process and the enthalpy change in breaking a single helical hydrogen bond is in the range of  $h = 3.8$  kJ/mol (0.9 kcal/mol) to 5.4 kJ/mol (1.3 kcal/mol) [55-57]. While  $h$  itself is independent of temperature, the temperature dependence of the equilibrium constant  $s(T)$  (growth parameter) follows van't Hoff's law according to

$$s(T) = e^{\frac{h}{R} \left( \frac{1}{T} - \frac{1}{T_1} \right)} \quad (6)$$

At  $T_1$  the growth parameter  $s$  is  $s(T_1) = 1$ .  $T_1$  defines the midpoint of the  $\alpha$ -helix  $\rightleftharpoons$  random coil for a sufficiently long and highly cooperative polypeptide chain. Under these conditions  $T_1$  is identical with the experimentally observed midpoint  $T_0$ . However, the chain length  $n$  has a dramatic effect on the melting behavior. Short chains melt at lower temperatures than long chains and the theory then predicts the midpoint temperature  $T_0$  at lower temperatures than  $T_1$ .

## 2. Thermodynamics of protein self-association and unfolding

---

The second parameter in Zimm-Bragg theory is the nucleation factor  $\sigma$  which is related to the probability of forming an  $\alpha$ -helix nucleus within a random coil sequence.  $\sigma$  determines the cooperativity of the system and is assumed to be temperature-independent.

Zimm-Bragg theory defines conditional probabilities for extending a given peptide chain by one additional segment where "segment" in the present context is identical to a single amino acid in the protein sequence. Adding a helix segment to an existing  $\alpha$ -helix requires the growth parameter  $s$ ; formation of an  $\alpha$ -helix nucleus within a random coil sequence is defined by the nucleation parameter  $\sigma s$ . The occurrence of a coil segment has the probability 1. In the nearest neighbor approximation these conditional probabilities can be summarized in the probability matrix  $M$  [54, 58].

$$M = \begin{pmatrix} 1 & 1 \\ \sigma s & s \end{pmatrix} \quad (7)$$

The partition function of a chain of  $n$  segments is then given by

$$Z = (1 \quad 1) M^n \begin{pmatrix} 1 \\ 0 \end{pmatrix} \quad (8)$$

Knowledge of the partition function allows the calculation of the  $\alpha$ -helix fraction according to

$$f_h = \frac{1}{n} \frac{\partial \ln Z}{\partial s} \quad (9)$$

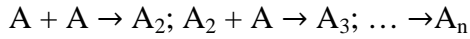
As  $s$  is a function of temperature,  $M$ ,  $Z$ , and  $f_h$  are equally temperature-dependent. The fraction of unfolded protein is

$$f_U(T) = (1 - f_h) \quad (10)$$

$f_U(T)$  can then be combined with equation (2) to calculate  $\Delta_N^U C_p(T)$ .

A convenient approach to calculate the helix-fraction is eq. (27) of reference [54] which can easily be programmed.

*Association/dissociation equilibrium of Apo A-I.* The association of Apo A-I is a separate process which must be distinguished from unfolding. It is described here by a chemical model which includes cooperativity and growth and has been applied successfully to describe surfactant association in micelles [59].



The formation of the dimer  $A + A \rightleftharpoons A_2$  is the nucleation step

$$c_{A_2} = \sigma K_a \cdot c_A^2 \quad (11)$$

which is followed by several growth steps

$$c_{A_3} = K_a \cdot c_{A_2} c_A = \sigma K_a^2 c_A^3 \quad (12)$$

$$c_{A_n} = K_a \cdot c_{A_{n-1}} \cdot c_A \quad (13)$$

$\sigma$  is the nucleation parameter (different from that of Zimm-Bragg theory) and  $c_A$  is the monomer equilibrium concentration. The equilibrium constant  $K_a$  is temperature-dependent according to van't Hoff's law. The corresponding enthalpy of association,  $\Delta H_a^0$ , is also temperature-dependent and is written as

$$\Delta H_a^0(T) = \Delta H_a^0 + \Delta C_{p,a}^0 (T - T_0) \quad (14)$$

## 2. Thermodynamics of protein self-association and unfolding

---

$T_0$  is an arbitrary reference temperature.  $\Delta C_{p,a}^0$  is the molar heat capacity change of the association reaction. All numerical values refer to protein monomers.

If  $c_A^0$  is the total concentration of monomer A and  $q = K_a c_A$  defined as growth parameter, mass conservation requires

$$c_A^0 = c_A \left( 1 + \sigma \sum_{j=2}^n j q^{j-1} \right) \quad (15)$$

We introduce a binding partition function  $Q$  which represents the sum of all concentrations found in the system referenced to the monomer concentration  $c_A$  (cf. [60])

$$c_A + c_{A_2} + \dots + c_{A_n} = c_A \left( 1 + \sigma \sum_{j=2}^n q^{j-1} \right) = c_A \cdot Q \quad (16)$$

$$Q = 1 + \sigma \sum_{j=2}^n q^{j-1} = 1 + \frac{\sigma(q - q^N)}{(1-q)} \quad (17)$$

The degree of dissociation (fraction of monomers) at a given total concentration,  $c_A^0$ , is given by

$$\alpha = \frac{c_A}{c_A^0} \quad (18)$$

and can be calculated as

$$\alpha = \left( q \frac{\partial Q}{\partial q} + Q \right)^{-1} \quad (19)$$

The temperature-dependence of  $\alpha$  is given by

$$\frac{d\alpha}{dT} = qQ^* \frac{\Delta H_a^0(T)}{RT^2} \left( -\frac{1}{\alpha^2} - Q^* K_a \cdot c_A^0 \right)^{-1} \quad (20)$$

where

$$Q^* = 2 \frac{\partial Q}{\partial q} + q \frac{\partial^2 Q}{\partial q^2} \quad (21)$$

We now consider a thought experiment where the protein is locked in its native conformation and a change in temperature influences only the association equilibrium but not the protein conformation. If performed in the DSC instrument the molar heat capacity change is predicted as:

$$\Delta C_{p,a}(T) = \Delta C_{p,a}^0 \cdot \alpha + \Delta H_a(T) \cdot \frac{d\alpha}{dT} \quad (22)$$

Knowing the temperature dependence of  $\Delta H_a$  and  $K_a$ , the degree of dissociation,  $\alpha$ , and the molar heat capacity change,  $\Delta C_{p,a}$ , can be predicted.

For completeness we mention two alternative association models which are discussed in the literature in connection with Apo A-I. The first is the *all-or-none* model



which can be described by

$$c_{A_n} / c_A^n = K_a^{n-1} \quad (24)$$

Defining again

$$q = c_A K_a \quad (25)$$

this leads to the binding partition function

$$Q = 1 + q^{n-1} \quad (26)$$

where the degree of dissociation can again be calculated with eq. 19.

The second model suggests a *monomer-dimer-tetramer-hexamer-octamer* equilibrium [61]. In the present notation the binding partition function of this model is given by

$$Q(n) = 1 + \sigma \sum_{j=1}^{n-1} q^{2j-1} = 1 + \sigma \frac{q - q^{2n-1}}{1 - q^2} \quad (27)$$

The nucleation parameter is included for generality and must be defined as  $\sigma = 1$  to make eq. (27) equivalent to the above mentioned model of reference [61]. Again eq. (19) can be used to derive the degree of dissociation  $\alpha$ .

## Results

*Isothermal titration calorimetry (ITC) of Apo A-I monomer  $\rightleftharpoons$  oligomer equilibrium.* Apo A-I self-associates in solution even at low protein concentrations [51, 61, 62], but thermodynamic aspects of Apo A-I self-association have not yet been investigated in detail. The availability of high-sensitivity titration calorimetry now permits the deduction of the enthalpy of association,  $\Delta H_a$ , binding constant,  $K_a$ , and association number,  $n$ , from dilution experiments. The calorimetric titration sequence is analogous to detergent demicellization experiments determining the critical micellar concentration [59, 63]. In the present study, the dilution involves oligomers of different size and the stoichiometry is not known. Also not known is the effect of temperature on the association-dissociation equilibrium.



Figure 1A displays the heat flow in a dilution experiment where Apo A-I (160  $\mu\text{M}$ ) was injected into PBS buffer. At 40  $^{\circ}\text{C}$  the heat of dissociation was endothermic but changed to exothermic when the experiment was performed below 20  $^{\circ}\text{C}$ . Integration of the calorimetric response peaks yielded the heats of reaction,  $\delta h_i$  (Fig. 1B). The first protein injection corresponded to a more than 100 fold dilution of the starting solution and resulted in a

Figure 1

complete dissociation of the Apo A-I complex. The molar heat of dissociation is then given by

$$\Delta H = \frac{\delta h_1}{\delta n} \quad (28)$$

where  $\delta h_1$  is the measured heat of dissociation of the *first* injection and  $\delta n$  is the molar amount of injected Apo A-I.

However, the experimentally derived  $\Delta H$  is not the full molar heat of dissociation,  $\Delta H_D^0$ . The thermodynamic and statistical analysis discussed below shows that the 160  $\mu\text{M}$  Apo A-I solution is composed of Apo A-I complexes (~95%) and a small fraction of monomers (~5%). The true heat of dissociation,  $\Delta H_D^0$  is thus larger than the measured value  $\Delta H$ . The correct value follows from the theoretical analysis of the dissociation isotherm as described in more detail below. Table 1 shows the measured  $\Delta H$  and the corrected heat of association,  $\Delta H_a^0 = -\Delta H_D^0$ .  $\Delta H_a^0$  has the opposite sign of

## 2. Thermodynamics of protein self-association and unfolding

---

the heat of dissociation. Taking into account the fraction of monomers,  $\alpha$ ,  $\Delta H_a^0$  is given by

$$\Delta H_a^0 = -\Delta H / (1 - \alpha) \quad (29)$$

Table 1

Continued addition of Apo A-I to the calorimeter cell causes dissociation to stop.

The degree of dissociation,  $\alpha_i$ , after  $i$  injections is given by

$$\alpha_i = \frac{\sum \delta h_i}{i \delta h_1} \quad (30)$$

The nominator is the cumulative heat *measured* for the first  $i$  injections, the denominator is the *predicted maximum heat*,  $i \cdot \delta h_1$ , expected for complete dissociation after  $i$  injections. The ITC dilution experiment thus provides both the dissociation enthalpy,  $\Delta H_D^0$ , and the dissociation isotherm  $\alpha = f(c_p^0)$ .  $c_p^0$  is the total concentration of protein in the calorimeter cell and increases with each injection.

ITC measurements were performed between 5 and 45 °C and Fig 2A displays the temperature dependence of the association enthalpy  $\Delta H_a^0$ . The enthalpy changes its sign at

Figure 2

about 20 °C and the slope of the straight line yields the molar heat capacity change for the association reaction as  $\Delta C_p^0 = -2.76 \text{ kJ mol}^{-1}\text{K}^{-1}$  ( $-0.66 \text{ kcal mol}^{-1}\text{K}^{-1}$ ). Apo A-I self-association is thermodynamically similar to the partitioning of hydrophobic substances between water and an organic phase [64]. The enthalpy of dissolving hydrophobic substances such as hexane in water is close to zero at room temperature while the heat capacity increment for the transfer from water into pure organic phase is large and negative. Apo A-I self-association paralleled this behavior, as the enthalpy of Apo A-I self-association was zero at room temperature and the heat capacity change strongly negative. Calorimetric experiments at 15-30 °C were not feasible because  $\Delta H_a^0 \sim 0 \text{ kcal/mol}$ .

Apo A-I dissociation as measured by ITC was analyzed with the cooperative association model. The result is shown in Fig. 1B (solid line) which simulates the dilution measurement at 40 °C and was calculated with an association constant  $K_a = 3.5 \times 10^5 \text{ M}^{-1}$ , a nucleation factor  $\sigma = 0.003$  and a maximum association number  $n = 8$ . An excellent fit between theory and experiment was obtained.

The cooperative model was further applied to investigate the influence of the association number 'n' on the quality of the simulation. A minimum of  $n = 6$  was required to generate a good fit of the ITC data over the whole temperature range. An increase in n from 6 to 20 provided simulations of similar quality, but reduced the values of the nucleation parameter  $\sigma$  and the association constant  $K_a$ . At  $n = 20$  a 'plateau' was reached where an increase in n had no further effect on  $\sigma$  or  $K_a$ . However, analytical ultracentrifugation data discussed below argue against an association number larger than  $n = 8$ .

## 2. Thermodynamics of protein self-association and unfolding

---

Fig. 2B shows the temperature dependence of the Apo A-I association constant  $K_a$  (addition of a monomer to an existing complex) for  $n = 8$ . The solid line is the predicted temperature dependence of  $K_a$  calculated with the van't Hoff equation and a temperature-dependent  $\Delta H_a^0$  (Fig. 2A). The simulations also showed that a nucleation parameter  $\sigma \ll 1$  was essential for the correct interpretation of the experimental data. Initial dimer formation is thermodynamically less favored than the addition of monomers to an existing complex.

As an alternative model we also evaluated the all-or-none model. A fit of the ITC data was possible with  $n = 6$ . However, the model assumes only monomers and hexamers without intermediates, is kinetically impossible, and disagrees with the results of analytical ultracentrifugation.

*Analytical ultracentrifugation (AUC) analysis of Apo A-I self-association.*

Previous studies on Apo A-I self-association used AUC measurements of serum-purified Apo A-I [61, 65]. We therefore compared the recombinant Apo A-I (with two additional C-terminal glycines) used in this study with serum-purified Apo A-I also using AUC. Fig. 3A shows sedimentation equilibrium runs at 6, 8 and 10 krpm for recombinant Apo A-I (160  $\mu\text{M}$ ) in PBS buffer. The protein concentration increases with increasing radius  $r$ , and thus each point in the concentration,  $c$ , vs. radius,  $r$ , profile corresponds to a *different equilibrium* between monomers and Apo A-I complexes. Quantitative analysis is possible by calculating both the total Apo A-I concentration at a given radius  $r$  and the slope of the  $\ln(c)$  vs.  $r^2$  curve at the same position. We determined local slopes of the  $\ln(c)$  vs.  $r^2$  function by linearization of 8-10 consecutive data points, computing the slope of this linearized interval, and then shifting the interval to the next

## 2. Thermodynamics of protein self-association and unfolding

---

data point. Figure 3B shows the apparent molecular mass,  $M_{app}$ , as a function of the corresponding total Apo A-I concentration. We assumed that monomeric and oligomeric Apo A-I molecules have the same specific optical absorption at 280 nm. Figure 3B summarizes data obtained for Apo A-I solutions at initial concentrations of 3, 40, and 160  $\mu\text{M}$  measured at 6 different rotor speeds between 4 krpm to 15 krpm. Data scatter is considerable but the semi-logarithmic plot clearly shows a horizontal lag phase up to  $\sim 3 \mu\text{M}$  where no association occurs and where  $M_{app}$  is identical to the molecular mass of monomeric Apo A-I. Above 3  $\mu\text{M}$   $M_{app}$  increases sigmoidially. The solid line in Fig. 3B corresponds to the best fit using the cooperative model with  $K_a = 3.5 \times 10^5 \text{ M}^{-1}$ ,  $n = 8$ , and  $\sigma = 0.003$ . Calorimetric measurements yielded  $K_a = 5.6 \times 10^5 \text{ M}^{-1}$  at 20 °C (represented by the dashed line in Fig. 3B) indicating a good agreement between AUC and ITC. The nucleation parameter  $\sigma$  determines the length of the monomeric lag phase as well as the steepness of the transition curve.

Figure 3C compares recombinant Apo A-I with Apo A-I purified from blood serum. It shows the degree of dissociation,  $\alpha$ , as determined by AUC measurements at 20 °C and 37 °C.

### Figure 3

The data allow two conclusions. (i) Recombinant and serum-derived Apo A-I yield identical results within experimental error. (ii) The AUC data can be described quantitatively by the cooperative association model as displayed by the solid lines in Fig. 3C. At 37 °C the simulation yielded  $K_a = 4 \times 10^5 \text{ M}^{-1}$ ,  $\sigma = 0.003$ ,  $n = 8$  which agrees perfectly with the ITC data. At 20 °C the AUC data predicted  $K_a = 8 \times 10^5 \text{ M}^{-1}$  which was slightly higher than expected on the basis of ITC measurements.

## 2. Thermodynamics of protein self-association and unfolding

---

*Differential scanning calorimetry (DSC) analysis of Apo A-I unfolding.* The thermodynamics of Apo A-I unfolding was quantified by measuring dilute solutions of Apo A-I with differential scanning calorimetry. Fig. 4 shows the melting curves for Apo A-I concentrations from 0.5 to 4.5 mg/mL. The maximum of the molar heat capacity occurred at  $T_0 = 52.6$  °C for all three samples and was independent of protein concentration. The heat of transition,  $\Delta H_N^U$ , was 422 kJ/mol (101 kcal/mol) and was also independent of the protein concentration, at least at 70.9  $\mu$ M and 160  $\mu$ M as the DSC scans were superimposable within experimental error. DSC scans were fully reversible if heating did not exceed 75 °C. Previous work on Apo A-I yielded DSC maxima between 57 and 63 °C and melting enthalpies between 58 to 200 kcal/mol [44, 45, 66]. The differences may be caused by differences in protein preparations and salt conditions and also by neglecting the difference between initial and final  $C_p$  values. (In differential scanning calorimetry the sharpness of a transition is an indicator of the purity of the substance, the homogeneity of the probe, and the cooperativity of the transition. The recombinant Apo A-1 (with 2 additional C- terminal glycines) used here yielded the sharpest transition compared to all published DSC data on Apo A-I. A survey of DSC data on Apo A-I of different origin reveals a complex situation. Unfolding curves composed of three consecutive non-two state transitions [44, 45], two consecutive two-state transitions [66] or just one broad transition [51] were reported. Likewise, the unfolding enthalpy  $\Delta_N^U H^0$  was 200 kcal/mol [44], 48 kcal/mol ([45], main peak), 84 kcal/mol [66], and estimated 200 kcal/mol [51]. The width of the melting curve at half-height was 14.3 °C in the present measurements, but ranged from 14 °C ([45], main peak) over 20 °C [66], 22 °C [45] to 25 °C [51]. In the latter case [51]

## 2. Thermodynamics of protein self-association and unfolding

---

the MALDI mass of the recombinant wild-type Apo A-1 is given as 29798 Da which is 1719 Da (ca. 14 amino acids) larger than the authentic human Apo A-1. This could explain the differences observed in association behavior and differential scanning calorimetry between the present study and reference [51].)

As Apo A-I unfolding was independent of protein concentration above 17  $\mu\text{M}$ , the association process described in the previous section did not influence unfolding. This is discussed below in the context of a quantitative comparison of the two different equilibria.

Figure 4

A general problem in evaluating DSC thermograms is the definition of the baseline [67]. In the present studies the baseline was defined by the linear part of the calorimetric scan at low temperature and was extrapolated beyond the main transition as shown in detail in Fig. 5. This appeared to be justified as it led to constant  $C_p$  values *before* and *after* the transition. The difference between the two linear parts is the molar heat capacity change  $\Delta_N^U C_p = 5.0 \text{ kJ/molK}$  (1.2 kcal/molK). A change in  $\Delta_N^U C_p$  was not reported in the earlier DSC experiments [44, 45, 51, 66]. However  $\Delta_N^U C_p$  changes of several kJ/molK are found for other proteins (e.g. T4 Lysozyme, 164 aa,  $\Delta_N^U C_p = 5.1 \text{ kJ/molK}$  [68], human growth hormone, 192 aa,  $\Delta_N^U C_p = 8 \text{ kJ/molK}$  [69]).

Figure 5

## 2. Thermodynamics of protein self-association and unfolding

---

Knowledge of  $\Delta_N^U C_p$  provides insight into the molecular nature of Apo A-I unfolding. At low temperatures ( $T \leq 20$  °C) amide hydrogens are well protected by hydrogen bonds in the native protein structure. This is true whether the site in question is deeply buried or at the solvent-exposed surface [70]. Hydrogen-deuterium exchange was thus used to determine the  $\alpha$ -helical segments of Apo A-I [70]. Thermal unfolding of Apo A-I increases the molecular fluctuations and H-bonds are transiently broken and brought in contact with solvent. While the increase in heat capacity is generally assigned to the exposure of apolar groups, a systematic study on cyclic peptides led to the conclusion: "The large apolar contribution suggests that a liquid hydrocarbon model of the hydrophobic effect does not accurately represent the apolar contribution to  $\Delta H^0$  of denaturation. Rather, significant enthalpic stabilizing contributions are found to arise from peptide groups (hydrogen bonding)" [71]. The heat capacity change upon water exposure of a single amide group has been estimated as  $\Delta_N^U C_p = 60 \pm 6 \text{ Jmol}^{-1}\text{K}^{-1}$  [71]. The increase of  $\Delta_N^U C_p = 5.0 \pm 0.5 \text{ kJ mol}^{-1}\text{K}^{-1}$  (1.22 kcal/molK) observed for Apo A-I could thus be caused by the exposure of about 83 amino acids, in agreement with the CD spectroscopy results to be discussed below.

Figure 5 shows the temperature-dependence of the heat capacity and compares the experimental data with the predictions of cooperative model (fig. 5A) and the  $N \rightleftharpoons U$  two-state model (fig. 5B). An improved fit of figure 5B could be obtained by superimposing several  $N \rightleftharpoons U$  two-state transitions. 2 or 3  $N \rightleftharpoons U$  two-state transitions were combined to simulate previous experimental DSC data as discussed above. The increase in the molar heat capacity between the fully folded and the unfolded protein was not considered in these earlier analyses.



*CD spectroscopy analysis of thermal Apo A-I unfolding.* The structural changes associated with thermal unfolding were investigated with CD spectroscopy. Figure 6A depicts CD spectra of Apo A-I in buffer measured in 10 °C steps between 25 °C and 85 °C. After heating to 85 °C and cooling to 25 °C the CD spectrum was virtually identical to the starting spectrum illustrating the reversibility of thermal unfolding. Inspection of figure 6A reveals spectral shapes characteristic of a predominantly  $\alpha$ -helical structure. However, a continuous loss of  $\alpha$ -helix structure occurs with increasing temperature.

Figure 6

The quantitative evaluation of the  $\alpha$ -helix fraction,  $f_h$ , is possible with

$$f_h = (\Theta_{222} + 3000) / (-39000) \quad (31)$$

where  $\Theta_{222}$  is the molar ellipticity per residue at  $\lambda = 222$  nm. The  $\alpha$ -helix content evaluated by equation (31) decreases from  $f_h = 45\%$  at 25 °C to 18% at 85 °C, consistent with earlier observations [44-46, 48, 72]. Surprisingly, the loss of  $\alpha$ -helix is compensated mainly by an increase in  $\beta$ -structure and not by random coil elements. This follows from simulations of the CD spectra in the range of 190-240 nm yielding the fractions of the main structural elements as shown in figure 6B. (Two different algorithms (cf. Materials and Methods) were applied and produced almost identical results.) The  $\alpha$ -helix content is found to be higher than estimated with eq. (31). It is constant at  $f_h \sim 50\% - 54\%$  below 45 °C and decreases to  $f_h = 21\%$  at 85 °C. The loss in  $\alpha$ -helix-fraction upon heating is  $\Delta f_h = 33\%$ . At the same time the  $\beta$ -structure

## 2. Thermodynamics of protein self-association and unfolding

---

contribution rises from 26% to 50% which has escaped notice in previous studies. The percentage of random coil segments increases modestly from 19% to 28%. The CD spectral simulations show that (i) the melting of Apo A-I is a multi-state process and (ii) the spectroscopic change of  $\Delta f_h = 33\%$  corresponds to the loss of  $(243 + 2) \times 0.33 = 81$  helical segments. This result is in excellent agreement with the thermodynamic analysis given above (i.e. 83 helical segments) based on the change of the molar heat capacity  $\Delta_N^U C_p$ . The solid line through the  $\alpha$ -helix data is the prediction of the Zimm-Bragg model.

Hydrogen bond enthalpy in a  $\beta$ -structure is much lower than that in an  $\alpha$ -helix. For the membrane-binding peptide (KIGAKI)<sub>3</sub>, composed of 18 amino acids,  $h_\beta$  is 0.96 kJ/mol (0.26 kcal/mol) for breaking a hydrogen bond in long stretches ( $n \geq 18$ ) of  $\beta$ -structure [73]. For shorter arrays of  $\beta$ -structure,  $h_\beta$  can be 0 kJ/mol or be even slightly negative [74]. Thus from a thermodynamic point of view the  $\alpha$ -helix  $\rightleftharpoons$   $\beta$ -structure transition can be similar or identical to the  $\alpha$ -helix  $\rightleftharpoons$  random coil transition, and  $\beta$ - and random coil-elements will be considered as thermodynamically equivalent in the present context. Significant differences between the enthalpies of  $\beta$ - and rc-segment formation should be reflected in the parameters of the Zimm-Bragg theory. However, for Apo A-I, and other proteins which we investigated, the enthalpy of helix disruption ( $h$ -value used in eq. (6)) was always in the range of 800 cal/mol to 1300 cal/mol.

As an aside it should be noted that a plot of the  $\lambda = 222$  nm ellipticity versus temperature (data of figure 6A) has its midpoint at 61 °C which is 8 °C higher than  $T_0$  of the caloric transition. The discrepancy between CD spectroscopy and DSC is also obvious from inspection of figure 6B. CD spectroscopy monitors changes of the secondary structure only, while DSC includes also the melting of the tertiary structure.

### Discussion

The present analysis is of general relevance for the understanding of the thermodynamic behavior of oligomeric systems. Our experimental and theoretical results shed light on two different problems, that is, the thermodynamics of (i) unfolding an  $\alpha$ -helical protein and (ii) the temperature- and concentration-dependence of a monomer  $\rightleftharpoons$  oligomer equilibrium. Cooperativity was found to play an essential role in both processes. The Zimm-Bragg theory was introduced as an alternative to the classical  $N \rightleftharpoons U$  two-state model for a consistent analysis of calorimetric and spectroscopic data on Apo A-I unfolding. The isodesmic self-association model was employed to describe the oligomerization of Apo A-I. The free energy for the addition of a monomer to any oligomer was assumed to be constant but the initial dimerization was less favorable by the nucleation factor  $\sigma$ , introducing cooperativity. Maximum self-association occurred at 21 °C whereas the mid-point of unfolding was at 52.6 °C. The measured heat of unfolding was ca. 100 kcal/mol and by a factor 5-10 larger than the heat of self-association. The unfolding enthalpy was independent of concentration up to 160  $\mu$ M. In the following we compare the temperature course of unfolding with that of Apo A-I dissociation. We provide a model calculation for the temperature- and concentration-dependence of  $C_p^0$  for a cooperative monomer  $\rightleftharpoons$  oligomer equilibrium.

*Thermodynamics of Apo A-I unfolding.* Crystal structure [42] and protein sequence analysis [75] predict that the Apo A-I region between residues 44 and 241 is largely  $\alpha$ -helical. The 2.2 Å crystal structure of C-terminal truncated Apo A-I (184 N-terminal residues) reveals an approximate half-circle (80% helix) with the N-terminal

## 2. Thermodynamics of protein self-association and unfolding

---

arranged in a loose bundle composed of four helices and an extended segment [42]. Unfolding of Apo A-I corresponds essentially to a disruption of  $\alpha$ -helical regions and, to a minor extent, to the unfolding of the four-helix tertiary structure. As a new approach we describe the Apo A-I unfolding with the cooperative Zimm-Bragg theory. Figure 5A compares the experimental DSC scan with the prediction of the cooperative  $h \rightleftharpoons \beta$ , rc model. The parameters used were: H-bond stability  $h = 4.6$  kJ/mol (1100 cal/mol), nucleation factor  $\sigma = 4.4 \times 10^{-5}$ ,  $T_1 = 339.7$  °K and  $n = 85$ . The predicted mid-point temperature for this short  $\alpha$ -helix was  $T_0 = 325.6$  °K, in agreement with the maximum of the measured  $C_p$  vs. T curve. Attempts to simulate the DSC curves with distinctly shorter chain lengths than  $n = 85$  were unsuccessful as the width of the transition region became too broad. Hydrogen exchange experiments indicate long stretches of  $\alpha$ -helix secondary structure between Apo A-1 residues 7 and 115 with a total of 95  $\alpha$ -helical residues [70]. It is the unfolding of this region which is most likely monitored in the DSC experiment. A second  $\alpha$ -helical region of 32 residues is found at positions 147 – 178 [70]. As Apo A-1 has an  $\alpha$ -helical content of 18% even at 85 °C (corresponding to ca. 40 residues) this  $\alpha$ -helix could account for the residual ellipticity observed in CD-spectroscopy (cf. figure 6).

The enthalpy per hydrogen bond can also be derived directly from the transition enthalpy without resorting to a particular model. As the unfolding enthalpy is  $\Delta_N^U H = 422$  kJ/mol (101 kcal/mol) and as CD spectroscopy suggests that ~85 segments are involved in the transition, an  $\alpha$ -helix stability of  $h = 422/85 \approx 5.0$  kJ/mol (1188 cal/mol) can be estimated, in good agreement with the value used in Zimm-Bragg theory.

Figure 5B displays the related calculations with the  $N \rightleftharpoons U$  model. The experimental transition temperature was  $T_0 = 325.6$  K, as defined by the maximum of

the  $C_p$  curve. The unfolding enthalpy  $\Delta_N^U H$  required for an optimum fit was 285 kJ/mol (68.2 kcal/mol). This value is much lower than the experimental result of 422 kJ/mol (101 kcal/mol). The  $N \rightleftharpoons U$  model also predicts a sharper transition than observed experimentally.

The theoretical transition enthalpy characterizing the two-state  $N \rightleftharpoons U$  equilibrium is often denoted with van't Hoff enthalpy,  $\Delta H_{vH}$ , and derived from CD-measurements. For Apo A-I  $\Delta H_{vH}$  is much smaller than the calorimetric transition enthalpy,  $\Delta_N^U H^0$ , and the ratio  $\Delta H_{vH} / \Delta_N^U H^0 < 1$  is considered to reflect the *low* cooperativity of the Apo A-I unfolding [44, 45, 66]. In contrast, a *high* cooperativity index  $n_{coop} = 7.8$  was defined by applying the Hill equation to describe the sigmoidicity of the thermal denaturation curve [46]. The Zimm-Bragg theory finally describes cooperativity in terms of the steepness of the transition curve. The smaller the nucleation parameter  $\sigma$  and the larger the number of hydrogen bonds to be broken, the more cooperative is the transition and the steeper the transition curve. In terms of the Zimm-Bragg theory Apo A-I unfolding is a highly cooperative process.

*Thermodynamics of Apo A-I self-association and monomer-oligomer probabilities.* Both AUC and ITC demonstrate that self-association of Apo A-I is a concentration-dependent process. Fig. 3B indicated that Apo A-I is monomeric below  $\sim 3 \mu\text{M}$  and self-associates at higher concentrations. The cooperative association model with  $n = 8$  and  $\sigma = 0.003$  gave the best fit to both the ITC and AUC data. Knowledge of  $K_a$  as deduced from the dissociation isotherm permits the calculation of the free energy,  $\Delta G_a^0$ , and entropy  $T\Delta S_a^0$  (see Table 1). At room temperature the enthalpy of

## 2. Thermodynamics of protein self-association and unfolding

---

association,  $\Delta H_a^0$ , is close to zero while the Gibbs free energy,  $\Delta G_a^0$ , is large and negative. This means that the entropy of association is large and positive and is the driving force for the association at temperatures below 20 °C. As the temperature increases, the reaction becomes exothermic and the contribution of entropy gradually decreases.

The Apo A-I solution contains states of oligomerization 1, 2, ...,j. The probability of their occurrence can be calculated with the partition function Q. If  $p_j$  is defined as the probability of j-mers in solution, i.e. the number of oligomers of size j divided by the total number of species in solution, then

$$p_j = \frac{n_j}{\sum_j n_j} \quad (32)$$

For the cooperative model one finds

$$p_1 = Q^{-1} \quad \text{and} \quad p_j = \sigma (K_a c_A)^{j-1} / Q \quad (33)$$

Figure 7 provides a comparison of the fraction of monomers,  $p_1$ , and octamers,  $p_8$ , plotted vs. the total monomer concentration  $c_A^0$  (maximum association number  $n = 8$ ).

Also

Figure 7

included are the degree of dissociation  $\alpha = c_A / c_A^0$  and the experimental results for  $\alpha$  obtained from the titration experiment shown in Fig. 1.

Figure 7 reveals that the degree of dissociation,  $\alpha$ , decreases faster than the monomer probability,  $p_1$ . This follows because only one  $A_8$  molecule is generated when eight monomers associate, and the loss of monomers thus proceeds faster than the growth in the number of oligomers. Monomers and octamers are the predominant species in solution. However, the sum  $p_1 + p_8$  goes through a minimum at a total Apo A-I concentration of ca.  $6.7 \times 10^{-4}$  M, with monomers and octamers accounting for only 70% of the total species. This indicates that the solution contains additional intermediates.

Earlier studies on Apo A-I self-association primarily relied on AUC measurements where a monomer-dimer-tetramer-octamer model was assumed [61, 62]. *Separate* association constants were defined for each association step. However, when applied to the present ITC data, this model did not provide satisfactory quantitative results.

Apo A-I association has also been reported in terms of an 'apparent molecular weight' [65].  $M_{app}$  can be calculated in the present notation as

$$M_{app} = \sum_{j=1}^n j p_j \cdot M_W^A \quad (34)$$

$M_W^A$  is the molecular mass of the Apo A-I monomer. Eq. (34) was used to simulate the data in Fig. 3B. Excellent agreement with the ITC experiments was obtained.

We have also analyzed previous  $M_{app}$  results for Apo A-I with the cooperative model discussed above. For example, simulating the  $M_{app}$  data given in reference [65] (figure 2, 0.13 M KCl) with the cooperative model required  $\sigma = 0.003$  and  $K = 6 \times 10^5 \text{ M}^{-1}$  for  $n = 8$ . These are exactly the values predicted by the present ITC experiments for the self-association at 20 °C.

## 2. Thermodynamics of protein self-association and unfolding

---

*Apo A-I unfolding vs. Apo A-I dissociation.* Protein association and denaturation can be tightly connected processes as demonstrated for a 54 amino acid fragment of GCN4 [76]. Increasing the protein concentration by a factor of 100 in this example shifts the midpoint of the unfolding transition by about 20 °C towards higher temperatures. In contrast, Apo A-I unfolding was independent of the protein concentration (up to 160  $\mu\text{M}$ ). Self-association reached its maximum at 21 °C and decreased both at lower and higher temperatures, while Apo A-I unfolding had its maximum change in the heat capacity (midpoint of unfolding transition) at 52.6 °C. Considering a 160  $\mu\text{M}$  (70.7 $\mu\text{M}$ ) Apo A-I solution at 45 °C, which is the onset temperature of the unfolding reaction, the fraction of monomers is 6.5% (12.8%), while that of octamers is 59% (51%), referenced to total monomeric Apo A-I. Hence at the beginning of the unfolding process the solution is mainly composed of oligomers. We therefore calculated the contribution of Apo A-I dissociation to the molar heat capacity change by the following thought-experiment. We considered an Apo A-I solution where the Apo A-I molecules were locked in their native conformation at all temperatures. The change in the molar heat capacity was thus exclusively caused by the dissociation of Apo A-I complexes. Using eqs. (19), (20), and (22) the molar heat capacity change of the dissociation equilibrium was calculated and compared with that of protein unfolding. Figure 8 displays

Figure 8



such calculations for three protein concentrations. As expected the heat capacity of the dissociation equilibrium depended on the total Apo A-I concentration,  $c_A^0$ . The maximum of the molar heat capacity shifted from 55 °C at 17  $\mu$ M Apo A-I to 72 °C at 160  $\mu$ M while the width of the transition was reduced. The predicted molar heat capacity was 3.7 kJ/molK (1.98 kJ/molK) for 70  $\mu$ M (160  $\mu$ M) Apo A-I at 53 °C which was much smaller than the molar heat capacity at the  $C_p$  maximum of the unfolding reaction of  $C_p^0 = 24.6$  kJ/molK. Figure 8 predicts that the dissociation of virtual, folded Apo A-I complexes should occur at temperatures *higher* than that of Apo A-I unfolding. An additional transition peak should appear in the  $C_p$  vs. T diagram. As this was not observed experimentally it is safe to conclude that Apo A-I unfolding and dissociation occur simultaneously. This is consistent with the observed concentration-independence of the unfolding transition. As the heat capacity change of the dissociation reaction makes only a small contribution (figure 8), the calorimetric  $\Delta_N^U H$  is dominated by the unfolding of secondary structural elements.

*Concluding Remarks.* We showed that protein self-association can be readily analyzed by the method of binding partition functions. This approach allowed comparison of different association models and provided analytic expressions to analyze experimental AUC and ITC results. The thermodynamic parameters of Apo A-I self-association are quite similar to those of other, more specific, protein-protein interactions. For example, the interaction of stathmin, a 17 kDa protein, with tubulin (~55 kDa) was investigated with ITC [77]. Similar to the present results the binding constants of the binary complex were  $10^6 - 10^7$   $M^{-1}$ . Likewise,  $\Delta H^0$  was also endothermic at low temperatures and attained zero values at 28 °C. The fact that some

## 2. Thermodynamics of protein self-association and unfolding

---

biological systems have very small reaction enthalpies at ambient temperature demonstrates that they minimize the temperature sensitivity of the corresponding chemical equilibria, leading to temperature-independent concentrations of the involved proteins. Another example supporting this conclusion is apolipoprotein C-1 showing a maximum of self-association at room temperature which is also reduced upon heating or cooling [78].

We further showed that the cooperative Zimm-Bragg model provided an accurate description of Apo A-I unfolding and should be considered as an alternative to the common two-state  $N \rightleftharpoons U$  model, at least for proteins with a high  $\alpha$ -helix content. For comparison, we analyzed experimental DSC results for a 22-kDa (N-terminal) fragment of Apo E2 which is about 50%  $\alpha$ -helical at 20 °C ([79], Fig.1). An excellent fit of the DSC curve was obtained with  $h = 5.02$  kJ/mol (1200 cal/mol) and  $\sigma = 3 \times 10^{-5}$ , parameters very similar to those of Apo A-I. As a second example we analyzed the calorimetric trace of a 50-residue peptide (figure 3 in reference [57]) with the Zimm-Bragg model and again obtained excellent agreement with experimental values using  $h = 930$  cal/mol and  $\sigma = 4 \times 10^{-3}$ . These results are consistent with a follow-up study of the same peptide with CD-spectroscopy resulting in  $h = 960 \pm 20$  cal/mol and  $\sigma = (2.9 \pm 0.3) \times 10^{-3}$  [80]. Application of the  $N \rightleftharpoons U$  model completely failed for this 50-residue peptide.

## Acknowledgement

We are indebted to Dr. Francis Müller and Eric André Kuszniir, Roche, for providing the AUC data for figure 3C. We are grateful to Howard Etlinger for carefully reading the manuscript and valuable comments.

## Legends to figures

*Figure 1: Dissociation reaction of Apo A-I measured with isothermal titration calorimetry (ITC).*

(A) Heat flow. A 160  $\mu\text{M}$  solution of Apo A-I in PBS buffer (138 mM NaCl, 10 mM sodium phosphate, pH 7.4, 0.02 %  $\text{NaN}_3$ ) was injected at 2  $\mu\text{L}$  aliquots into the calorimeter cell ( $V_{\text{cell}} = 0.2 \text{ mL}$ ) containing only buffer. The heat of reaction,  $\delta h_i$ , arises from the dissociation reaction of Apo A-I oligomers as each injection corresponds to a ca. hundred-fold dilution of protein concentration. The measurement was made at 40 °C. At room temperature the heat of dissociation is close to zero and the disassociation reaction is not detectable by ITC.

(B) Integrated heats of reaction,  $\delta h_i$ , as a function of injection number. The solid line shows the theoretical analysis based on the cooperative association model. Maximum association number  $n = 8$ , association constant  $K_a$  (40 °C) =  $3.5 \times 10^5 \text{ M}^{-1}$ ,  $\sigma = 0.003$ , measured heat of dissociation  $\Delta H = 49.1 \text{ kJ/mol}$  (11.74 kcal/mol). The corrected heat of dissociation was 51.3 kJ/mol (12.3 kcal/mol) as the starting solution contained 4.4% monomers.

*Figure 2: Thermodynamic parameters of Apo A-I self-association.*

(A) Enthalpy,  $\Delta H_a^0$ , of Apo A-I self-association as determined with isothermal titration calorimetry.

(B) Temperature-dependence of the association constant  $K_a$ .  $K_a$  was calculated by fitting the dilution isotherms of the calorimetric titration experiments with the cooperative association model using  $n = 8$  and  $\sigma = 0.003$ . The solid line predicts the

## 2. Thermodynamics of protein self-association and unfolding

---

temperature dependence of  $K_a$  by combining the van't Hoff equation with the temperature-dependent  $\Delta H_a^0$  of fig. 2A.

*Figure 3: Apo A-I self-association measured with analytical ultracentrifugation (AUC).*

(A) Sedimentation equilibrium experiments. Apo A-I at a concentration of 160  $\mu\text{M}$  in PBS buffer was centrifuged for 96 hrs at 6 krpm (black line), 8 krpm (red) and 10 krpm (blue) at 20  $^\circ\text{C}$ .

(B) Apparent molecular mass,  $M_{\text{app}}$ , as a function of total Apo A-I concentration. 3 concentrations were simultaneously measured. 3  $\mu\text{M}$  (blue data points, cuvette size 12 mm); 40  $\mu\text{M}$  (green data points, cuvette size 3 mm); 160  $\mu\text{M}$  (red data points, cuvette size 1.4 mm). Measurements at 6 krpm (■), 8 krpm (▲), 10 krpm (◆), 12 krpm (●) and 15 krpm (★). Analyses were limited to a maximum optical density of  $\text{OD} = 2$ . The solid line was calculated with the cooperative association model using  $n = 8$ ,  $\sigma = 0.003$ ,  $K_a = 3.5 \times 10^5 \text{ M}^{-1}$ . The dashed line corresponds to  $K_a = 5.6 \times 10^5 \text{ M}^{-1}$  predicted by ITC at 20  $^\circ\text{C}$ .

(C) Degree of dissociation,  $\alpha$ , as a function of total protein concentration. Recombinant Apo A-I (■) is compared with serum-purified Apo A-I (◆). Measurements were made at 20  $^\circ\text{C}$  (blue points) and 37  $^\circ\text{C}$  (red points). The solid lines are the predictions of the cooperative association model with  $n = 8$ ,  $\sigma = 0.003$ , and  $K_a = 4.0 \times 10^5 \text{ M}^{-1}$  (37  $^\circ\text{C}$ , red line) or  $K_a = 8 \times 10^5 \text{ M}^{-1}$  (20  $^\circ\text{C}$ , blue line).

*Figure 4: Differential scanning calorimetry (DSC) of recombinant Apo A-I.*

Apo A-I unfolding reaction measured at 17.7, 70.9 and 160  $\mu\text{M}$ . The transition maximum occurred at 52 - 53  $^\circ\text{C}$  and was concentration independent. The normalized

## 2. Thermodynamics of protein self-association and unfolding

---

DSC scans at 70.9 and 160  $\mu\text{M}$  are superimposable. The heating rate was 1  $^{\circ}\text{C}/\text{min}$ . All measurements were made in buffer (10 mM sodium phosphate, 138 mM NaCl, pH 7.4, 0.02%  $\text{NaN}_3$ ). The measurement at 17.7  $\mu\text{M}$  was at the limit of sensitivity and could not be used for an evaluation of unfolding enthalpy.

*Figure 5: Interpretation of Apo A-I thermal unfolding comparing two models.*

The experimental result (black line) is the DSC scan of a 160  $\mu\text{M}$  Apo A-I solution in PBS buffer measured at a heating rate of 1  $^{\circ}\text{C}/\text{min}$ . (A) Zimm-Bragg model (red line) using  $\sigma = 4.4 \times 10^{-5}$ ,  $h = 1100$  cal/mol,  $n = 85$ ,  $\Delta_{\text{N}}^{\text{U}}\text{C}_{\text{p}}^0 = 5.0$  kJ/mol. Predicted  $T_0 = 325.6$  K. The midpoint of the  $h \rightarrow \beta$ , rc transition of an infinitely long  $\alpha$ -helix is at  $T_1 = 339.7$  K.

(B)  $\text{N} \rightleftharpoons \text{U}$  2 two-state model (red line) using  $\Delta_{\text{N}}^{\text{U}}\text{H} = 285$  kJ/mol (68.2 kcal/mol),  $\Delta_{\text{N}}^{\text{U}}\text{C}_{\text{p}}^0 = 5.0$  kJ/mol, and  $T_0 = 325.6$  K

*Figure 6: Thermal unfolding analysis of recombinant Apo A-I by CD spectroscopy.*

(A) Far-UV-CD spectra of Apo A-I for temperatures between 25  $^{\circ}\text{C}$  (black line) to 85  $^{\circ}\text{C}$  (blue line) recorded at 10  $^{\circ}\text{C}$  steps. Apo A-I concentration was 0.5 mg/mL (17.7  $\mu\text{M}$ ) in buffer (100 mM NaF, 10 mM sodium phosphate, pH 7.4). Measurements at a lower concentration of 0.1 mg/mL (3.6  $\mu\text{M}$ ) yielded similar spectra in the range of 25 - 65  $^{\circ}\text{C}$ .

(B) Deconvolution of the CD spectra in terms of 3 structural elements. (■)  $\alpha$ -helix, (●)  $\beta$ -sheet, (◆) random coil. The  $\beta$ -turn element is not shown as it was always close to zero. Figure 6 demonstrates that the loss in  $\alpha$ -helix content is mostly compensated by an increase in  $\beta$ -structure. The solid line is the predicted  $\alpha$ -helix

## 2. Thermodynamics of protein self-association and unfolding

---

content as calculated with the Zimm-Bragg theory using a nucleation parameter  $\sigma = 4.4 \times 10^{-5}$ , a hydrogen bond enthalpy per helix residue of  $h = 1100$  cal/mol, and  $n = 85$  as deduced from the DSC and CD unfolding experiments.

*Figure 7: Self-association of Apo A-I. Probabilities of monomers and octamers.*

(■) Apo A-I degree of dissociation,  $\alpha$ , as derived from the ITC experiment shown in figure 1. Solid lines: predicted probabilities (mole fractions) of monomers,  $p_1$ , and octamers,  $p_8$ , as a function of the total protein monomer concentration,  $c_A^0$ , at 40°C. Calculations with the cooperative association model  $\sigma = 0.003$ ,  $K_a = 3.5 \times 10^5 \text{ M}^{-1}$ , maximum association number  $n = 8$ .

Figure 8: Computed DSC scans for a solution containing virtual Apo A-I oligomers which dissociate but remain folded.

Three different protein concentrations were compared. The melting curves were calculated with the cooperative association model. The temperature dependence of the association constant was  $\Delta H_a$  (kcal/mol) =  $-0.659 (T-273) + 13.288$  and the association constant at 273 K was  $3.5 \times 10^5 \text{ M}^{-1}$ . The temperature dependence of  $K_a$  was identical to that in figure 5B. The maximum association number is  $n = 8$  and the cooperativity parameter  $\sigma = 0.003$ . Blue line: 17.7  $\mu\text{M}$ , red line 70.7  $\mu\text{M}$ , magenta line 160  $\mu\text{M}$ .

A) Molar heat capacity change,  $C_p^0$ . The maximum of the dissociation reaction shifts to higher temperatures with increasing protein concentration. B) Degree of dissociation,  $\alpha$

## 2. Thermodynamics of protein self-association and unfolding

**Table 1**

Thermodynamic parameters of Apo A-I self-association equilibrium calculated with the cooperative association model

Tem p C	$C_{\text{Apo A-I}}$ $\mu\text{M}$	$\Delta H^{\text{a)}$ kcal/mol	Maximum association number $N = 8$				
			$\Delta H_{\text{a}}^{\text{0b)}$ kcal/mol	$\sigma$	$K_{\text{a}}$ $\text{M}^{-1}$	$\Delta G_{\text{a}}^{\text{0}}$ kcal/mol	$T\Delta S_{\text{a}}^{\text{0}}$ kcal/mol
5	160	-7.7	8.14	0.003	2.8E+05	-6.90	15.04
5	160	-8.51	9.03	0.003	2.6E+05	-6.86	15.89
10	160	-6.95	7.19	0.003	4.8E+05	-7.33	14.52
10	160	-7.03	7.31	0.003	4.0E+05	-7.23	14.55
35	160	7.34	-7.59	0.003	4.9E+05	-7.99	0.40
40	80	9.22	-10.1	0.003	3.3E+05	-7.87	-2.20
40	160	11.74	-12.3	0.003	3.5E+05	-7.91	-4.37
45	160	18.5	-19.8	0.003	2.4E+05	-7.80	-11.99

<sup>a)</sup>  $\Delta H$  = heat of dissociation as measured in the calorimetric experiment. While the precision of an individual calorimetric measurement is high ( $\pm 0.2$  kcal/mol) the reproducibility is determined by different factors and is of the order of  $\pm 1.3$  kcal/mol.

<sup>b)</sup>  $\Delta H_{\text{a}}^{\text{0}}$  is the enthalpy of protein association,  $\Delta H_{\text{a}}^{\text{0}} = -\Delta H/(1-\alpha)$ , where  $\alpha$  is the fraction of monomers in the starting solution.

## References

1. Segrest, J. P., Li, L., Anantharamaiah, G. M., Harvey, S. C., Liadaki, K. N., and Zannis, V. (2000) Structure and function of apolipoprotein A-I and high-density lipoprotein, *Curr Opin Lipidol* 11, 105-115.
2. Frank, P. G., and Marcel, Y. L. (2000) Apolipoprotein A-I: structure-function relationships, *J Lipid Res* 41, 853-872.
3. Mei, X., and Atkinson, D. (2011) Crystal structure of C-terminal truncated apolipoprotein A-I reveals the assembly of high density lipoprotein (HDL) by dimerization, *J Biol Chem* 286, 38570-38582.
4. Borhani, D. W., Rogers, D. P., Engler, J. A., and Brouillette, C. G. (1997) Crystal structure of truncated human apolipoprotein A-I suggests a lipid-bound conformation, *Proc Natl Acad Sci U S A* 94, 12291-12296.
5. Gursky, O., and Atkinson, D. (1996) Thermal unfolding of human high-density apolipoprotein A-1: Implications for a lipid-free molten globular state, *Proc Natl Acad Sci USA* 93, 2991-2995.
6. Suurkuusk, M., and Hallen, D. (1999) Denaturation of apolipoprotein A-I and the monomer form of apolipoprotein A-I<sub>Milano</sub>, *Eur J Biochem* 265, 346-352.
7. Saito, H., Dhanasekaran, P., Nguyen, D., Holvoet, P., Lund-Katz, S., and Phillips, M. C. (2003) Domain structure and lipid interaction in human apolipoproteins A-I and E, a general model, *J Biol Chem* 278, 23227-23232.
8. Silva, R. A., Hilliard, G. M., Fang, J., Macha, S., and Davidson, W. S. (2005) A three-dimensional molecular model of lipid-free apolipoprotein A-I determined



- by cross-linking/mass spectrometry and sequence threading, *Biochemistry* 44, 2759-2769.
9. Arnulphi, C., Jin, L., Tricerri, M. A., and Jonas, A. (2004) Enthalpy-driven apolipoprotein A-I and lipid bilayer interaction indicating protein penetration upon lipid binding, *Biochemistry* 43, 12258-12264.
  10. Silva, R. A., Huang, R., Morris, J., Fang, J., Gracheva, E. O., Ren, G., Kontush, A., Jerome, W. G., Rye, K. A., and Davidson, W. S. (2008) Structure of apolipoprotein A-I in spherical high density lipoproteins of different sizes, *Proc Natl Acad Sci U S A* 105, 12176-12181.
  11. Swaney, J. B. (1983) Reconstitution of apolipoprotein A-I from human high density lipoprotein with bovine brain sphingomyelin, *J Biol Chem* 258, 1254-1259.
  12. Jayaraman, S., Abe-Dohmae, S., Yokoyama, S., and Cavigliolo, G. (2011) Impact of self-association on function of apolipoprotein A-I, *J Biol Chem* 286, 35610-35623.
  13. Sreerama, N., and Woody, R. W. (2004) On the analysis of membrane protein circular dichroism spectra, *Protein Sci* 13, 100-112.
  14. Reed, J., and Reed, T. A. (1997) A set of constructed type spectra for the practical estimation of peptide secondary structure from circular dichroism, *Anal Biochem* 254, 36-40.
  15. Zimm, B. H., and Bragg, J. K. (1959) Theory of the phase transition between helix and random coil in polypeptide chains, *J Chem Phys* 31, 526-535.
  16. Chou, P. Y., and Scheraga, H. A. (1971) Calorimetric measurement of enthalpy change in the isothermal helix-coil transition of poly-L-lysine in aqueous solution, *Biopolymers* 10, 657-680.

## 2. Thermodynamics of protein self-association and unfolding

---

17. Rialdi, G., and Hermans, J., Jr. (1966) Calorimetric heat of the helix-coil transition of poly-L-glutamic acid, *J Am Chem Soc* 88, 5719-5720.
18. Scholtz, J. M., Marqusee, S., Baldwin, R. L., York, E. J., Stewart, J. M., Santoro, M., and Bolen, D. W. (1991) Calorimetric determination of the enthalpy change for the alpha-helix to coil transition of an alanine peptide in water, *Proc Natl Acad Sci U S A* 88, 2854-2858.
19. Davidson, N. (1962) *Statistical Mechanics*, pp 385, McGraw-Hill, New York, N.Y.
20. Beck, A., Li-Blatter, X., Seelig, A., and Seelig, J. (2010) On the interaction of ionic detergents with lipid membranes. Thermodynamic comparison of n-alkyl- $^+N(CH_3)_3$  and n-alkyl- $SO_4^-$ , *J Phys Chem B* 114, 15862-15871.
21. Wyman, J., and Gill, S. J. (1990) *Binding and Linkage. Functional chemistry of biological macromolecules*, University Science Books, Mill Valley, CA.
22. Vitello, L. B., and Scanu, A. M. (1976) Studies on human serum high density lipoproteins. Self-association of apolipoprotein A-I in aqueous solutions, *J Biol Chem* 251, 1131-1136.
23. Swaney, J. B., and O'Brien, K. (1978) Cross-linking studies of the self-association properties of apo-A-I and apo-A-II from human high density lipoprotein, *J Biol Chem* 253, 7069-7077.
24. Heerklotz, H., and Seelig, J. (2000) Titration calorimetry of surfactant-membrane partitioning and membrane solubilization, *Biochim Biophys Acta* 1508, 69-85.
25. Privalov, P. L., and Gill, S. J. (1989) The hydrophobic effect - a reappraisal, *Pure Appl Chem* 61, 1097-1104.

26. Formisano, S., Brewer, H. B., Jr., and Osborne, J. C., Jr. (1978) Effect of pressure and ionic strength on the self-association of Apo-A-I from the human high density lipoprotein complex, *J Biol Chem* 253, 354-359.
27. Brouillette, C. G., Dong, W. J., Yang, Z. W., Ray, M. J., Protasevich, II, Cheung, H. C., and Engler, J. A. (2005) Forster resonance energy transfer measurements are consistent with a helical bundle model for lipid-free apolipoprotein A-I, *Biochemistry* 44, 16413-16425.
28. Privalov, P. L., and Dragan, A. I. (2007) Microcalorimetry of biological macromolecules, *Biophys Chem* 126, 16-24.
29. Carra, J. H., Murphy, E. C., and Privalov, P. L. (1996) Thermodynamic effects of mutations on the denaturation of T4 lysozyme, *Biophys J* 71, 1994-2001.
30. Kasimova, M. R., Milstein, S. J., and Freire, E. (1998) The conformational equilibrium of human growth hormone, *J Mol Biol* 277, 409-418.
31. Chetty, P. S., Mayne, L., Lund-Katz, S., Stranz, D., Englander, S. W., and Phillips, M. C. (2009) Helical structure and stability in human apolipoprotein A-I by hydrogen exchange and mass spectrometry, *Proc Natl Acad Sci U S A* 106, 19005-19010.
32. Murphy, K. P., and Gill, S. J. (1991) Solid model compounds and the thermodynamics of protein unfolding, *J Mol Biol* 222, 699-709.
33. Saito, H., Dhanasekaran, P., Nguyen, D., Deridder, E., Holvoet, P., Lund-Katz, S., and Phillips, M. C. (2004)  $\alpha$ -Helix formation is required for high affinity binding of human apolipoprotein A-I to lipids, *J Biol Chem* 279, 20974-20981.
34. Meier, M., and Seelig, J. (2007) Thermodynamics of the coil  $\rightleftharpoons$  beta-sheet transition in a membrane environment, *J Mol Biol* 369, 277-289.

## 2. Thermodynamics of protein self-association and unfolding

---

35. Meier, M., and Seelig, J. (2008) Length dependence of the coil <--> beta-sheet transition in a membrane environment, *J Am Chem Soc* 130, 1017-1024.
36. Nolte, R. T., and Atkinson, D. (1992) Conformational analysis of apolipoprotein A-I and E-3 based on primary sequence and circular dichroism, *Biophys J* 63, 1221-1239.
37. Thompson, K. S., Vinson, C. R., and Freire, E. (1993) Thermodynamic characterization of the structural stability of the coiled-coil region of the bZIP transcription factor GCN4, *Biochemistry* 32, 5491-5496.
38. Honnappa, S., Cutting, B., Jahnke, W., Seelig, J., and Steinmetz, M. O. (2003) Thermodynamics of the Op18/stathmin-tubulin interaction, *J Biol Chem* 278, 38926-38934.
39. Gursky, O., and Atkinson, D. (1998) Thermodynamic analysis of human plasma apolipoprotein C-1: high-temperature unfolding and low-temperature oligomer dissociation, *Biochemistry* 37, 1283-1291.
40. Acharya, P., Segall, M. L., Zaiou, M., Morrow, J., Weisgraber, K. H., Phillips, M. C., Lund-Katz, S., and Snow, J. (2002) Comparison of the stabilities and unfolding pathways of human apolipoprotein E isoforms by differential scanning calorimetry and circular dichroism, *Biochim Biophys Acta* 1584, 9-19.
41. Scholtz, J. M., Qian, H., York, E. J., Stewart, J. M., and Baldwin, R. L. (1991) Parameters of helix-coil transition theory for alanine-based peptides of varying chain lengths in water, *Biopolymers* 31, 1463-1470.

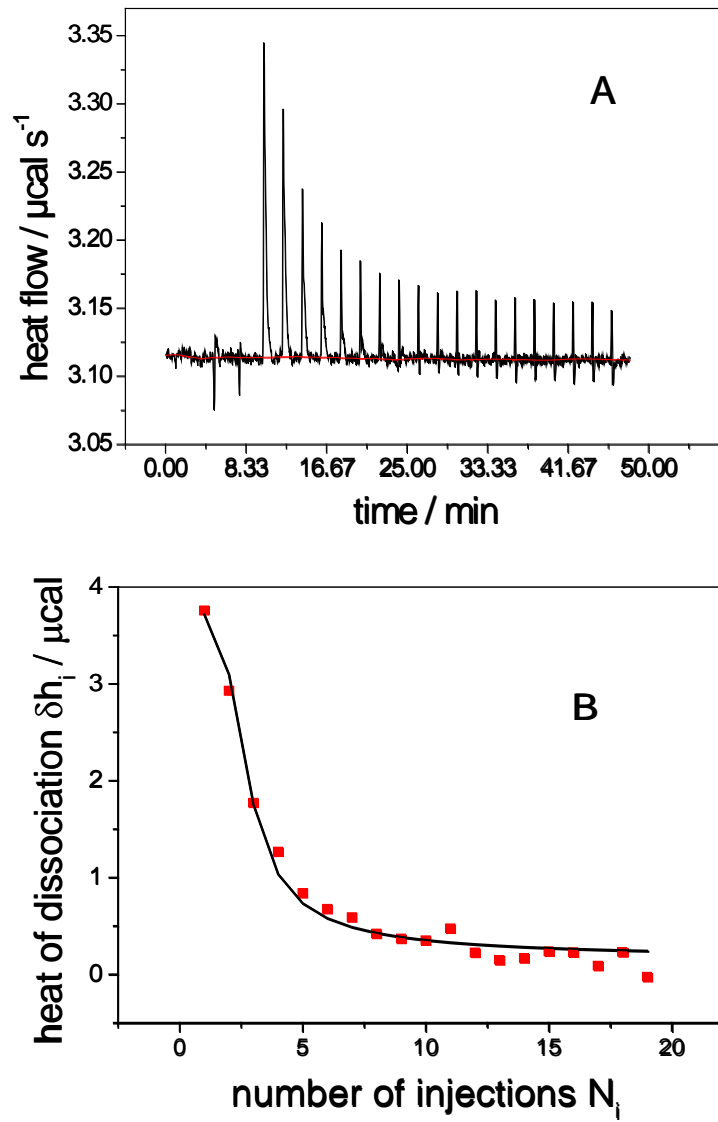
**Figures**

Figure 1

## 2. Thermodynamics of protein self-association and unfolding

---

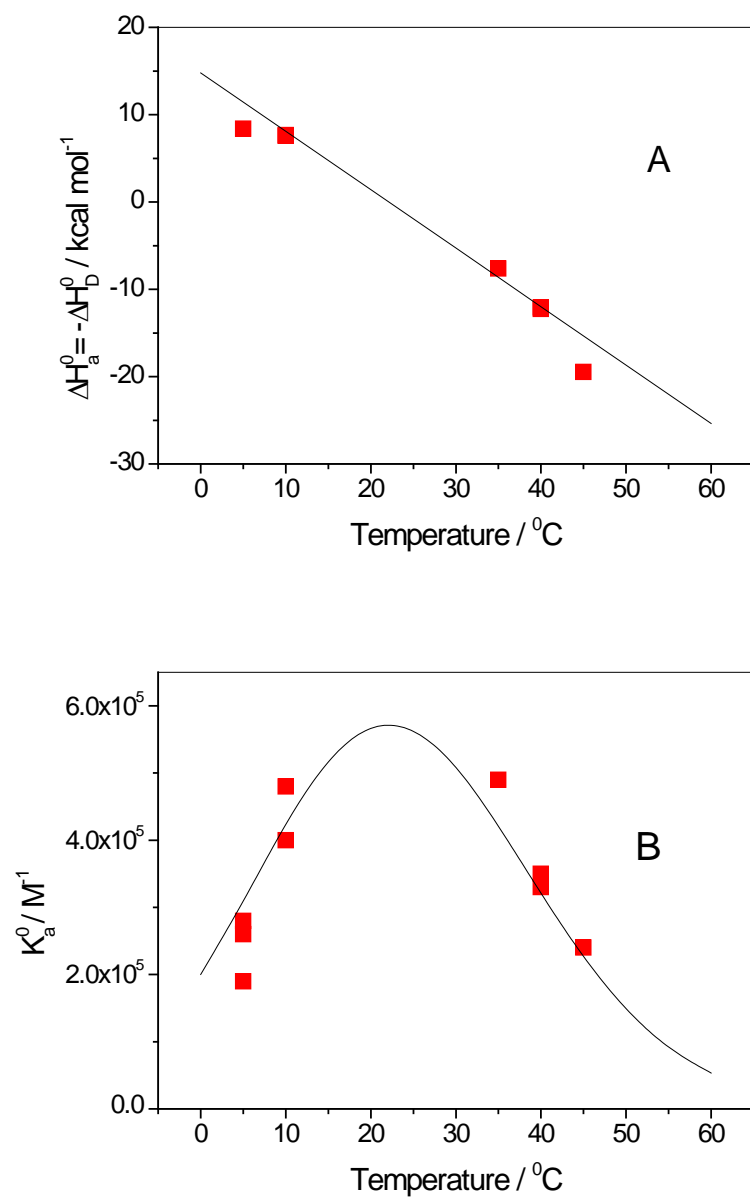


Figure 2

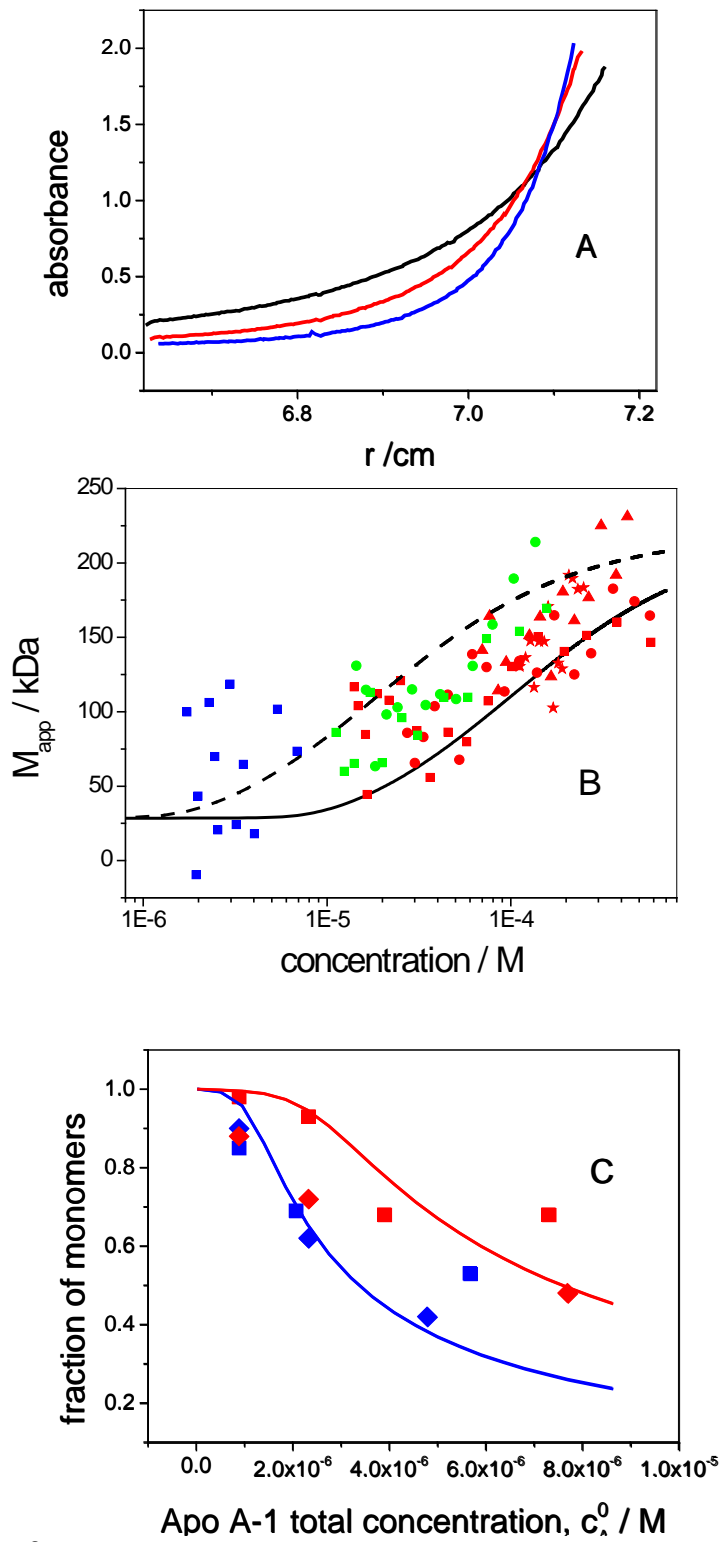


Figure 3

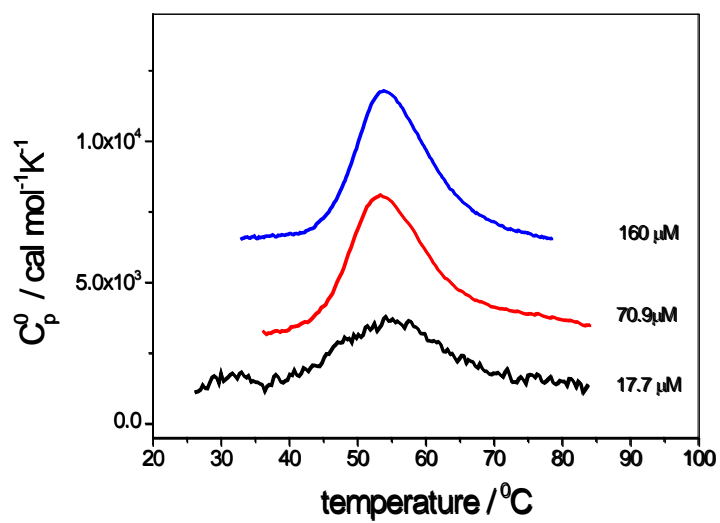


Figure 4

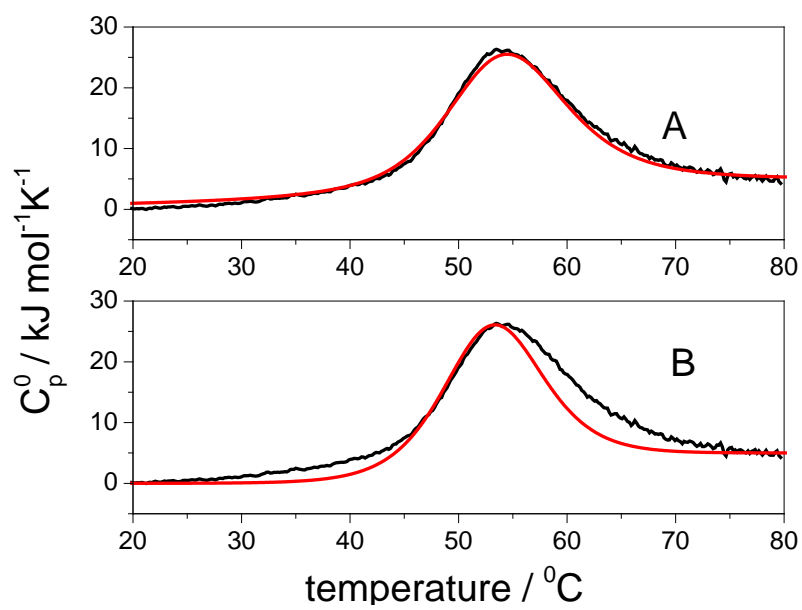


Figure 5



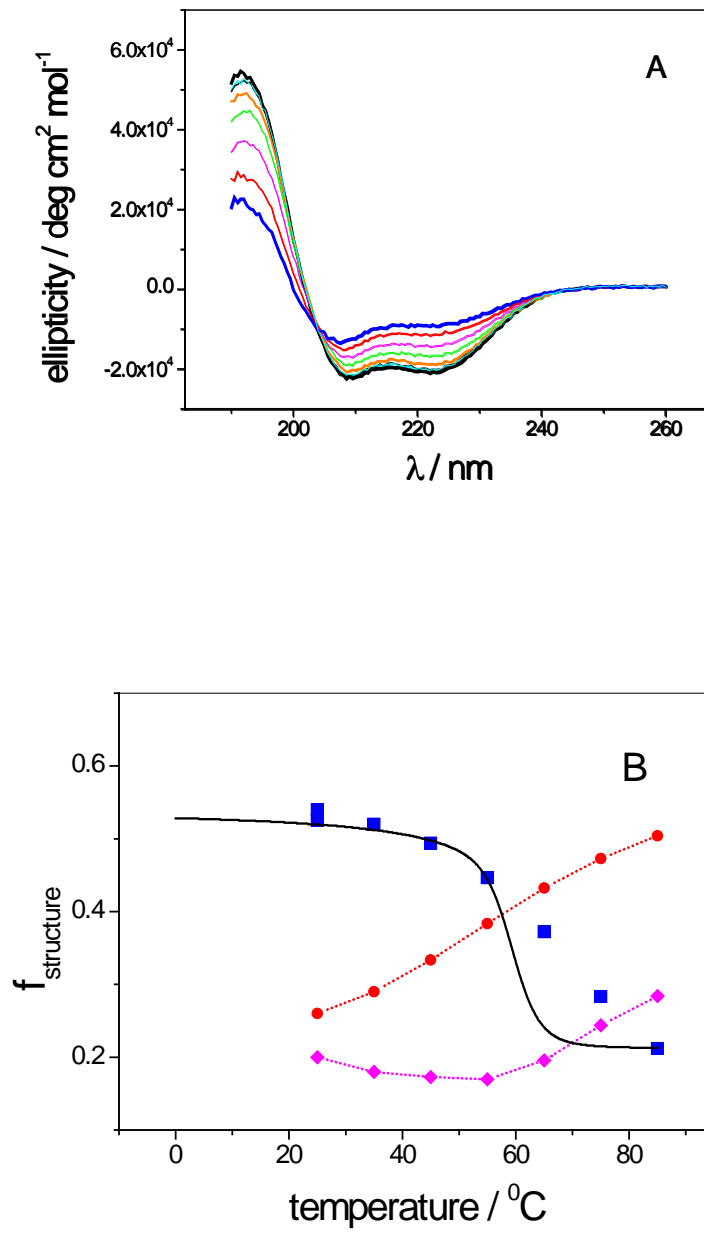


Figure 6

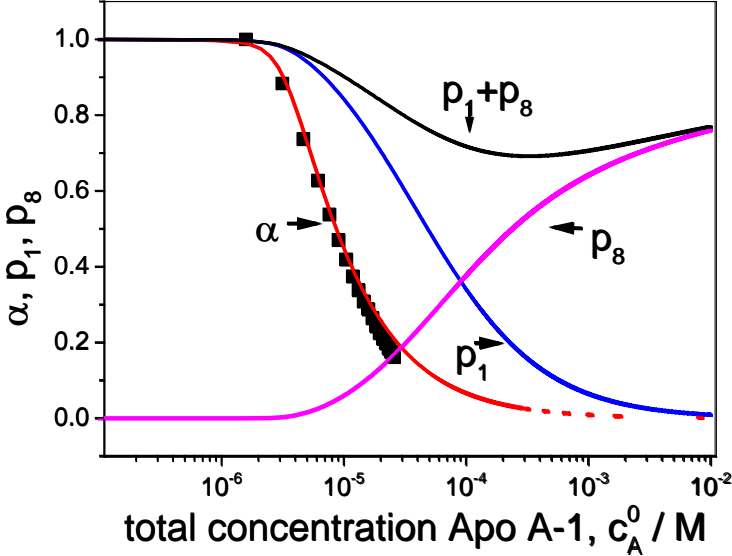


Figure 7

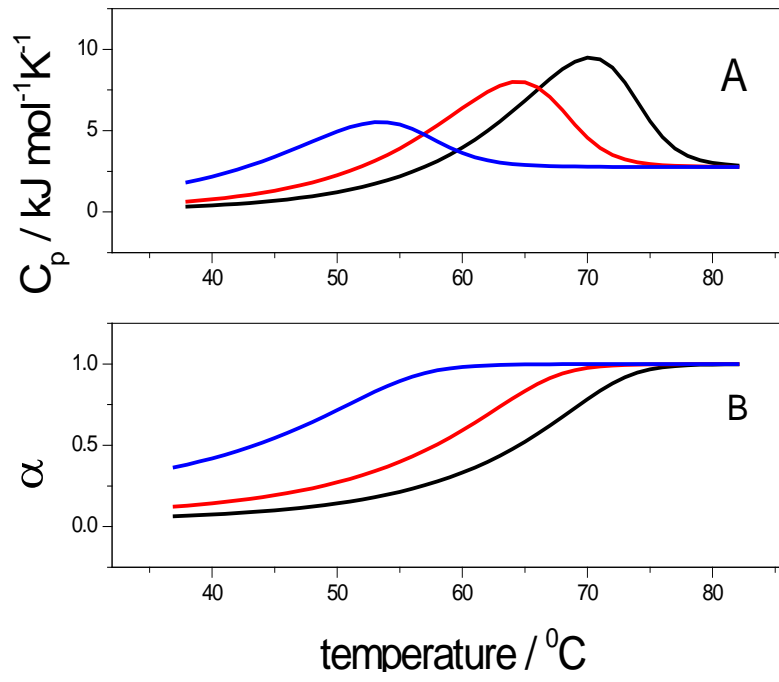


Figure 8

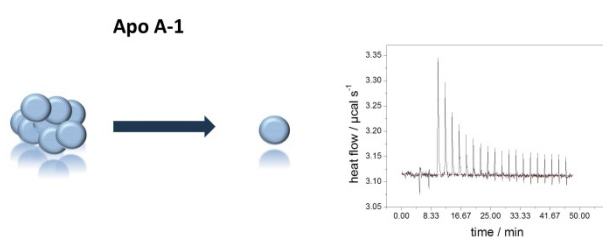
## 2. Thermodynamics of protein self-association and unfolding

---

For Table of Contents Use Only

### Thermodynamics of protein self-association and unfolding. The case of Apolipoprotein A-I.

Fabian Zehender, André Ziegler, Hans-Joachim Schönfeld, and Joachim Seelig



## Appendix: Dynamic light scattering and analytical ultracentrifugation with Apo A-1

### Dynamic light scattering (DLS)

To determine the size of Apo A-1 self-associates, dynamic light scattering (DLS) was performed in a Zetasizer Nano ZS (Malvern Instruments Ltd., Worcestershire, UK) device. Light scattering was recorded and analyzed in terms of an autocorrelation function (Chapter 2: Materials and Methods), which was translated into a size distribution by software provided from Malvern instruments. The size distribution by intensity was converted into a size distribution by volume via software.

Table 1: Comparison of DLS measurements with Apo A-1 at a concentration of 7 and 160  $\mu\text{M}$  in PBS buffer.

Sample	160 $\mu\text{M}$	7 $\mu\text{M}$
<b>Attenuator</b>	9	<b>11</b>
<b>Measurement Position / mm</b>	4.65	4.65
<b>Temperature / °C</b>	19.9	20
<b>Average PDI</b>	0.190	0.207

Apo A-1 solutions in PBS (+ 0.02 %  $\text{NaN}_3$ ) at a concentration of 7 and 160  $\mu\text{M}$  were measured in the DLS device.

## 2. Thermodynamics of protein self-association and unfolding

---

The size distribution by volume is shown in Figure 1. Measurements at concentrations of 7  $\mu\text{M}$  were at the border of sensitivity of the device. The diameter of Apo A-1 oligomers was calculated to be the same for both (11 nm) concentrations contradicting the results obtained by AUC and ITC where concentration dependent oligomerization was found (Chapter 3: Published article). There, Apo A-1 was found to be mainly monomeric at 7  $\mu\text{M}$  and oligomeric (8 Apos) at a concentration of 160  $\mu\text{M}$ .

The attenuator of the DLS device has already reached its highest value of 11 for measurement at 7  $\mu\text{M}$  Apo A-1 (Figure 1 and Table 1). Thus the question whether a solution of 7  $\mu\text{M}$  Apo A-1 has already reached the threshold of sensitivity is debatable. On the other hand, the increased viscosity at 160  $\mu\text{M}$  could lead to non-ideal effects that could have falsified the results.

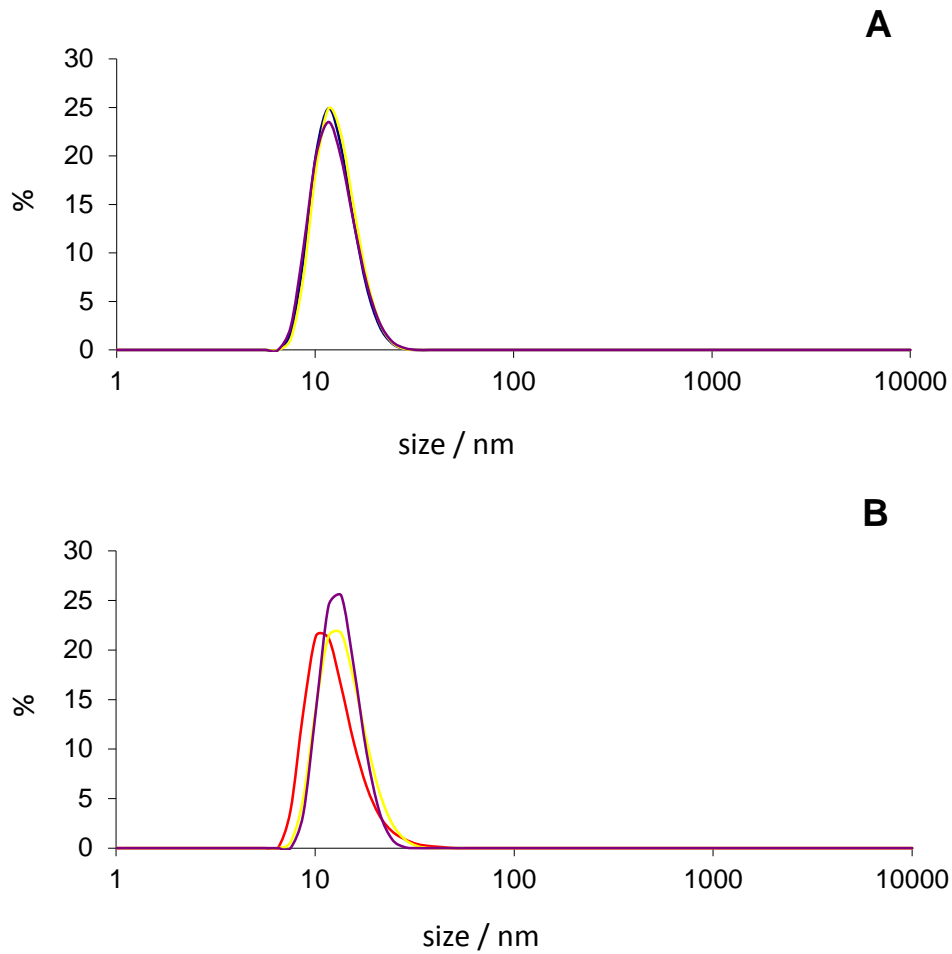


Figure 1: Size distribution by volume of three identical DLS measurements with 7  $\mu\text{M}$  (A) and 160  $\mu\text{M}$  (B) Apo A-1 in PBS buffer.

### **Diameter calculation of an eight monomer self-associate**

On basis of the DLS data the diameter of a possible octamer was calculated:

The molecular weight of a complex of six monomers is

$$8 \cdot 28'200 \text{ g/mol} = 225'600 \text{ g/mol.}$$

## 2. Thermodynamics of protein self-association and unfolding

---

Mass 8 molecules:  $m = 3.7456 \cdot 10^{-19} \text{ g}$

Volume 8 molecules:  $V = 3.7456 \cdot 10^{-19} \text{ g} / 0.73 \text{ g/cm}^3 = 5.1310 \cdot 10^{-19} \text{ cm}^3$

Radii:  $V = 4/3 \pi r^3 = 5.1310 \cdot 10^{-19} \text{ cm}^3$

$r = 4.9663 \cdot 10^{-7} \text{ cm} = 4.69 \text{ nm}$

Diameter:  $d = 9.93 \text{ nm}$

The result of almost 10 nm is in a similar range as the resulting size of 11.5 nm (160  $\mu\text{M}$ ) measured by DLS

Analogous the number of monomers in one oligomer was calculated via the measured particle size. The calculation yielded 12 Apos per oligomer, which is in a similar range to the assumption of eight Apos derived by AUC and ITC measurements for highly concentrated samples, such as 160  $\mu\text{M}$ .

### **Analytical ultracentrifugation**

Additional measurements in a XL-I centrifuge (Beckman Coulter, Indianapolis, IN; Rotor: Axi50) were performed with Apo A-1 and alternative models were used to analyze the data.



Apo A-1-solutions (10.8 mg/ml) were dialysed (Visiking, MWT 14000 cutoff, 3 days, 4 x 1:1000) against PBS buffer (+ 0.02 % NaN<sub>3</sub>). Subsequently the concentration was determined by UV-VIS spectroscopy. The buffer of the last dialysis bath was used to fill the reference compartments of the analytical ultracentrifuge cells.

### **Experimental determination of $v_{\text{bar}}$**

The specific partial volume,  $v_{\text{bar}}$  which was used for analyzing AUC data in the published article (Chapter 3) was calculated to be 0.736 ml/g as a sum of the specific partial volume of each amino acid of Apo A-1. However, a calculated value can differ from the real  $v_{\text{bar}}$  of a protein due to possible cavities and hydration effects of the macromolecule. When analyzing a sedimentation equilibrium run the resulting molecular mass is very sensitive to changes in the specific partial volume. Hence  $v_{\text{bar}}$  was attempted to be found experimentally.

Apo A-1 was dissolved in PBS buffer (+ 0.02 % NaN<sub>3</sub>) with different D<sub>2</sub>O concentrations in order to prepare buffers of different densities. The concentration of Apo A-1 (3.5  $\mu\text{M}$ ) was chosen to exhibit a sufficient absorption ( $A_0 \approx 0.15$ ) in a centerpiece with 12 mm path length but at low enough protein concentration so that the solution contains only monomers. The sedimentation equilibrium was measured at 8, 12, 15, 20, 25 und 30 krpm. The last five scans of measurements at 12, 15, 20 and 25 krpm were averaged and analyzed as described in as follows.

The concentration at a certain point in the cells  $a(r)$  is described by

$$a(r) = a_0 \cdot \exp\left[\frac{M_b \omega^2}{2RT} (r^2 - r_0^2)\right],$$

## 2. Thermodynamics of protein self-association and unfolding

---

$a_0$  is the initial absorbance at the beginning of the experiment.  $M_b$  is the buoyant weight,  $\omega$  is the angular velocity,  $R$  the ideal gas constant and  $T$  the temperature.  $r_0$  is the radius value of the sample-air interface (meniscus) and  $r$  is the radius, that is defined between the meniscus and the bottom of the cell.

Transformation yields

$$\frac{\ln(a(r))}{\ln(a_0)} = \frac{M_b \omega^2}{2RT} (r^2 - r_0^2).$$

The left side of the equation of each cell at each of the mentioned rotational velocities was fitted linearly against the radius  $r^2 - r_0^2$ .

The slope of the fit is

$$slope = \frac{M_b \omega^2}{2RT}.$$

Referred to

$$M_b = M_w (1 - v_{bar} \rho) = M_w - M_w v_{bar} \rho$$

the buoyant weight  $M_b$  was fitted linearly against the density  $\rho$  of the corresponding  $D_2O/H_2O$ -PBS buffer.  $v_{bar}$  is the specific partial volume. The slope of the fit is

$$slope = M_w v_{bar}$$

## 2. Thermodynamics of protein self-association and unfolding

and the axes intercept equates to the molecular mass  $M_w$ . The slope was divided by 28.2 kDa in order to yield the specific partial volume  $v_{\text{bar}}$ .

Table 2: Results of analytical ultracentrifugation measurements with Apo A-1 in PBS and H<sub>2</sub>O/D<sub>2</sub>O solutions aiming to determine the specific partial volume  $v_{\text{bar}}$  of the protein.

velocity	<i>krpm</i>	<b>12</b>	<b>15</b>	<b>20</b>	<b>25</b>
intercept / $M_w$	<i>kDa</i>	49.0	38.7	33.32	24.4
$v_{\text{bar}}$	<i>ml/g</i>	<b>1.3</b>	<b>1.0</b>	<b>0.9</b>	<b>0.6</b>
standard deviation	<i>ml/g</i>	0.7	0.4	0.1	0.1
$R^2$		0.40	0.58	0.93	0.90

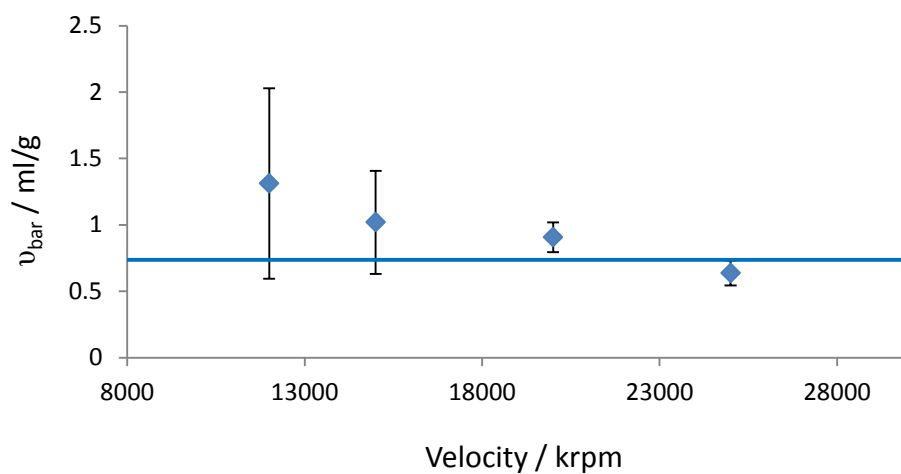


Figure 2: Calculated  $v_{\text{bar}}$  of Apo A-1 is shown as a function of the velocities of the equilibria used for the calculation. The error of the results increased at lower velocities.  $v_{\text{bar}}$  as a sum of the  $v_{\text{bar}}$ s of each amino acid is depicted as a blue horizontal line.

## 2. Thermodynamics of protein self-association and unfolding

---

Table 2 and Figure 2 show the results of the calculations.  $v_{\text{bar}}$  varies with the velocity at which equilibrium was attained. At lower velocities higher values of  $v_{\text{bar}}$  as well as higher errors were observed. The increase of errors at lower velocities is probably due to the small slope of the concentration gradients in the AUC cells. Presumably this causes larger scattering of  $M_{\text{bs}}$  and thus larger errors. Furthermore a small deviation from equilibrium could play a role. However, this is unlikely as it was tested if equilibrium was attained by SedFit software.

Apo A-1 was described to self-associate at concentrations above 0.1 mg/ml ( $\approx 3.5 \mu\text{M}$ ). Self-association could alter the hydration of the protein yielding smaller values of  $v_{\text{bar}}$ . Considerable higher concentrations than  $3.5 \mu\text{M}$  of Apo A-1 were reached mainly in the region of the bottom of the cell, especially at higher velocities. This might lead to smaller values of  $v_{\text{bar}}$  for measurements at high velocities compared to those at low velocities. On the other hand, with increasing velocities the molecular mass  $M_w$ , determined by intercept, decreased (Table 2).

### **Sedimentation Velocity (SV)**

Performing the SV mode the sample is spun down to the bottom at relatively high (42 krpm) and constant radial velocity. The sedimentation is detected by means of optical systems and followed by acquiring scans every five minutes.

## 2. Thermodynamics of protein self-association and unfolding

Table 3: Sedimentation coefficients of Apo A-1 in PBS buffer at different concentrations. Sedimentation coefficient distributions were obtained by SedFit software analysis. The main peaks are written in **bold red**, others are in **blue**, whereas very small peaks are written *italic* and black.

detection	concentration c	sedimentation - coefficient S		
	mg/ml		$10^{-13}s$	
interference	0.09	<b>1.9</b>	4.6	
absorbance	0.09	<b>2</b>		
interference	0.28	<b>2.1</b>	4.6	
absorbance	0.28	<b>2.2</b>	<b>4.6</b>	
interference	0.57	1.8	<b>4.6</b>	
absorbance	0.57		<b>4.8</b>	
interference	1.13		<b>4.8</b>	
interference	2.25		<b>4.6</b>	6.5
interference	9.72		<b>4.3</b>	

Table 3 shows sedimentation constants at different protein concentrations derived by SedFit software analysis. If several peaks were observed, they are categorized into small, normal, and main peaks. The main peaks are plotted as a function of protein concentration in Figure 3. At concentrations above 0.28 mg/ml oligomers with a sedimentation coefficient of  $4.6 \cdot 10^{-13}$  s are mainly populated. However, the results suggest the existence of only two species with sedimentation coefficients S of  $S \approx 2 \cdot 10^{-13}$  s and  $S \approx 4.6 \cdot 10^{-13}$  s except one outlier at 2.25 mg/ml with a small peak at  $S = 6.5 \cdot 10^{-13}$  s. The presence of only two oligomeric states of Apo A-1 is contradicting the results obtained by ITC and AUC SE measurements, where oligomers of different

## 2. Thermodynamics of protein self-association and unfolding

---

sizes were suggested. Calculation of the molecular weight from the sedimentation coefficients is difficult due to the lack of the frictional ratio of oligomers and the monomer. An approximate calculation of the molecular weight is shown as follows.

The sedimentation coefficient  $S$  is defined as

$$S = \frac{M(1 - \nu\rho)}{N_A 6\pi r \eta}$$

$M$  is the molecular weight,  $\nu$  is the specific partial volume,  $\rho$  is the density of the solvent,  $N_A$  the Avogadro number,  $r$  is the radius and  $\eta$  is the viscosity of the solvent.

Assuming the following parameters

$$\begin{aligned} S &= 4.6 \cdot 10^{-13} \text{ s} & \eta &= 0.01 \text{ Ns/m}^2 & \rho &= 10^{-3} \text{ kg/m}^3 \\ d &= 9.93 \text{ nm} & \nu_{\text{bar}} &= 0.73 \text{ ml/g}, \end{aligned}$$

in the above mentioned equation and solving for the molecular mass  $M$  yields

$$M = 90.72 \text{ kDa.}$$

Divided by the mass of one Apo A-1 molecule results in  $n = 3$  Apos per oligomer. The same calculation for the sedimentation coefficient of  $S = 2.0 \cdot 10^{-13} \text{ s}$  and a radius of an Apo A-1 monomer of  $r = 2.48 \text{ nm}$  (calculated analog to the radius of an octamer, see below) yielded a molecular mass of 20.86 kDa. This is less than the molecular mass of one Apo A-1 molecule (28.2 kDa), suggesting, that the approximation underestimates the molecular weight of the species. Consequently, the number of Apos per oligomer  $n$

= 3 is less than suggested by Sedimentation equilibrium results in combination with ITC results ( $n = 8$ , as discussed in Chapter 3: Published article). However, the approximation indicated that Apo A-1 is oligomeric at least at concentrations beginning at 0.5 mg/ml.

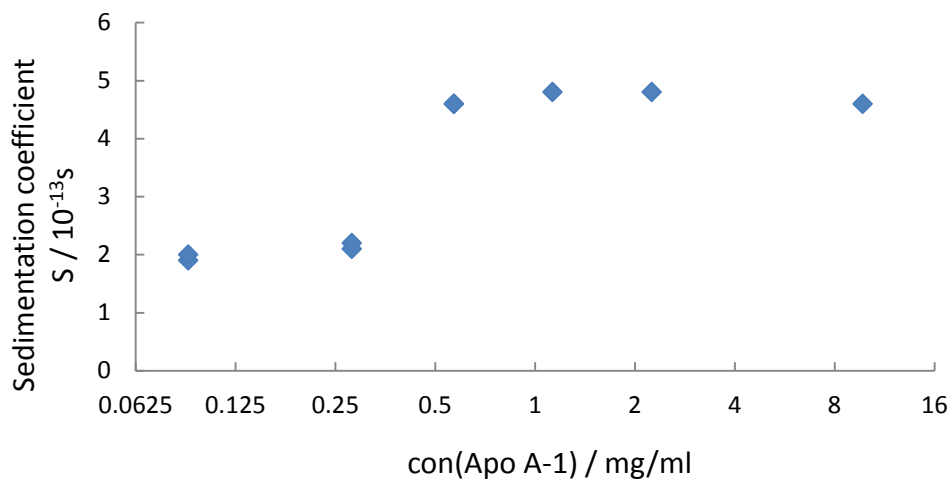


Figure 3: Apo A-1's main sedimentation coefficients of a sedimentation velocity measurement is shown as a function of its concentration. The results suggest two different oligomeric states, the larger at higher concentrations.

### **Sedimentation Equilibrium (SE)**

SE measurements were analyzed by calculating the apparent molecular mass of short intervals in the concentration gradient in the published article (Chapter 3). An alternative approach of analyzing this data was done by means of SedPhat software with different fitting models.

## 2. Thermodynamics of protein self-association and unfolding

---

Figure 4 shows the concentration profile in a cell after sedimentation of the protein at 42 krpm. The upper part shows the enlarged baseline. It is almost zero in the upper part of the cell, hence a baseline absorbance of zero was used for further analysis.

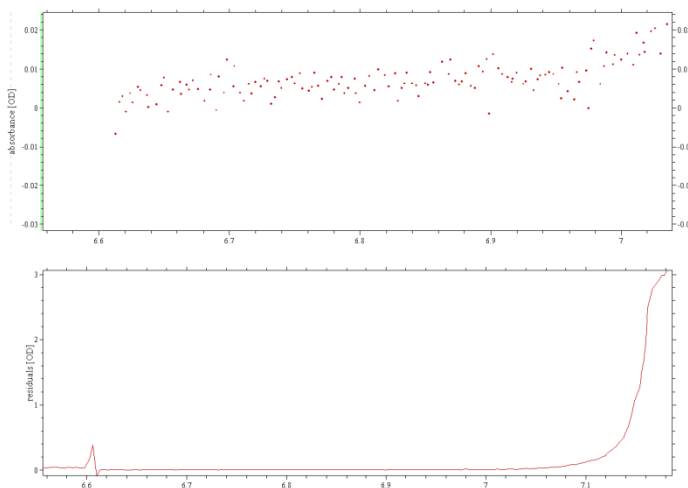


Figure 4: Concentration profile of a 160  $\mu\text{M}$  Apo A-1 sample in PBS buffer after 40 h at 42 krpm in order to determine the baseline absorbance. The profile is enlarged in the upper part of the figure.

In Figure 5 an equilibrium concentration gradient of a 160  $\mu\text{M}$  sample is shown at 8 krpm. A single species model was fitted to the data in SedPhat software. The fitted absorbance data and thus the concentration were smaller than the measured ones at lower radii and vice versa. Therefore the model seems not applicable, since it does not account for different oligomeric equilibria in the concentration gradient. The root mean square deviation (rmsd) of 0.045 is significantly higher than deviations caused by the noise of the detection system (0.005). An apparent molecular mass of 114 kDa is the result of this model, corresponding to a tetramer.



## 2. Thermodynamics of protein self-association and unfolding

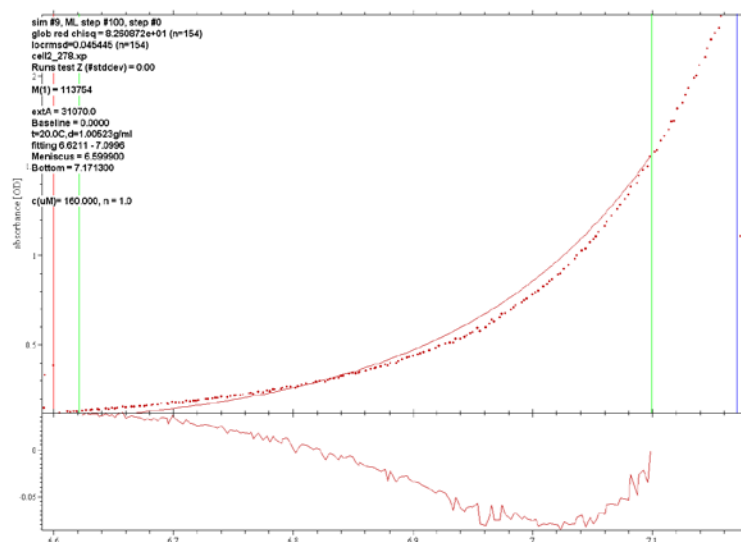


Figure 5: SedPhat-analysis of an 8 krpm sedimentation equilibrium run with 160  $\mu\text{M}$  Apo A-1 in PBS buffer by means of a single species model. The concentration profile is shown in the upper part. The red vertical line is the meniscus of the solution, whereas the blue vertical line stands for the bottom of the cell. The model was fitted to the data in between the green vertical lines. The part below shows the deviation of the fit and the data in absorbance units.

As an alternative a monomer-n-mer-model was chosen. Two species without intermediates were assumed in this model, a monomer and the highest associate  $n$ .  $n$  was set to be five in Figure 6. A global fit of a 160  $\mu\text{M}$  Apo A-1 solution in equilibrium at 6 and 8 krpm is shown. A set of different  $n$  values was chosen, while the rmsd was used as criteria of the fit quality. The rmsd of the fits are shown in Figure 7 as a function of the number of the highest associate  $n$ . The best fit is attained with  $n = 5$  corresponding to a pentamer, but rmsd values of fits with  $n$  between 4 – 7 were on a similar level.

## 2. Thermodynamics of protein self-association and unfolding

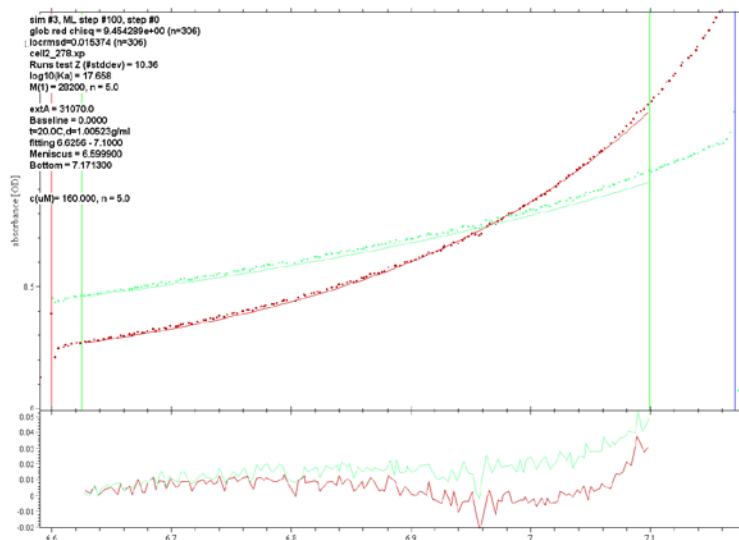


Figure 6: SedPhat analysis of 160  $\mu\text{M}$  Apo A-1 (in PBS buffer) in equilibrium at 6 and 8 krpm. A monomer-n-mer model with  $n = 5$  was used to fit to the data. The concentration profiles are shown in the upper part. The red vertical line is the meniscus of the solution, whereas the blue vertical line stands for the bottom of the cell. The model was fitted to the data in between the green vertical lines. The part below shows the deviations of the fits and the data in absorbance units.

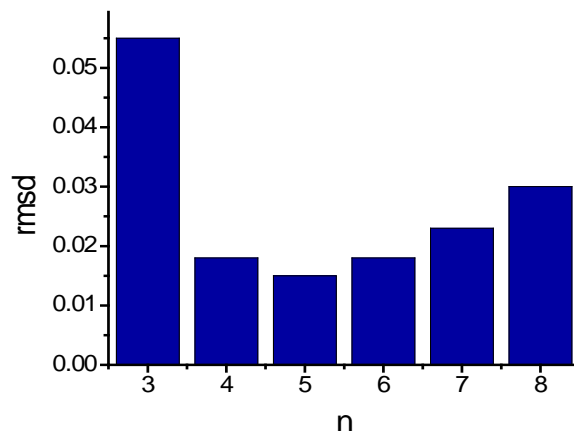


Figure 7: An AUC SE run with 160  $\mu\text{M}$  Apo A-1 in PBS buffer was analyzed with a “monomer-n-mer” model in SedPhat software. A bar chart of the rmsd value of each fit with different  $n$  values is depicted. Fits between  $n = 4 - 7$  show a similar low rmsd values indicating good quality of the fit.

### 3. Lipid binding of Apo A-1 mimetic peptides

#### Introduction

Atherosclerosis is a clinical syndrome affecting a large number of people worldwide. Low serum high-density lipoprotein (HDL) levels were identified as an independent risk factor of cardiovascular disease. HDL is one of the key players in reverse cholesterol transport (RCT). RCT is a multi-step process resulting in the net movement of cholesterol from peripheral tissues back to the liver via the plasma [1]. The liver can eliminate excess cholesterol by secreting cholesterol or bile acids into the bile.

Apo A-1 is a 28 kDa protein consisting of 10 repeating sequence homologies. It is the main protein constituent of HDL (70 % of protein in HDL) present in plasma at a concentration of  $\approx 35 \mu\text{M}$  in mice and humans.

Large parts of Apo A-1 are in an amphipathic  $\alpha$ -helical secondary structure. Amphipathic helices, a common feature of apolipoproteins, are grouped into seven distinct classes: A, H, L, G, L, C and M [2]. They differ in charge, charge distribution and charge density. Class A amphipathic helices are described by zwitterionic, negatively charged residues at the center of the polar face and positively charged residues clustering in the polar-nonpolar interface (Figure 1). The  $\alpha$ -helices in Apo A-1 feature mainly a class A amphipathic motif. This structural motif imparts hydrophilic and hydrophobic regions and is found in many biologically active peptides and proteins. The polar and nonpolar face is oriented along the long axis of the  $\alpha$ -helix. This distribution of physico-chemical properties forms a structural complement to that of

### 3. Lipid binding of Apo A-1 mimetic peptides

phospholipids and facilitates the interaction of the two types of molecules [2]. The interaction of Apo A-1 related peptides with lipids in the aqueous environment was first described by Segrest et al. [3].

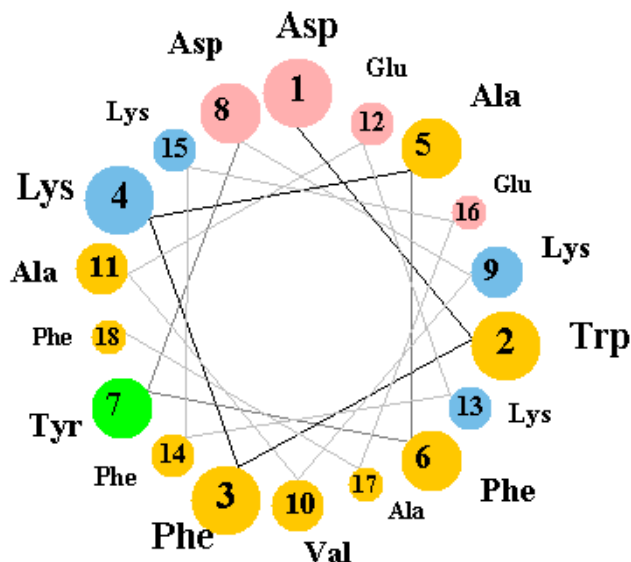


Figure 1: Helical wheel presentation of the peptide 4F on <http://cti.itc.virginia.edu/~cmg/Demo/wheel/wheelApp.html>. Nonpolar residues are depicted in yellow, polar but uncharged are in green, acidic are in rose and basic residues are in blue. The closer the residues are to the beholder the bigger are the circles. The amphipathic character of the peptide is visible by the separation of the hydrophilic and charged residues on the upper side and the hydrophobic on the lower part of the scheme. The criteria of class A amphiphilic helices are fulfilled with negatively charged residues clustered at the center of the polar face of the helix and positively charged residues at the polar/nonpolar interface.

The amphipathic helix motif class A in Apo A-1 is responsible for lipid binding. Hence, a 18 amino acid long model peptide of the amphipathic class A motif was designed and designated 18A. The sequence DWLKAFYDKVAEKLKEAF of this peptide had no sequence homology to Apo A-1 and is not present in any of the naturally occurring proteins. Together with DMPG lipids, discoidal complexes were formed that showed

structural similarities to those of Apo A-1. The complexes mediated cellular cholesterol efflux in cell culture similar to complexes with Apo A-1 [4]. The lipoprotein particles were, analog to HDL, able to activate the lecithin-cholesterol acyltransferase (LCAT), an important protein of the RCT. These and many other properties caused the classification of 18A as Apo A-1 mimetic peptide. Refinement of the peptide design by addition of an acetyl group to the amino terminus and an amide to the carboxyl terminus yielded increased helicity of the peptide upon addition to lipids [5]. The blocking of the termini also increased the cholesterol efflux and LCAT activation efficiency significantly. Further detailed studies of the physical and chemical characteristics of class A amphipathic peptides revealed that the hydrophobic region determines the biological activity of the peptides. Hence exchange of nonpolar residues in 18A with phenylalanine generated new peptides with increased hydrophobicity and increased affinity to lipids. The new peptides were designated 3F, 4F, 5F, ... depending on the total number of phenylalanines in the 18A sequence [6]. 4F showed highest activity in arterial wall cell cultures and prevented lesions better than other 18A analogs when tested in animal models [7]. Tandem helical peptides are obtained by an interruption of the helical sequence with a proline residue. A molecule composed of two 18As bridged by a proline (designated 37pA) was also investigated with respect to its Apo A-1 mimetic characteristics. 37pA exhibits greater lipid binding affinity and greater ability to promote cholesterol efflux from cultured cells [4, 8-10]. The best studied Apo A-1 mimetic peptide however is 4F.

Apo A-1 and its mimetic peptides were tested extensively *in vivo*. Administration of Apo A-1 and a mutant version Apo A<sub>Milano</sub>-1 resulted throughout all studies in healthful changes in terms of cardiovascular disease. The requirement of intravenous

### 3. Lipid binding of Apo A-1 mimetic peptides

---

administration and large amounts of the protein ruled out the approach for pharmacological application [11]. Therefore the hope lies in Apo A-1 mimetic peptides.

The plasma concentration of D-4F, the D enantiomer of L-4F used in our studies, was measured to be maximal 130 nM after oral administration to mice and only 4 nM after a single oral dose in humans. 4F was found to improve arterial vasoreactivity [12] and to be antiatherogenic in diabetes [13]. The peptide also improved insulin resistance and reduced adiposity in male obese mice [14, 15].

Clinical trials with 4F have not yet led to clear results. The peptide was always well tolerated but the therapeutic results were ambiguous. Improvements of clinical markers like LDL-induced monocyte chemotactic activity were achieved after oral administration with a single dose of D-4F [16]. Though, intravenous and subcutaneous administration of L-4F yielded no biomarker change of HDL function [17].

Most of the work with Apo A-1 mimetic peptides was done in cell culture and in animal models. Doing so, cardio-protective effects of these peptides were proven empirically. However, *in vivo* consequences of different peptide designs are still not predictable. These peptides have high potential of improving cardiovascular disease but mechanistic understanding and a detailed insight into lipid binding is lacking. We therefore studied in detail the binding of 4F and partly 4F-Pro-4F (denoted P) to lipids.

## Materials and Methods

### Materials

The peptides 4F (Ac-DWFKAFYDKVAEKFKKEAF-NH<sub>2</sub>) and P (Ac-DWFKAFYDKVAEKFKKEAFPDWFKAFYDKVAEKFKKEAF-NH<sub>2</sub>) were obtained from PEPTIDE 2.0 Inc. (Chantilly, USA). Phosphate buffered saline (PBS), consisting of 10 mM sodiumphosphate (Merck, Darmstadt, Germany) and 138 mM NaCl (Merck), dissolved in Nanopure water and charged with 0.02 % NaN<sub>3</sub> (Sigma) at pH 7.4 (25 °C) was used to dissolve the peptides if not specified differently. Alternatively, a buffer (HEPES) consisting of 10 mM HEPES (Roth) without any salt was used with and without 10 % DMSO (Merck). Buffers were filtered through sterile 0.2 µM regenerated cellulose and PTFE filters (Nano).

### Methods

#### a. Dynamic light scattering (DLS)

Measurements were performed at 25 °C in a Zetasizer Nano ZS ZEN3600 (Malvern; Worcestershire, UK), equipped with a HeNe laser (633 nm) and a backscattering detector (scattering angle of 173°). Solutions (PBS + 0.02 % NaN<sub>3</sub>, pH 7.4; 10 mM HEPES, pH 7.4 ± 10 % DMSO) were filtered (PES; 0.22 µm; Millipore; Billerica, MA) and measured in rectangular cuvettes (1 cm). The intensity autocorrelation functions

### 3. Lipid binding of Apo A-1 mimetic peptides

---

were evaluated using a second-order cumulant analysis yielding the translational diffusion coefficient  $D$ . The mean hydrodynamic diameter ( $D_H$ ) was calculated from  $D$  by using the Stokes-Einstein equation. The size distributions were calculated from the diffusion coefficient distribution using the CONTIN routine, and the resulting intensity counts were volume-weighted [18].

#### **b. High sensitivity isothermal titration calorimetry (ITC)**

ITC was performed using either the ITC-200 or the VP titration calorimeter from Microcal (Northampton, MA). The cell volumes were 200  $\mu\text{L}$  and 1.4 mL, respectively, and the injection volume varied between 2  $\mu\text{L}$  and 10  $\mu\text{L}$ . Solutions were degassed under vacuum for about 10 min. Usually the calorimeter cell contained the peptide solution and the lipid vesicles were in the injection syringe. The heat flow associated with lipid binding was integrated by the software provided with the instrument and analyzed with a multisite binding model [18-20].

#### **c. Circular dichroism (CD)**

CD spectra were obtained with a CD spectrometer Chirascan (Applied Photophysics Ltd., Leatherhead, UK) in the wavelength range of 180 nm - 260 nm using a total acquisition time of 10 min per spectrum. Measurements were done at 25 °C with peptide concentrations of 176  $\mu\text{M}$  in 100 mM NaF, 10 mM sodium phosphate, pH 7.4 at 25 °C. Quartz platelets with path lengths of  $d = 0.1$  mm were used and a baseline with pure buffer was recorded and subtracted from the sample spectra. The CD-spectra were



simulated with the non-commercial software CDpro [21] based on reference spectra of 43 proteins (data set # 1).

#### **d. Analytical ultracentrifugation (AUC)**

A Beckman XL-I ultracentrifuge (Beckman Coulter, Indianapolis, IN USA) with UV- and Interference detection was used. Peptide solutions were measured in PBS and HEPES buffer at concentrations between 100 and 200  $\mu\text{M}$ . Sedimentation velocity (SV) measurements were done at 20 °C. Depending on the protein concentration, the center piece length was 3 or 12 mm. The rotational speeds in the SV runs were 3, 10 and 18 krpm.

#### **e. Static light scattering**

Measurements were performed either in a black 96-well plate suitable for fluorescence measurements (Corning) in a Spectramax M2 (Molecular Device, Sunnyvale, CA USA) plate reader with a light source at 350 nm and detection at 360 nm or in a rectangular 2 mm cuvette in a FP 6500 Spectrofluorometer (JASCO Co., Tokyo, Japan) with emission and detection at 360 nm.

#### **f. Tryptophan fluorescence**

Measurements were performed in a rectangular 5 mm cuvette in a FP 6500 Spectrofluorometer (JASCO Co., Tokyo, Japan). Emission spectra between 300 – 450

### 3. Lipid binding of Apo A-1 mimetic peptides

---

nm were collected with excitation at 290 nm. The samples were mixed and incubated at room temperature for one hour, before measuring in the spectrometer.

#### **g. Preparation of Lipid Vesicles**

A defined amount of lipids in chloroform was first dried under a nitrogen stream and subsequently overnight in high vacuum. Typically, 1-3 mL of buffer (PBS + 0.02 % NaN<sub>3</sub>, pH 7.4 at 25 °C) were added to the lipids, and the suspension was rigorously vortexed. For preparation of small unilamellar vesicles (SUVs), the lipid suspension was kept in an ice bath and sonified under a constant nitrogen stream using a titanium tip ultrasonicator until the solution became transparent (40 min without cholesterol and 60 min with Cholesterol). Titanium debris was removed by centrifugation (Eppendorf tabletop centrifuge, 10 min at 12 000 rpm). The lipid concentration was calculated on basis of the weight of the dried lipid. Large unilamellar vesicles (LUVs) were prepared by the extrusion method [22]. After the dried lipid had been vortexed with buffer, six freeze and thaw cycles were performed with the lipid suspension and extruded through polycarbonate filters (13 times through 100 nm filters).

## Results

### Association behavior of peptides 4F and P

Apolipoprotein A-1 was shown to self-associate [22-25]. At concentrations below 3  $\mu\text{M}$  Apo A-1 is monomeric starting to oligomerize with increasing concentrations. The self-association behavior of Apo A-1 is described in Chapter 3 with a model similar to those used to describe the micellization of detergents [26]. Since the amphipathic character of the helices in Apo A-1 are similar to those of Apo A-1 mimicking peptides 4F and P we investigated if these peptides also self-associate.

#### Dynamic light scattering (DLS)

Self-association of the peptide 4F was studied with DLS. Figure 2 compares the autocorrelation curves of a suspension of 100 nm phospholipid vesicles (lipid concentration = 1.85 mM, in orange) with a solution of peptide 4F ( $c_{\text{pep}} = 100 \mu\text{M}$ , in blue). The curve describes the autocorrelation as a function of time. Autocorrelation is the degree of similarity of the fluctuations in scattering intensity which arise from Brownian motion of scattering particles. An initial scattering of a particle at the time  $t_0$  is compared with subsequent measurements of scattering after additional times  $t_0+t_1(+t_2+\dots)$ . An autocorrelation value of 1 stands for perfect correlation and can only occur at time zero. Since the particle is diffusing out of the detection volume a sigmoidal decay of the autocorrelation is observed in a plot of the autocorrelation against the logarithm of the time. The time it takes to diffuse out of the detected volume

### 3. Lipid binding of Apo A-1 mimetic peptides

---

is determined by the diffusion coefficient  $D$ , which depends on the size of the particle. The measured diffusion coefficient of the phospholipid vesicles was  $D = 4.90 \cdot 10^{-12} \text{ m}^2 \text{ s}^{-1}$  calculated with the Stokes-Einstein equation. For the 100 nm vesicles shown in Figure 2 the autocorrelation decreased to the half of the value after about 45  $\mu\text{s}$ . In this time the vesicles moves 21 nm. Small particles are diffusing very rapidly and large particles diffuse slowly.

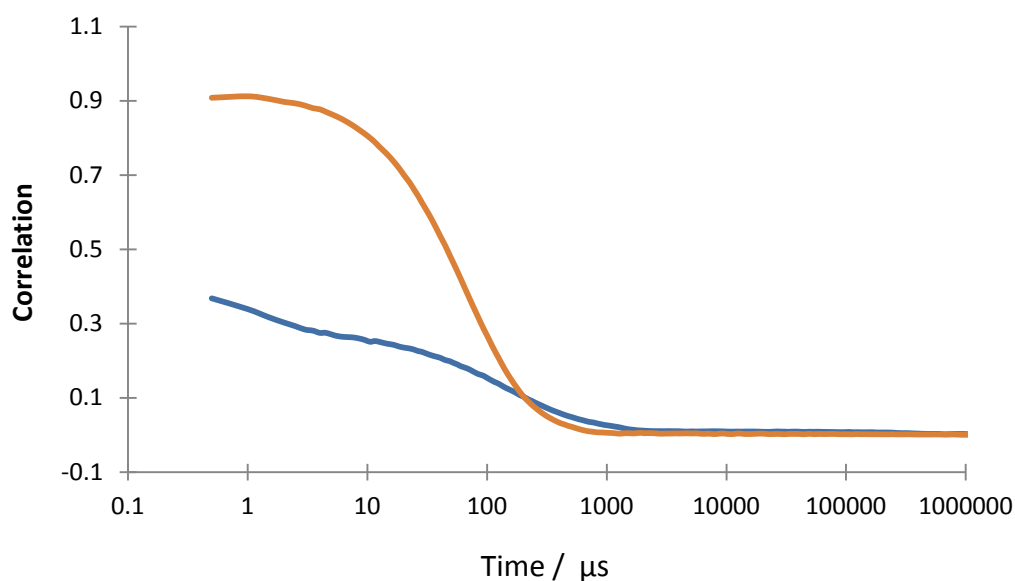


Figure 2: Autocorrelation of light scattered by particles in buffer is shown as a function of time. DLS measurements of 1.85 mM 100 nm POPC LUVs (orange line) and of 100  $\mu\text{M}$  4F peptide dissolved in PBS buffer (blue line) are depicted. LUVs yielded a typical sigmoidal shape of the autocorrelation curve in contrast to the peptide, which is too small to be investigated by DLS.

In the experiment shown in Figure 2 the second measurement follows 0.5  $\mu\text{s}$  after the initial one. If a particle diffuses very fast, the detection limit of the device is reached. This threshold is reached for particles with diameter  $\leq 4 \text{ nm}$ . For such solutions the initial autocorrelation is less than 0.5. The autocorrelation curve of the peptide 4 F (blue

### 3. Lipid binding of Apo A-1 mimetic peptides

curve in Figure 2) does not show the typical sigmoidal shape and starts below 0.4. Assuming a specific partial volume  $v_{\text{bar}} = 0.73 \text{ g/cm}^3$  of the peptide, a hexamer would still be below the detection limit of the DLS device.

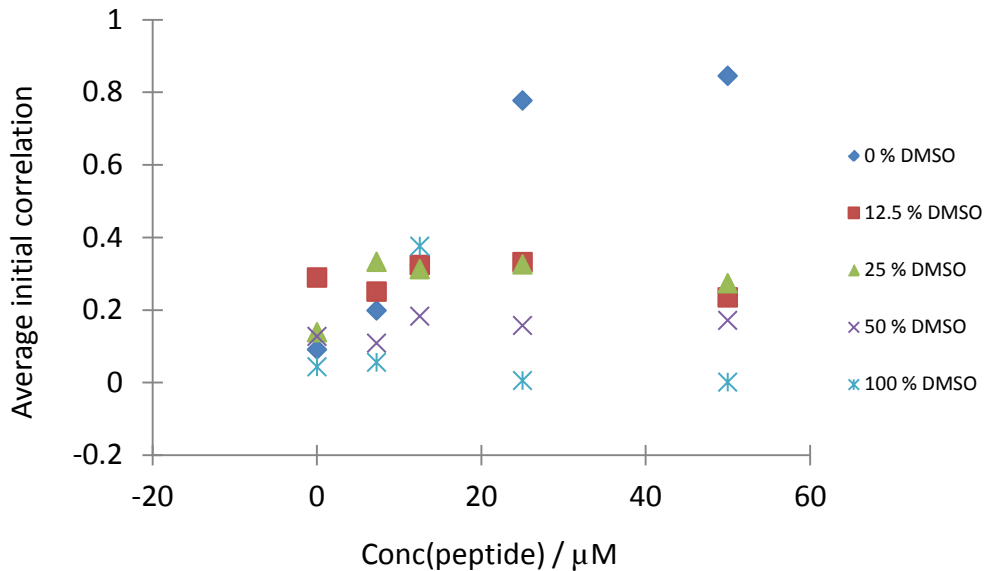


Figure 3: DLS measurements with 4F at different peptide and DMSO concentrations. To simplify the graph, only the initial value of the autocorrelation curves is shown. Autocorrelation curves with significant aggregates would yield initial autocorrelation values of approximately 1. Except of two samples particles are too small to be investigated by DLS.

Analogous to the peptide measurements shown in Figure 2 a set of different conditions were investigated. The peptides were dissolved in PBS buffer at five different concentrations. For each concentration five different DMSO concentrations were chosen in the range of 0 – 50 % resulting in a total of 25 different samples. In the following, only the autocorrelation at  $t = t_0$  ( $AC_{t_0}$ , as average of three measurements with the same sample) is shown in order to simplify the analysis. In Figure 3 the  $AC_{t_0}$  is plotted against the concentration of the peptide. The figure indicates that 4F in the presence of DMSO exhibits  $AC_{t_0}$  values below 0.4. In contrast, the two solutions without DMSO at

### 3. Lipid binding of Apo A-1 mimetic peptides

---

the two highest peptide concentrations (25 and 50  $\mu\text{M}$ ) show  $AC_{10}$  values of  $AC_{10} \approx 0.8$ . These results suggest the absence of large self-associates under most conditions, except at the two highest peptide concentrations in solutions without DMSO. Particle sizes could not be calculated by the Zetasizer software due to poor autocorrelation curves and high polydispersity indices ( $PDI \geq 0.3$ ). A high PDI is an indicator of the presence of particles of different size. A solution exhibiting a PDI below 0.25 is considered to be monodisperse, values above 0.3 are considered to indicate polydisperse solutions.

#### **Static light scattering**

DLS measurements have certain limitations. The DLS result neither quantifies the amount of scattering particles nor differentiates between particles of different chemical nature if they have the same size. Thus, a perfect auto-correlation curve could be measured in a peptide solution free of any peptide associates but containing tiny impurities such as dust particles. To distinguish between real associates and tiny impurities in the peptide solution, static light scattering was performed in a fluorescence plate reader (Spectramax M2) at 350/360 nm. The scattering is shown in Figure 4 as a function of the concentration. The same mixtures as before were prepared. The graph indicates that there is a rather constant scattering intensity independent of the peptide concentration and that there are only small differences as a function of the DMSO concentration, expect for one solution of 25  $\mu\text{M}$  4F, 0 % DMSO.

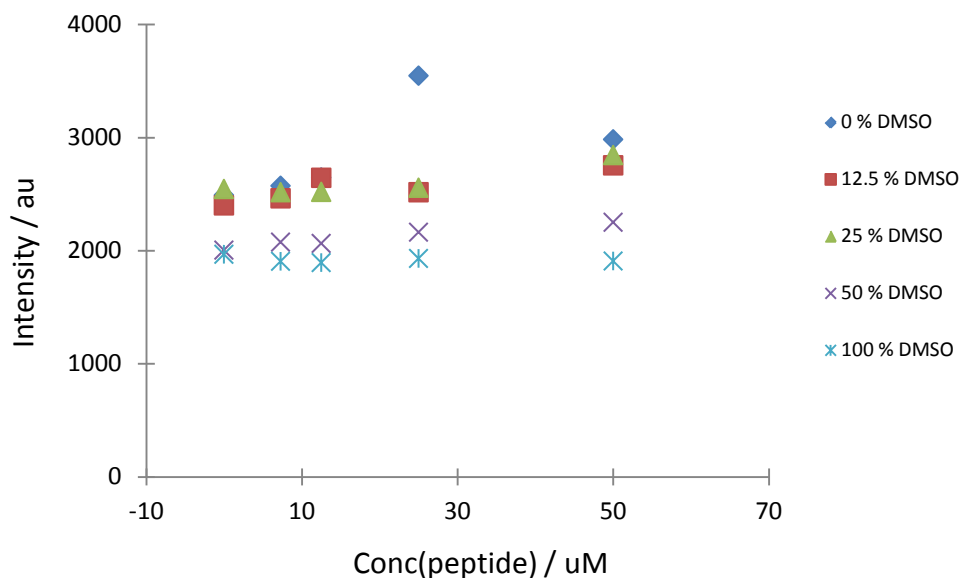


Figure 4: Light scattering intensities of 4F in buffers with varying percentages of DMSO (v/v) are shown in dependence of five different peptide concentrations. The scattering intensities were not significantly dependent on peptide and DMSO concentrations.

### Analytical ultracentrifugation

The peptide aggregation was further studied by analytical ultracentrifugation as it allows the measurement of higher concentrations than is possible with dynamic and static light scattering. 4F (200 µM) and P (100 µM) were dissolved in PBS buffer and spun at 10 krpm for 10 hours. The results are depicted in Figure 5 and Figure 6. The absorbance at 280 nm is plotted against the radius. The radius begins in the center of the rotor leading to values of about 6 - 7.5 cm in the area of the windows of the cell. The g-forces due to rotation cause sedimentation of particles having a specific density greater than the solvent. On the other hand an increased concentration gradient yields an enlarged diffusion flow, described by Fick's laws. These opposing processes come to equilibrium, as soon as the sedimentation flow compensates the diffusional flow. At a

### 3. Lipid binding of Apo A-1 mimetic peptides

---

given specific density large particles experience a large sedimentation rate and a small diffusional rate. Consequently large self-associates sediment at lower rotational velocities than small monomers. If a peptide is sedimented to the bottom of the AUC cell, it is no longer detectable. In case of 4F, integrating the absorbance from meniscus to bottom yielded the same value before and after the AUC run. This proves that the protein was not sedimented to the bottom of the cell and lead to the conclusion, that no big aggregates were formed. The experiment was repeated with 10 hours at 42 krpm, again with 200  $\mu\text{M}$  4F in the AUC and still no sedimentation and meniscus depletion was observed.

Trying to dissolve 100  $\mu\text{M}$  P in PBS buffer led to huge aggregates, which were visible even by eye. The solution with its aggregates was filled into AUC cells and spun at 3 and 10 krpm for 8 hours and 5 hours, respectively (Figure 7). The absorbance of 100  $\mu\text{M}$  P at 280 nm the length of the centrifugation cell was constant 0.26 at the first as well as at the last scan but should be 1.37. This means that over 90 % of the peptide was sedimented to the cell bottom, while 10 % were kept in solution without any further tendency to aggregate and sediment. Therefore 4F was used in PBS buffer, while P was used in HEPES-buffer together with 10 % DMSO.



### 3. Lipid binding of Apo A-1 mimetic peptides

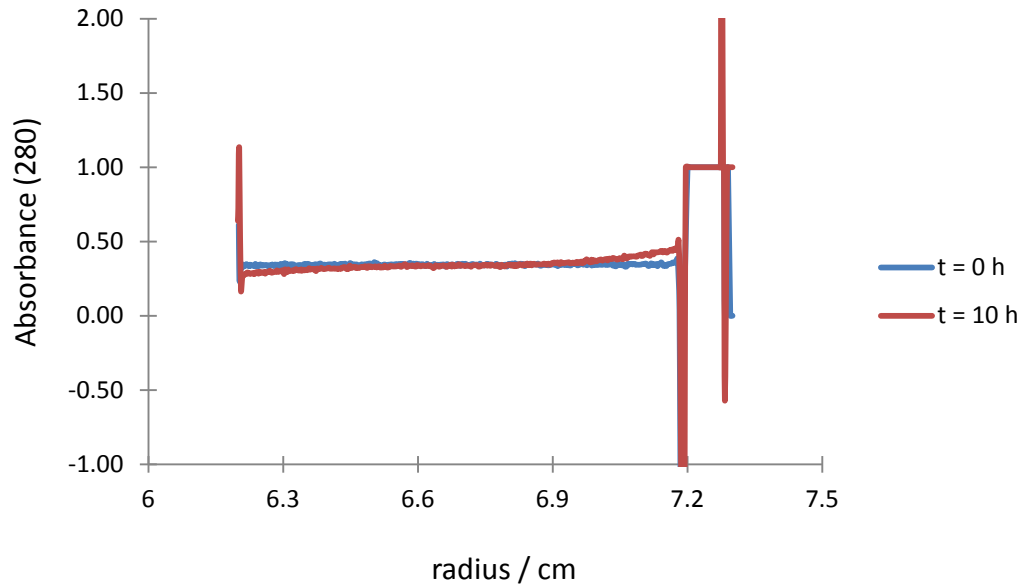


Figure 5: Analytical Ultracentrifugation scans of 200  $\mu\text{M}$  4F in PBS buffer at 10 krpm at the beginning of the measurement (blue line) and after 10 hours (red line). Analysis confirmed mass conservation of the peptide, meaning that all peptide is remained in solution.

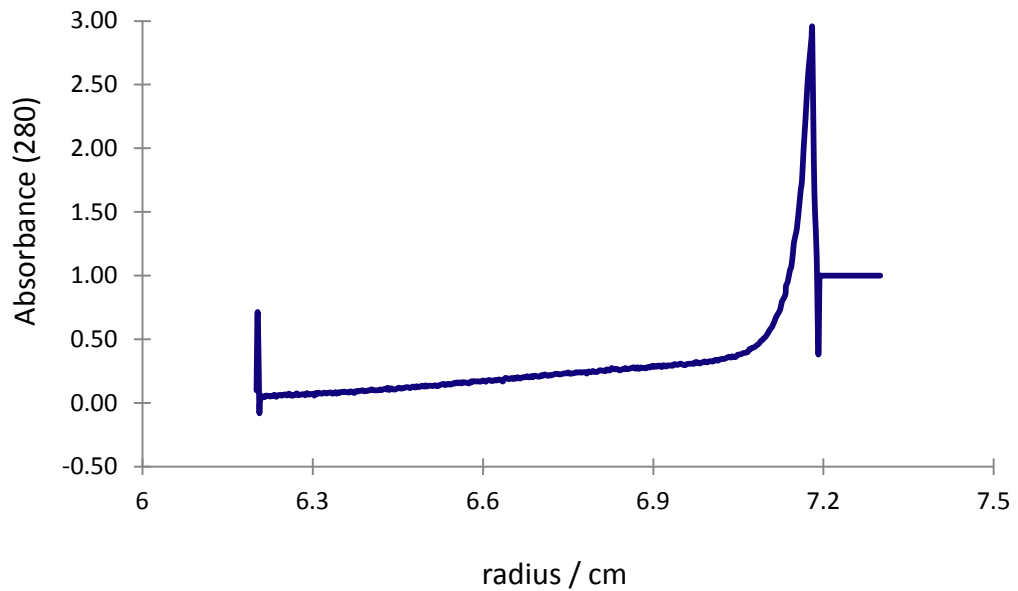


Figure 6: Analytical ultracentrifugation run with 200  $\mu\text{M}$  4F in PBS at 42 krpm after 10 hours. Sedimentation and meniscus depletion were not observed.

### 3. Lipid binding of Apo A-1 mimetic peptides

---

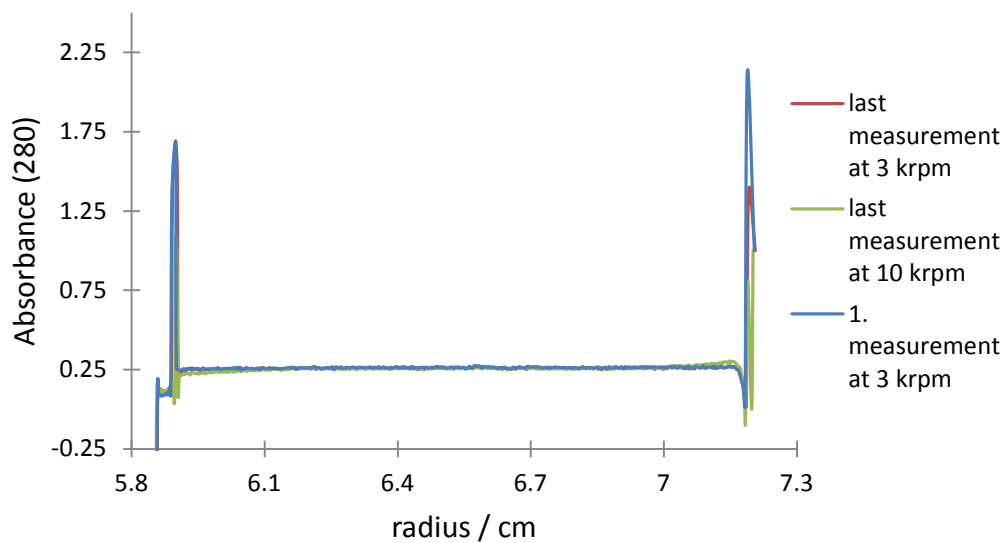


Figure 7: Analytical ultracentrifugation runs with 100  $\mu\text{M}$  P at 3 and 10 krpm. The initial and the last scan after eighth hours at 3 krpm are depicted in blue, respectively in red. The last scan after 5 hours at 10 krpm is depicted in green. The detected concentration is about 10  $\mu\text{M}$  and does not tend to sediment. This means that 90 % of the initial concentration is sedimented, which was visible even by eye.

#### **Isothermal Titration calorimetry (ITC)**

The self-association of Apo A-1 is described in Chapter 3. The dissociation reaction was measured by diluting a concentrated Apo A-1 solution (160  $\mu\text{M}$ ) in the ITC device and monitoring the heat changes.

Similar ITC dilution experiments were performed to test if reversible associates are also present in 4F solutions (Figure 8). Concentrated solutions of 4F (200  $\mu\text{M}$ ) were injected into PBS buffer at different temperatures. The titration experiments showed a small endothermic reaction ( $\approx$  1-3 kcal/mol), which could indicate dissociation. The

### 3. Lipid binding of Apo A-1 mimetic peptides

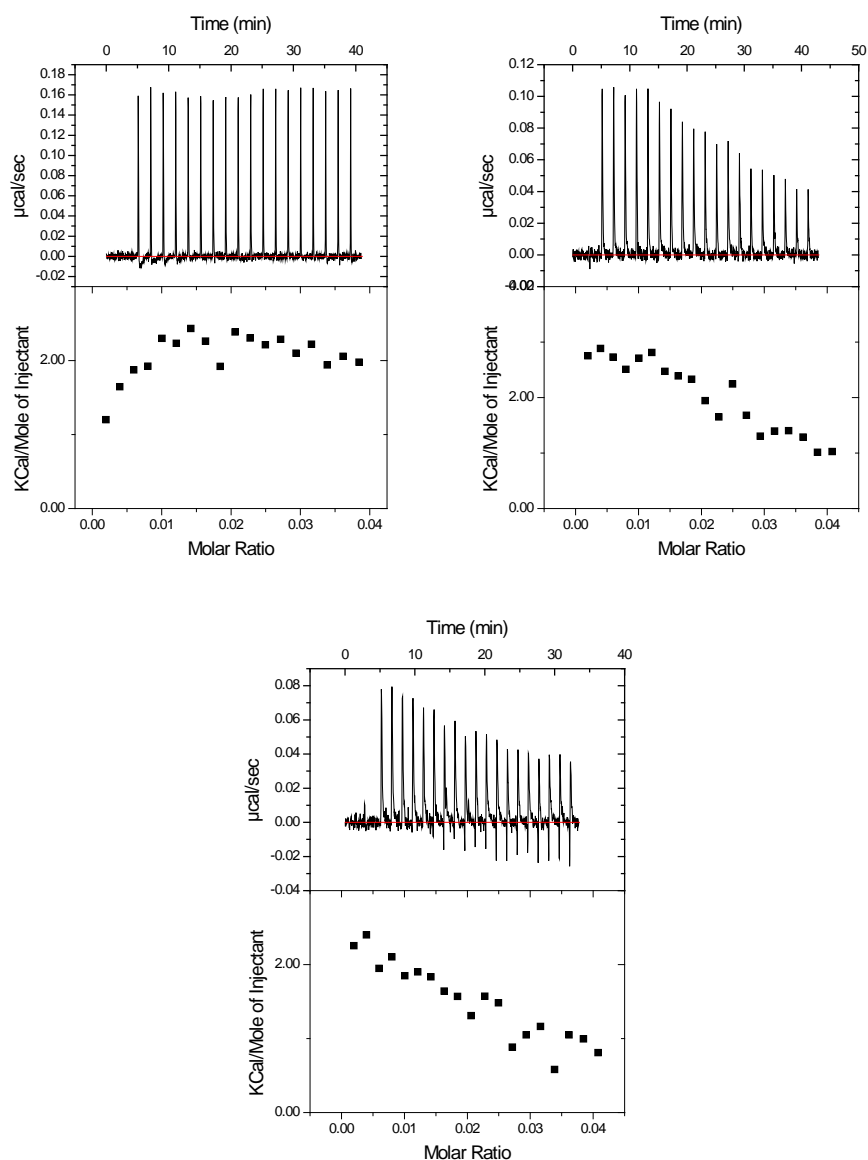


Figure 8: ITC measurements: Titration of  $200 \mu\text{M}$  4F into PBS buffer at  $40^\circ\text{C}$  (first figure),  $20^\circ\text{C}$  (second figure) and  $10^\circ\text{C}$  (third figure). Reversible self-associates of a highly concentrated peptide solution could dissociate by a dilution effect due to injection into pure buffer. The heat of reaction are slightly decreasing, except of the measurement at  $40^\circ\text{C}$ . This could be a sign of a dissociation reaction, which is not detectable at  $40^\circ\text{C}$  either because there are no oligomers at this temperature, that could dissociate or because the enthalpy of dissociation has its zero crossing at  $40^\circ\text{C}$ .

heat peaks were almost constant at temperatures of  $40^\circ\text{C}$  and decreased at lower temperatures. The dependency on temperature might be a sign of different

### 3. Lipid binding of Apo A-1 mimetic peptides

---

monomer/oligomer equilibrium with the existence of more oligomers at lower temperatures and vice versa. Another possibility could be that the enthalpy of dissociation is zero at about 40 °C.

#### **Binding of peptides 4F and P to lipid membranes**

Binding of peptides to lipid membranes was investigated mainly by means of ITC. However, ITC results do not give any information about detailed processes and the driving force of the observed reactions. Therefore ITC experiments were compared with several other methods to characterize the reaction in detail. Static and dynamic light scattering were used to investigate the influence of the peptides on the vesicle structure. Circular dichroism spectroscopy was performed to investigate secondary structural changes of the peptides induced by lipid binding. Tryptophan fluorescence was measured to get insight into the change of the environment of the tryptophans due to lipid binding.

#### **Static light scattering**

Static light scattering measurements were performed to distinguish between insertion of the peptides into vesicles or micellization of vesicles. In the first case the radius and the scattering of the particles would slightly rise, in the second case scattering would almost diminish due to dissolution of the 100 nm vesicles. Static light scattering measures the intensity of light, scattered by particles in the solution of the cuvette. The scattering intensity is proportional to the sixth power of the particles diameter.

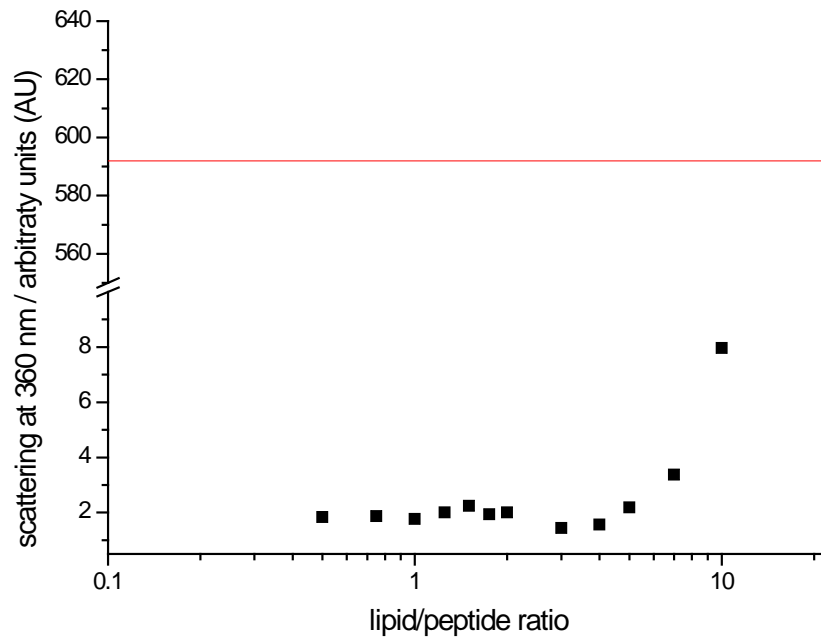


Figure 9: Static light scattering of POPC LUVs (5 mM) titrated into peptide 4F (200  $\mu$ M) after 15 h incubation. The scattering intensity of the mixtures is shown as a function of lipid-to-peptide ratios (black dots) together with a pure LUV suspension (5 mM, red line). The low detected scattering intensity in presence of 4F indicates micellization of vesicles by 4F even at a 1:10 peptide to lipid ratio.

Samples prepared by titrating POPC LUVs (5 mM) into a 4F solution (200  $\mu$ M) with an incubation period of 15 h at room temperature. Figure 9 shows light scattering of the samples in dependence of the lipid-to-peptide ratios. The scattering intensity of the mixtures (2-9 arbitrary units (AU), 0 - 1.43 mM POPC) up to lipid-to-peptide ratio  $\approx$  3 is much lower than expected for intact 100 nm vesicles (590 AU, 5 mM POPC). The low scattering intensity shows that the lipid vesicles were dissolved upon peptide addition, even at lipid-to-peptide ratios of 10. The scattering intensity is also proportional to the number of particles (concentration). However, the ratio of the lipid concentrations of the measurement with pure LUVs and the highest lipid concentration

### 3. Lipid binding of Apo A-1 mimetic peptides

---

in the mixtures is 3.5 (1.43 mM vs. 5 mM POPC) and does not explain the difference of scattering intensity of factor 65 between those two measurements (9 AU vs. 590 AU).

#### **Tryptophan fluorescence**

Peptide 4F contains a single tryptophan, and the change of tryptophan fluorescence was measured as a function of the peptide-to-lipid ratio (Table 1). Simultaneously, the mixtures were measured with dynamic light scattering (DLS).

Fluorescence studies with indol dissolved in varying mixtures of ethanol/cyclohexane showed strong a dependence of the emission spectra on the environment of the fluorophor.

Depending on the environment, the maximum of the tryptophan emission when excited with UV light at  $\lambda_{\text{ex}} = 280 - 300 \text{ nm}$  is found between  $\lambda_{\text{max}} = 308 - 350 \text{ nm}$  [27]. The fluorescence maximum is at  $\lambda_{\text{max}} = 350 \text{ nm}$  for tryptophan in a hydrophilic environment like water but shifts to smaller wavelength by exposure to a hydrophobic environment like the interior of a membrane. Peptides, which are completely bound to lipid membranes showed a maximal fluorescence at  $\lambda_{\text{max}} = 332 \text{ nm}$  in many cases [28]. In apoazurin Pfl the tryptophan is located in a completely apolar environment in the interior of the protein, which leads to a blue-shifted ( $\lambda_{\text{max}} = 308 \text{ nm}$ ) emission characteristic comparable to indole in cyclohexane [27]. Tryptophan acts as a reporter of the environment of the tryptophan side chain as the fluorescence emission maxima shift to smaller wavelength, e.g. when the peptide binds to lipids. Binding of proteins and peptides to lipid vesicles can be performed either qualitatively by detecting a blueshift or in detail by calculating a binding constant out of the experimental data.

### 3. Lipid binding of Apo A-1 mimetic peptides

In Figure 10 the fluorescence emission spectra of the samples (Table 1) are shown. The change of the emission maxima is depicted in Figure 11. The emission maxima shifted to smaller wavelength ( $\lambda_{\max} = 335$  nm) with increasing lipid-to-peptide ratios. This indicates a binding of peptides to lipid membranes as eluded above. Assuming the formation of an  $\alpha$ -helix of all residues, the helical wheel representation suggests the tryptophan to be located on the hydrophilic side, but near the interface of the amphiphilic plane, which is going through the long axis of the helix Figure 1. Hence, binding of the nonpolar side of the helix to lipid membranes would position this residue in a nonpolar environment.

Table 1: Table of 4F and POPC lipid mixtures and resulting sizes used for tryptophan – fluorescence and dynamic light scattering measurements. Sizes and the polydispersity indices (PDI) were measured by DLS. Asterisks on the PDI values indicate bad quality of correlation diagrams, the sizes should be interpreted with caution in these cases.

Sample	Peptide	POPC SUVs	L-to-P ratio	Fluor. max.	Size by DLS	PDI (DLS)
<i>No</i>	$\mu M$	<i>mM</i>		<i>nm</i>	<i>nm</i>	
1	100	0	0	349	-	-
2	100	0.25	2.5	339	10.8	0.47*
3	100	0.5	5	337	26.8	0.63
4	100	1	10	336	583.1	0.50*
5	100	1.85	18.5	334.5	655.4	0.54*
6	0	1.85	-	-	35.0	0.21

### 3. Lipid binding of Apo A-1 mimetic peptides

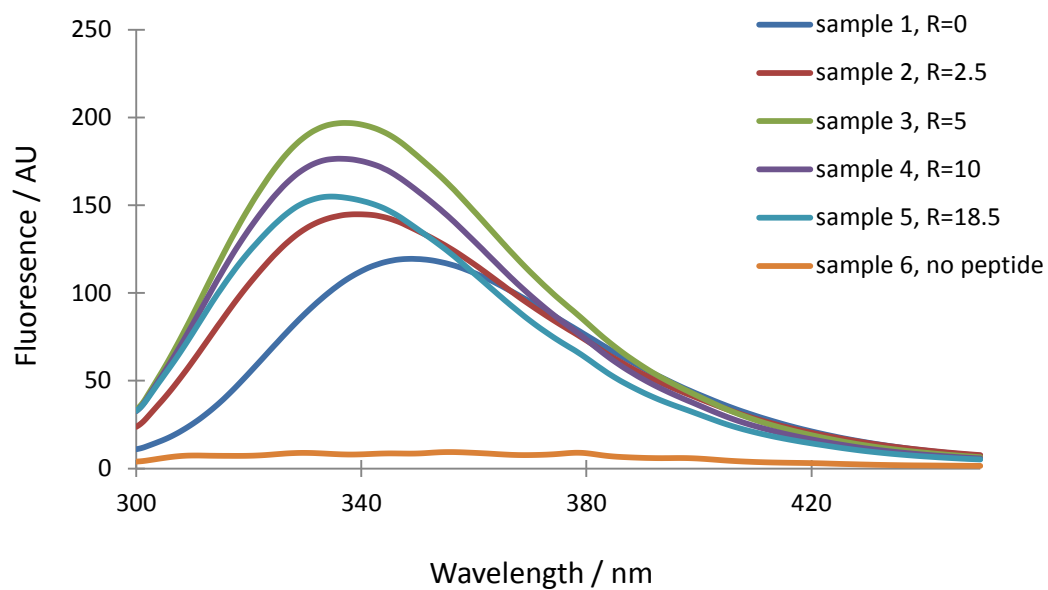


Figure 10: Tryptophan fluorescence spectra of different 4F/lipid mixtures (see Table 1) excited at 290 nm. The peptide concentration was 100  $\mu\text{M}$  4F, except of sample 6, and the lipid-to-peptide ratio (R) is marked in the legend. The fluorescence maxima of the spectra are shifted to smaller wavelength with higher lipid-to-peptide ratios due to interaction of these molecules.

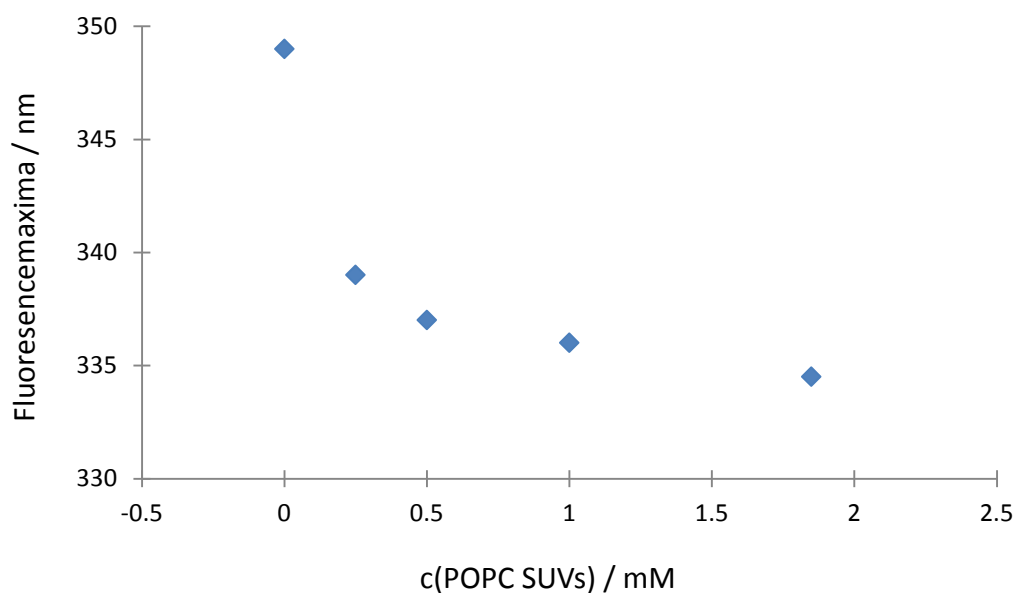


Figure 11: The tryptophan fluorescence maxima of 4F (100  $\mu\text{M}$ ) at different lipid mixtures (see Table 1) are depicted. A blueshift of the emission maxima with increasing lipid concentration is significant.



#### **Dynamic light scattering (DLS)**

Figure 12 shows autocorrelation curves of various lipid-to-peptide ratios (Table 1, same mixtures as used for Trp-fluorescence) by means of DLS measurements. The inflexion point of autocorrelation curves gives a hint of the particle size. The higher the x-value of the inflexion point the bigger are the particles. Table 1 contains volume weighted size distributions. The particle size of the SUVs (35 nm) decreased at small lipid-to-peptide ratios to 10.8 nm, but increased with increasing lipid-to-peptide ratios to 655.4 nm. This was also easily observed by eye, as the slightly turbid SUV suspension turned into a clear solution at a lipid-to-peptide ratio of 2.5, but got milky beginning at lipid-to-peptide ratios of 10.

In comparison to results obtained by static light scattering the particle size at a lipid-to-peptide ratio of ten must be different. While static light scattering indicate very small particles like micelles, the size of the DLS measurement is calculated to be 583 nm. This discrepancy might be explained by different reaction conditions. In the static light scattering the concentration of 4F was 143  $\mu\text{M}$  and LUVs were used, while dynamic light scattering was performed with 100  $\mu\text{M}$  4F and SUVs.

### 3. Lipid binding of Apo A-1 mimetic peptides

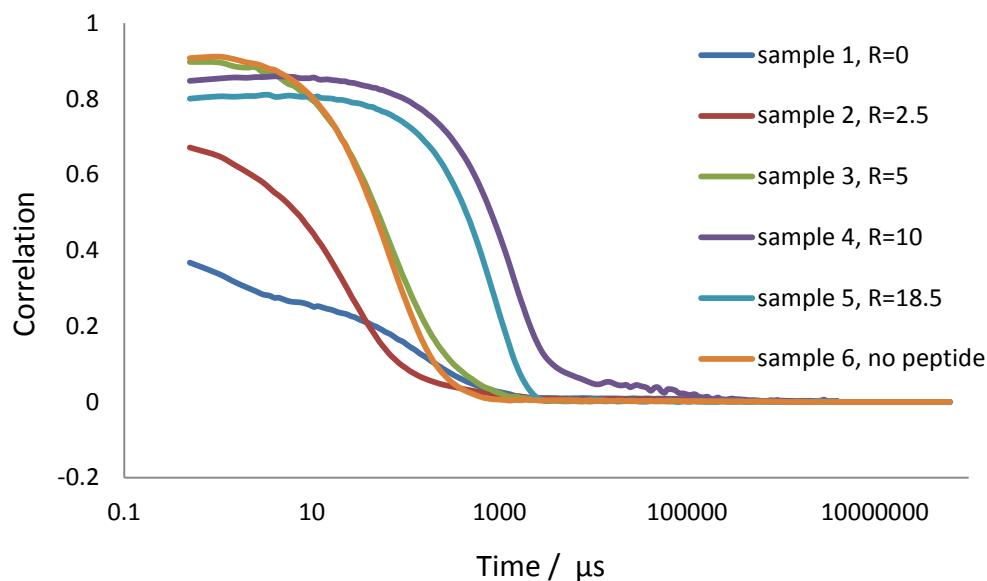


Figure 12: Autocorrelation curves of 100  $\mu\text{M}$  4F and various POPC lipid concentrations (see Table 1) used for tryptophan fluorescence were also measured by DLS. The peptide concentration was 100  $\mu\text{M}$  4F, except for sample 6 (pure lipid), and the lipid-to-peptide ratio (R) is marked in the inset. The x-value of the inflexion point correlates with the size of particles in solution. The orange line is a measurement of the peptide without lipids. Small lipid concentrations decrease, whereas high concentrations increase the size of the particles at a constant peptide concentration of 100  $\mu\text{M}$  4F.

### Circular dichroism spectroscopy (CD)

The secondary structure of the peptide 4F was checked with CD spectroscopy, without and with different amounts of POPC lipids (Table 2). In Figure 13 CD spectra at different lipid-to-peptide ratios are shown for 4F. Analysis of the spectra with three different algorithms of the software CDpro is depicted in Figure 14 as a function of the lipid concentration. Free peptide consisted mostly of  $\alpha$ -helix ( $\approx 40\%$ ), about 35%  $\beta$ -sheet& $\beta$ -turn and 25% of random coil structure. The  $\alpha$ -helical part of the peptides increased with increasing lipid-to-peptide ratios at the expense of  $\beta$ -sheet& $\beta$ -turn and

### 3. Lipid binding of Apo A-1 mimetic peptides

random coil fractions (Figure 14). The results suggest that binding of the peptide 4F to lipids induce a random coil and  $\beta$ -sheet &  $\beta$ -turn to  $\alpha$ -helix transition.

Table 2: Circular dichroism (CD) measurements with mixtures of the peptide 4F together with various POPC LUV concentrations. Chloride ions of the PBS buffer were exchanged by fluoride.

Sample	LUVs	4F	L-to-P ratio
<i>No</i>	$\mu M$	$\mu M$	
1	588	0	-
2	74	176	0.4
3	294	176	1.7
4	588	176	3.3
5	0	176	0

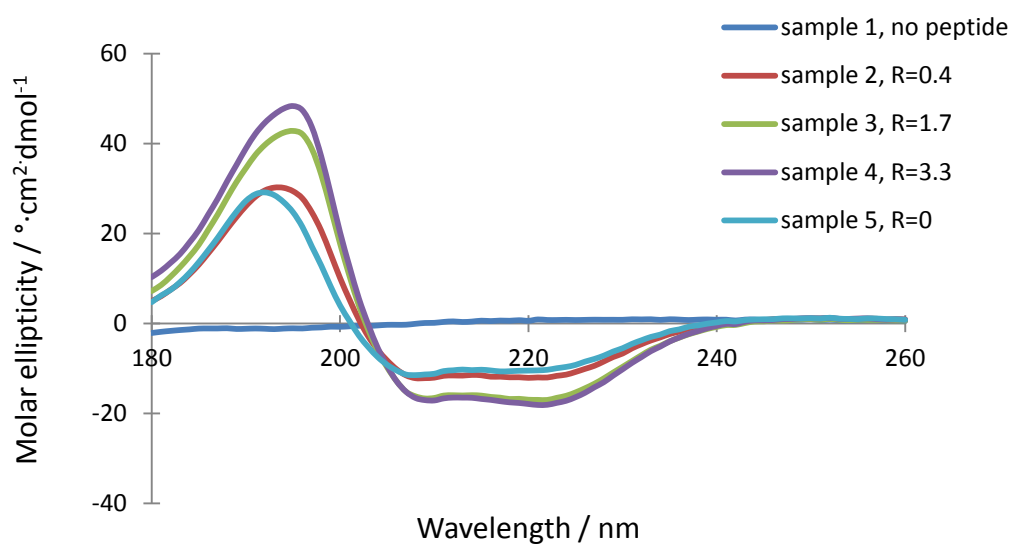


Figure 13: Circular dichroism spectra of 4F at different peptide to lipid ratios (see Table 2). The peptide concentration was 176  $\mu M$  4F, except of sample 1, and the lipid-to-peptide ratio (R) is marked in the inset. The spectra suggest predominantly  $\alpha$ -helical secondary structure, which even increased at higher lipid-to-peptide ratios.

### 3. Lipid binding of Apo A-1 mimetic peptides

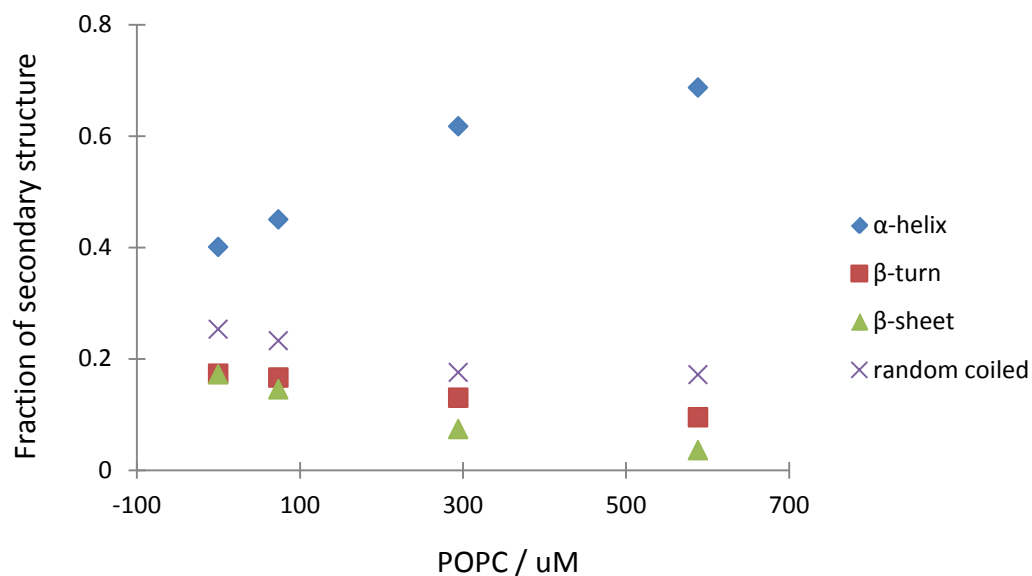


Figure 14: Analysis of CD measurements with 4F (176  $\mu\text{M}$ ) at different peptide to lipid ratios (Table 2) by CDpro with three algorithms. The peptide is highly  $\alpha$ -helical which increased at higher lipid concentrations drastically at the expense of  $\beta$ -structure and random coil parts.

### Isothermal titration calorimetry (ITC)

#### *Binding of the peptide 4F to lipid membranes*

Binding of the peptides to lipid vesicles was further investigated by means of ITC. Small or large unilamellar vesicles were prepared by sonication or extrusion procedure, respectively. The size and the monodispersity of the vesicles were determined by DLS measurements of diluted lipid vesicle suspensions (50  $\mu\text{M}$ ). LUVs ( $\approx 105$  nm) were always monodisperse with a PDI of 0.05. On the other hand, SUVs ( $\approx 35$  nm) showed a PDI of 0.25 - 0.3, even after variation of the sonication procedure. This is at the border of polydispersity as alluded to above. The size distribution (by volume) of representative DLS measurements of POPC SUVs and LUVs is shown in Figure 15.

### 3. Lipid binding of Apo A-1 mimetic peptides

The distribution analysis with SUVs showed the main peak at  $\approx 35$  nm and a second second small peak at  $\approx 180$  nm. In comparison, the analysis of LUVs indicated only the main peak at  $\approx 105$  nm.

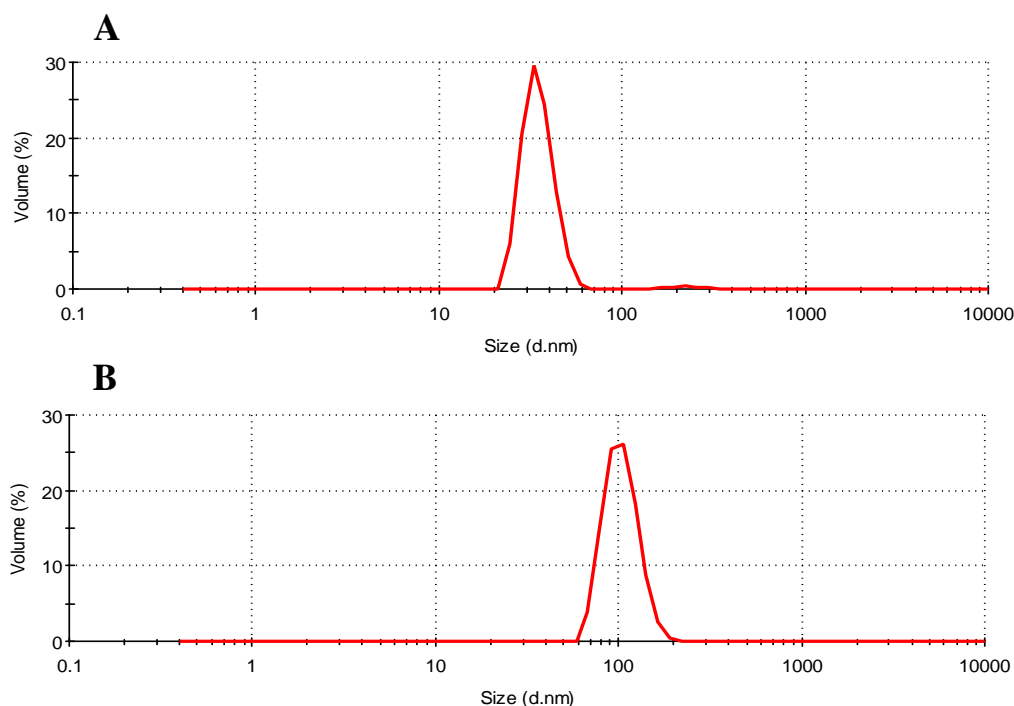


Figure 15: Size distribution by volume for POPC SUVs (A, 18.5  $\mu$ M) and LUVs (B, 50  $\mu$ M) determined by dynamic light scattering.

A typical ITC titration is shown in Figure 16 A. Figure 16 A shows 2  $\mu$ L injections (19 times) of POPC LUVs (5 mM) into 203  $\mu$ L of 200  $\mu$ M 4F dissolved in PBS buffer at 40  $^{\circ}$ C. The spacing of the injections was increased to a maximum of 300 s at lipid-to-peptide ratios between 1 and 2 as a slow kinetics of this exothermic reaction was observed in this range.

At the first injection probably most of the injected lipid was bound as 4F was in excess over lipid. As more vesicles were injected, the concentration of free peptide decreased,

### 3. Lipid binding of Apo A-1 mimetic peptides

---

and the heats of reaction became progressively smaller until all peptide was bound to lipid membranes. Further injections did not yield any significant heat changes. Integration of the heat flow over time resulted in the heat of binding for each titration step and is plotted as a function of the lipid-to-peptide ratio in Figure 16 B. The molar binding enthalpy of 4F is then determined from the total heat released in the titration ( $\approx -216.7 \mu\text{cal}$ ) and the amount of peptide in the calorimeter cell (40.6 nmol). Therefore the heat of reaction is  $\Delta H \approx -5.34 \text{ kcal/mol}$  for the experiment shown in Figure 16.

For a complete thermodynamic characterization of the binding process including the binding constant,  $K$ , and the entropy,  $\Delta S$ , the calorimetric data were analyzed with a multisite binding model, which was also used to describe the binding equilibrium of other peptides [20, 29]. In this model, the peptide is supposed to have  $n$  independent and equivalent binding sites for a ligand such as POPC. The binding model is represented by the following equation:

$$\frac{[P]_b}{[L]_t} = \frac{nK[P]}{1 + K[P]} \quad (1)$$

$[P]$  and  $[P]_b$  are the concentrations of free and bound peptide, respectively,  $[L]_t$  is the total concentration of ligand, that is POPC lipid. In the analysis, the lipid concentration  $[L]_t$  may differ from the nominal concentration. This is caused by a peptide binding only to the vesicle outside (only 50 % of the lipid). In contrast 100 % lipid is available upon micellization. The concentration of the lipid vesicles was varied in order to give consideration to the fact that only the outer lipid leaflet of intact vesicles is exposed to the peptides, whereas all lipids are exposed after micellization of vesicles. Practically this was done by minimizing the mean square deviation of the fit at a fixed stoichiometry of  $n = 1$ .  $K$  is the intrinsic binding constant, and the stoichiometry  $n$  is the

number of peptide molecules bound per ligand. The stoichiometry could also be derived directly from the experimental binding isotherm by the ratio at the midpoint of the transition. In consequence of mass conservation, the concentration of bound peptide can be described by the following equation:

$$[P]_b = \frac{1}{2} \left( \frac{1}{K} + [P]_t + n[L]_t \right) - \frac{1}{2} \sqrt{\left( \frac{1}{K} + [P]_t + n[L]_t \right)^2 - 4n[L]_t[P]_t} \quad (2)$$

The index t denotes the total concentration of peptide and lipid in the calorimeter cell after each injection step. The peptide concentration changes during the titration with lipid vesicles due to dilution effects. The concentration of bound peptide is linked to the calorimetric data by the following equation:

$$\delta Q_i = \Delta H_{peptide}^0 \delta [P]_{b,i} V \quad (3)$$

where  $\delta Q_i$  is the heat absorbed or released at the *i*th injection.  $\Delta H_{peptide}^0$  is the binding enthalpy of peptide,  $\delta [P]_{b,i}$  is the change (increase) in bound peptide concentration upon injection *i*, and *V* is the volume of the calorimeter cell. The solid line in Figure 16 is the best least-squares fit to the data using 1-3 with the following set of parameters:  $n = 1$ ,  $K = 7.52 \cdot 10^4 \text{ M}^{-1}$ , and  $\Delta H_{peptide}^0 = -5.73 \text{ kcal/mol}$  Table 3.  $\Delta H_{peptide}^0$  is consistent with the simple calculations given above. The entropy  $\Delta S$  is calculated by the binding constant (calculated with *K*), the enthalpy of reaction and the temperature.

### 3. Lipid binding of Apo A-1 mimetic peptides

---

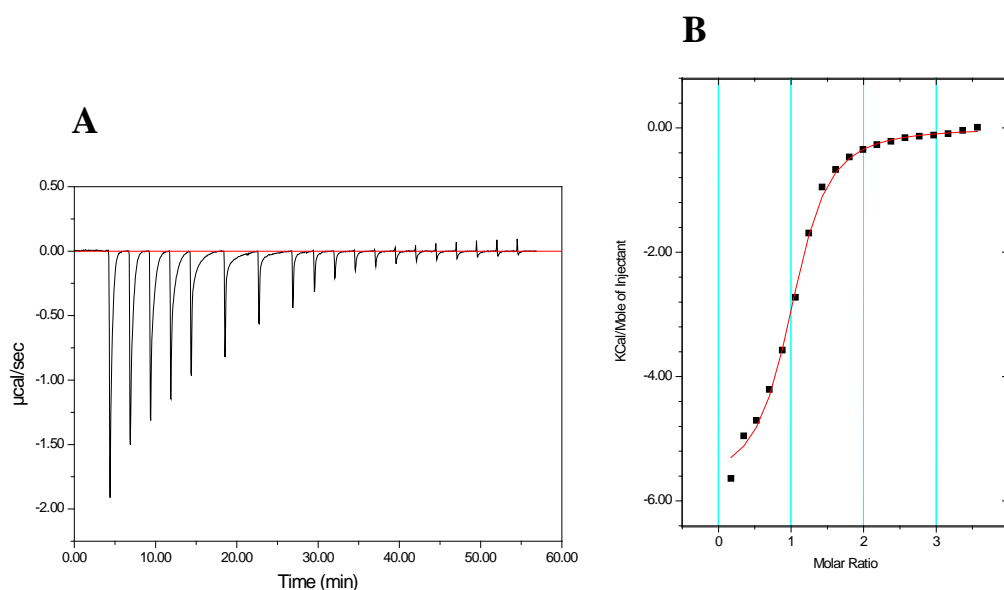


Figure 16: Example of a typical thermogram and binding isotherm of 5 mM POPC LUVs titrated into 200  $\mu\text{M}$  4F at 40  $^{\circ}\text{C}$  in PBS buffer (+ 0.02 %  $\text{NaN}_3$ ). In A the heat flow due to the binding reaction is shown time dependently. The integrated peaks are depicted (B) in dependence of the lipid to peptide ratio and a binding model with  $n$  identical binding sites ( $\Delta H = -5.73 \text{ kcal/mol}$ ,  $K = 7.52 \cdot 10^4$ ,  $n = 1$ ) is fitted to the data. Buffer: PBS + 0.02 %  $\text{NaN}_3$ .

The binding reaction was measured at different temperatures ranging from 5 to 45  $^{\circ}\text{C}$ . Thermograms and binding isotherms are collected in the appendix (Figure 26) and thermodynamic parameters are summarized in Table 3. The heat flow of experiments with the two lowest temperatures (5 and 15  $^{\circ}\text{C}$ ) was very small and reached almost the detection limit of the microcalorimeter. The reaction enthalpy decreased with increasing temperatures leading to a negative change of the heat capacity of  $\Delta C_p = -137 \text{ J mol}^{-1} \cdot \text{K}^{-1}$  as shown in Figure 17. The negative algebraic sign of the heat capacity change is a hallmark of hydrophobic interactions as driving force of the reaction [30, 31]. The binding constants  $K$  are in accordance with van't Hoff's law, that changes only slightly



### 3. Lipid binding of Apo A-1 mimetic peptides

with the temperature in a range of  $K \approx 5 \cdot 10^4 \text{ M}^{-1}$  within the errors of the measurement (Figure 18). Hence, also the Gibbs free reaction enthalpy does not change significantly. A decrease of enthalpy and entropy of reaction with increasing temperature at an almost constant Gibbs free enthalpy was observed. This process is called enthalpy-entropy-compensation and found in many other reactions. Remarkable is the increase in lipid accessibility from about 70 to 90 % of the total lipid amount at 45 °C indicating almost complete dissolution of the vesicles (Table 3).

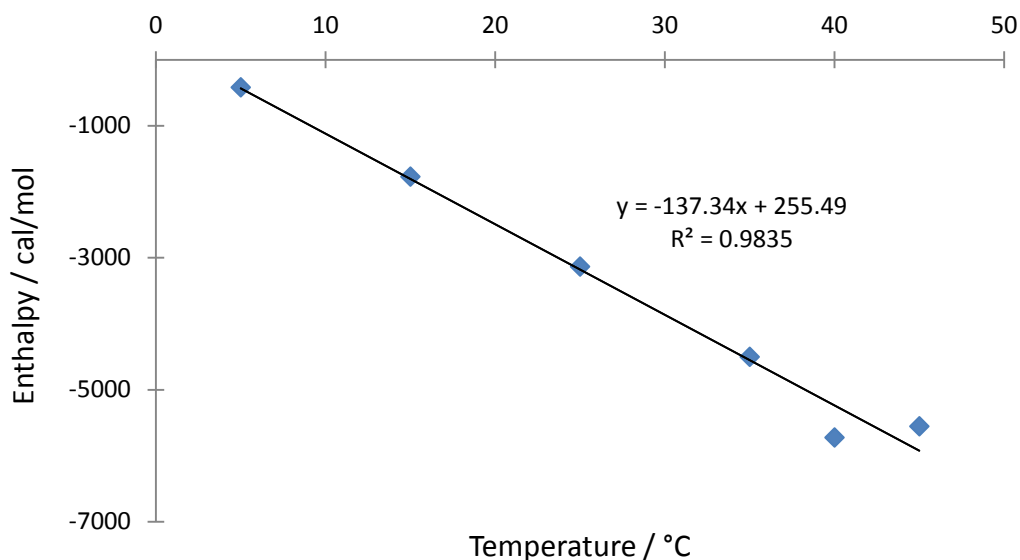


Figure 17: Temperature dependency of the reaction enthalpy. Measurements of 5 mM POPC LUVs titrated into 200  $\mu\text{M}$  4F are shown. The change of heat capacity of  $-137 \text{ cal mol}^{-1} \text{ K}^{-1}$  is derived by the slope of the linear fit. The negative algebraic sign is a hallmark of hydrophobic interactions.

### 3. Lipid binding of Apo A-1 mimetic peptides

---

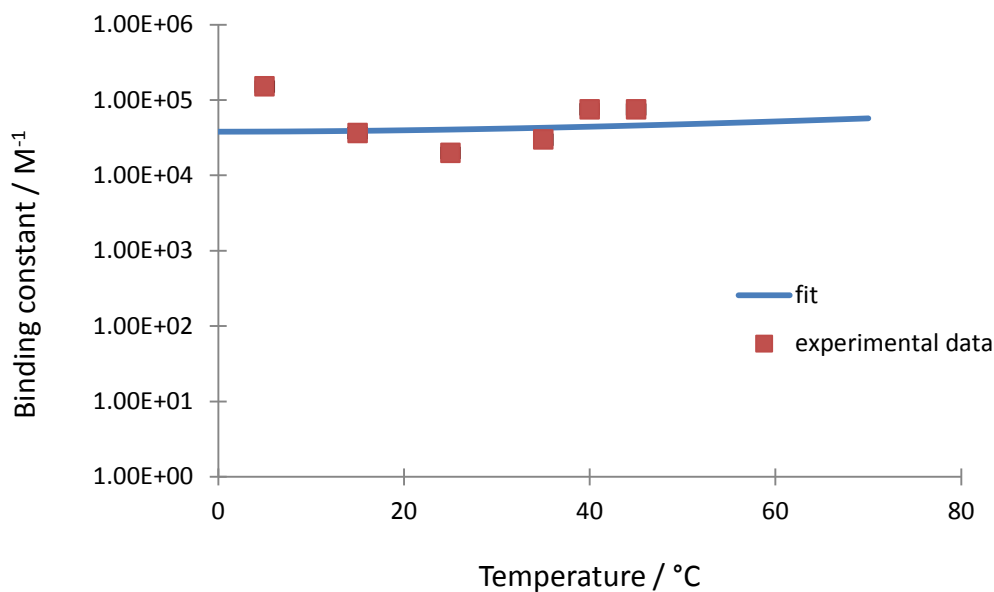


Figure 18: Binding constant of 4F to POPC LUVs in as a function of the reaction temperature. The binding constants of each measurements (red squares) are in the range of  $4 \cdot 10^4 \text{ M}^{-1}$  and follow van't Hoff's law (blue line).

#### ***Binding of the peptide 4F to cholesterol***

The binding of the peptide 4F to cholesterol was also investigated in detail. Due to the poor solubility of cholesterol two strategies were chosen to make solution reactions possible. One was the incorporation of cholesterol into methyl- $\beta$ -cyclodextrin rings as investigated by Herklotz et al. [32]. The other approach was the preparation of lipid vesicles with POPC and cholesterol.

#### *Cholesterol in m- $\beta$ -Cyclodextrin*

Cyclodextrins are cyclic oligosaccharides. In particular,  $\beta$ -cyclodextrin is composed of seven glycopyranoside units, which are topologically organized as a toroid with a smaller and a larger opening, exposing primary and secondary hydroxyl groups to the solvent. Hence the molecules are well soluble in water. The ring interior is less hydrophilic than the aqueous phase, facilitating the incorporation of hydrophobic molecules such as cholesterol. The methylated m- $\beta$ -cyclodextrin has an enhanced affinity to cholesterol. In cell culture it is used together with cholesterol in order to load cells with cholesterol.

Pure m- $\beta$ -cyclodextrin (20 mM) or m- $\beta$ -cyclodextrin (20 mM) containing 1 mM cholesterol were filled into the syringe of the titration calorimeter and were injected into a solution of 4F (100  $\mu$ M) in the cell. Injection of pure m- $\beta$ -cyclodextrin into peptide yielded relatively high ( $\approx 20$   $\mu$ cal) and a linearly decreasing heat release. This is typical for a dilution reaction and does not indicate direct binding of the peptide to m- $\beta$ -cyclodextrin (Figure 19, below). In contrast ITC experiments of m- $\beta$ -cyclodextrin (20 mM) with incorporated cholesterol (1 mM) shows the sigmoidal shape of a multi-site binding isotherm (Figure 19).

### 3. Lipid binding of Apo A-1 mimetic peptides

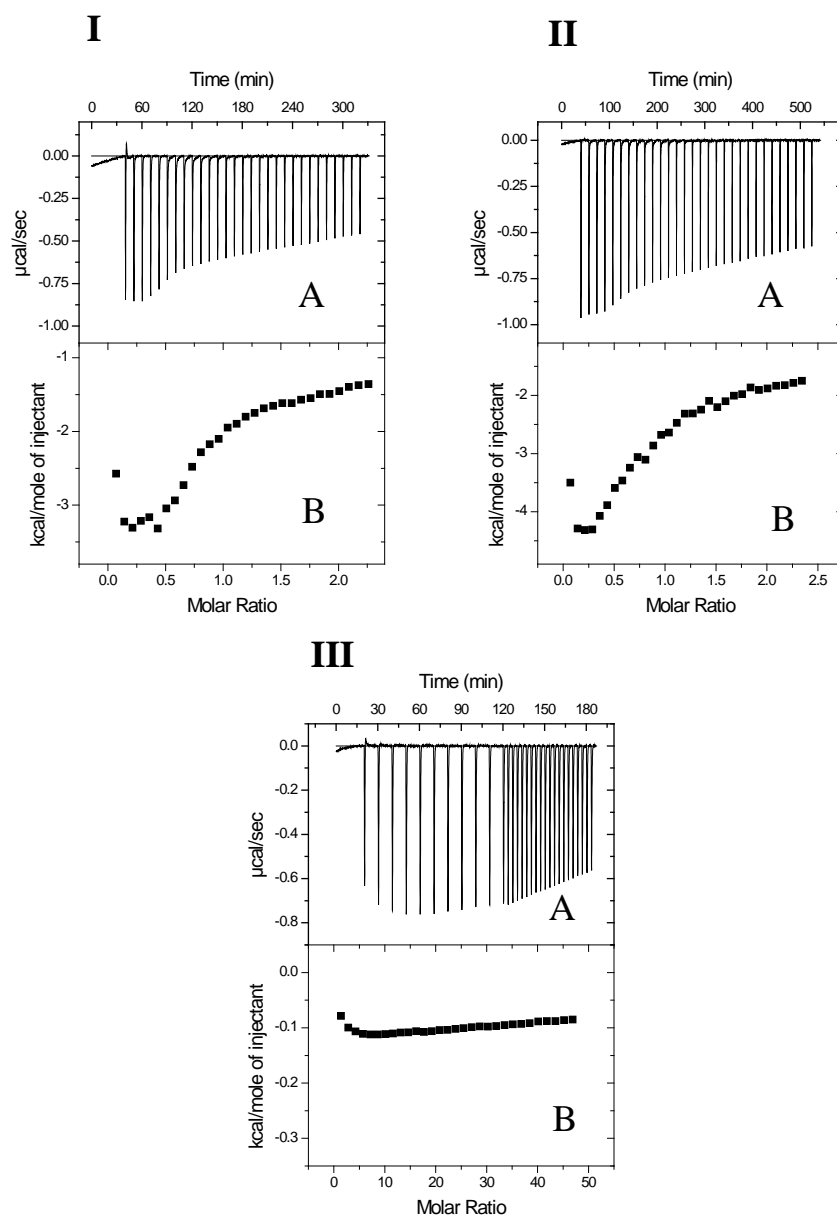


Figure 19: Titration of m- $\beta$ -cyclodextrin into peptide 4F at 15 °C (I,III) and 5 °C (II). (A) Calorimetric traces were obtained by titration of cyclodextrin (20 mM) into 4F (100  $\mu$ M). Cholesterol (1 mM) was complexed by cyclodextrin in (II) and (III). Each heat peak corresponds to injection of 10  $\mu$ L cyclodextrin with or without cholesterol into the microcalorimeter cell. (B) Heats of reaction were obtained by integration of heat peaks and were plotted as a function of the peptide-to-cholesterol (I, II) and peptide-to-cyclodextrin (III) ratio, respectively. Buffer: 10 mM Hepes + 10 % DMSO.

#### *Cholesterol in unilamellar vesicles*

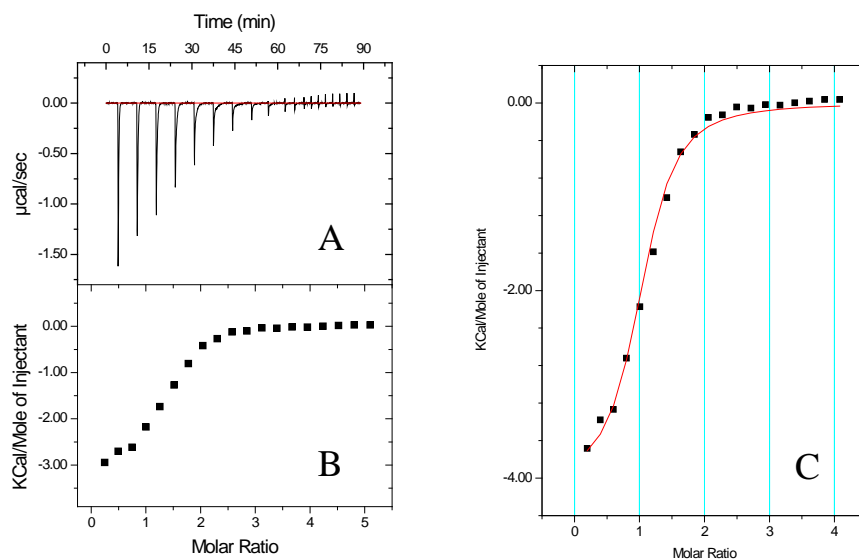
The second approach was the preparation of lipid vesicles containing a well-defined cholesterol amount of cholesterol to elucidate the potential binding of cholesterol to the peptide 4F. LUVs were prepared using the extrusion method above 40 °C [33] in order to produce vesicles with a homogeneous distribution of cholesterol (5, 10 and 20 % cholesterol). The PDI of LUVs was about 0.05 in different buffers, increasing to about 0.1 with cholesterol, whereas the diameter changed slightly from approximately 100 nm to approximately 110 nm. The vesicles were filled into the syringe at a concentration of 5 mM and were injected into a solution of 200  $\mu$ M peptide 4F at 40 °C as shown in Figure 20. The analysis was made with the same model as discussed above, resulting thermodynamic parameters are summarized in Table 3 and depicted in Figure 21. The reaction enthalpies clearly increased from -5697 to -2672 cal/mol with increasing cholesterol fractions (0 - 20 %, Figure 21), while the reaction entropy increased from 3.06 to 10.6 cal mol<sup>-1</sup> K<sup>-1</sup>. The binding constants were in the range of 10<sup>4</sup> M<sup>-1</sup> and decreased linearly with increasing cholesterol fraction of the vesicles. The stoichiometry was  $n = 1$  while the accessible lipid increased with increasing cholesterol percentage of the vesicles from 80 to 100 %.

Measurements were also made with SUVs (Appendix Figure 27). POPC SUVs had a high polydispersity index PDI of about 0.3 which increased to 0.4 in presence of cholesterol. The diameter of the vesicles without cholesterol was about 35 nm with an accounting for approximately 90 % of total material. With an increasing cholesterol percentage the diameter increased to approximately 45 nm, whereas the fraction of these vesicles decreased to about 75 % of total lipid. More than 60 min sonication time yielded large particles in the range of 230 nm with a PDI of 0.14.

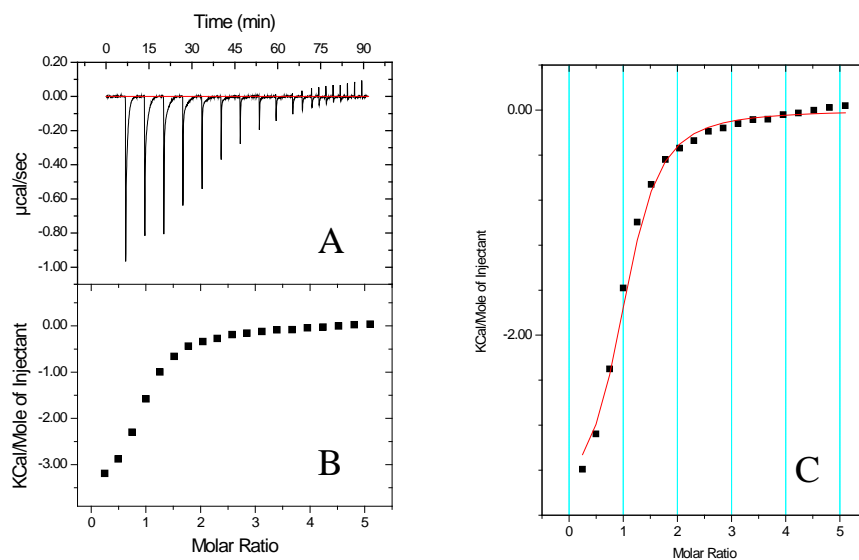
### 3. Lipid binding of Apo A-1 mimetic peptides

---

**I**



**II**



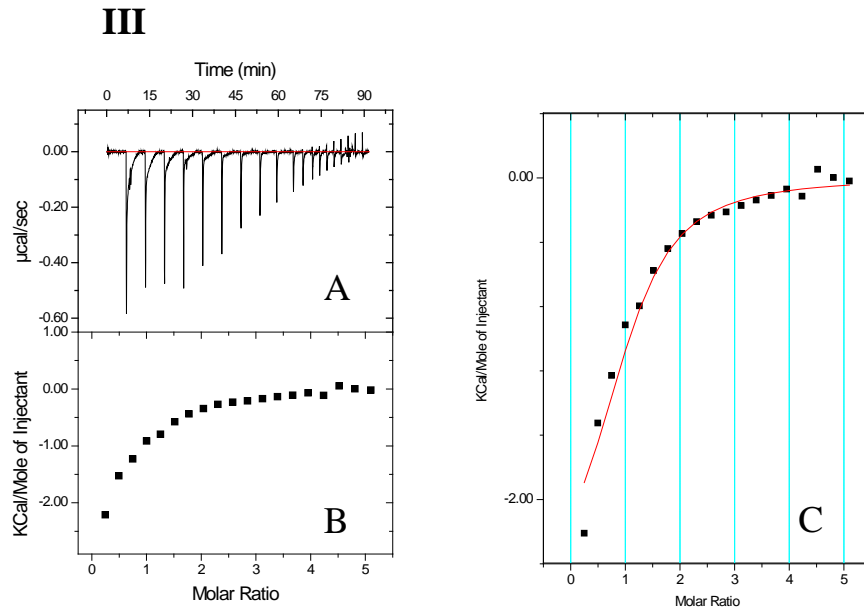


Figure 20: Titration of POPC LUVs with cholesterol into peptide 4F at 40 °C. (A): Calorimetric traces were obtained by titration of POPC LUVs (5 mM) with cholesterol (I: 5 %, II: 10 %, III: 20 %) into 4F (200  $\mu\text{M}$ ). Each heat peak corresponds to injection of 2  $\mu\text{L}$  lipids into the microcalorimeter cell. (B): Heats of reaction were obtained by integration of heat peaks and were plotted as a function of the peptide-to-lipid ratio. This experimentally obtained binding isotherm was fitted (I:  $\Delta H = -4.06 \text{ kcal/mol}$ ,  $K = 6.40 \cdot 10^4$ ,  $n = 1$ ; II:  $\Delta H = -3.53 \text{ kcal/mol}$ ,  $K = 4.20 \cdot 10^4$ ,  $n = 1$ ; III:  $\Delta H = -2.67 \text{ kcal/mol}$ ,  $K = 1.49 \cdot 10^4$ ,  $n = 1$ ) with a multisite-binding model in (C). Buffer: PBS + 0.02 %  $\text{NaN}_3$ .

### 3. Lipid binding of Apo A-1 mimetic peptides

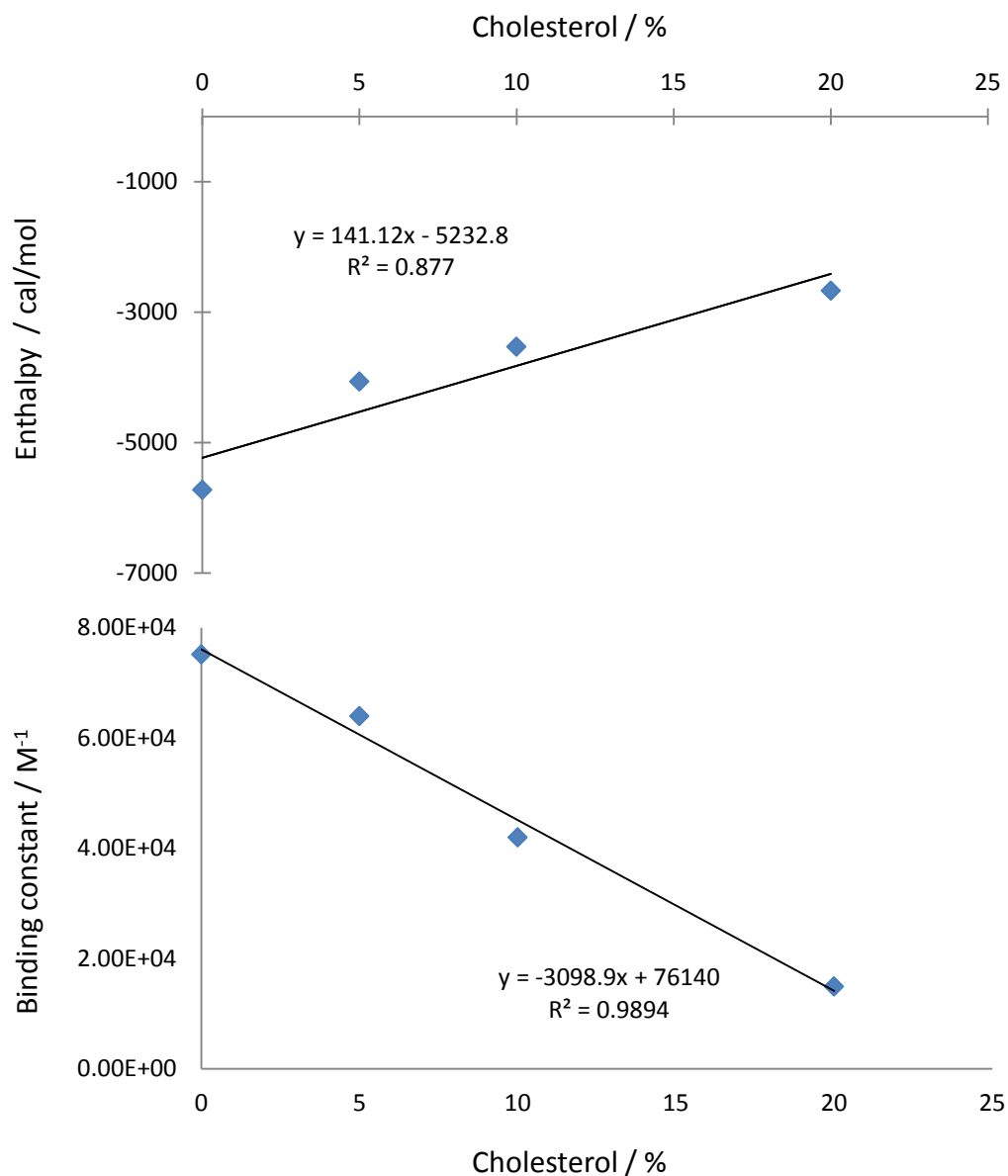


Figure 21: Binding of peptide 4F to lipid vesicles (LUVs) containing cholesterol. Above: Reaction enthalpy of 4F to POPC/cholesterol LUVs as a function of cholesterol content. Below: Binding constants of 4F to POPC/cholesterol LUVs as a function of the cholesterol percentage. Multi-site binding model with a POPC:4F stoichiometry of  $n = 1$ .



#### **Binding of the peptide P to lipid membranes**

Peptide P corresponds to a 4F dimer covalently bridged by a proline. It exhibits a greater *in vivo* HDL binding and anti-inflammatory potency [10]. In order to avoid aggregation of peptide P 10 % DMSO was added to the buffer. The experiments were performed with POPC LUVs as well as with SUVs. Lipid vesicles were filled into the syringe at a concentration of 3 mM (LUVs) and 1 mM (SUVs) and titrated into a solution of peptide P at a concentration of either 80 or 40  $\mu\text{M}$ . The ITC titration results at 40 °C and the integrated heat peaks are shown in Figure 22. Conspicuous is the devolution of the heat flow during the first injection steps. The enthalpy first decreased, increased for a short period and then decreased again. One may speculate that an initial micellization reaction is reversed as more lipid is added. The experimental binding isotherm of reactions with LUVs and SUVs at 40 °C led to a binding constant of the order of  $10^5 \text{ M}^{-1}$  which was about one order of magnitude larger than that of the smaller peptide 4F. However, the stoichiometry is quite different with 2 and 0.4 and also the accessible lipid percentage of 65 and 100 % for LUVs and SUVs, respectively. In comparison to 4F the enthalpy of reaction is much more exothermic in case of 4F (4F/LUVs:  $\Delta H = -5726$  vs. P/LUVs:  $\Delta H = -1751$  kcal/mol, P/SUVs:  $\Delta H = -3624$  kcal/mol, Table 3).

However, reaction conditions were different, due to the presence of DMSO in solutions of the peptide P. Therefore experiments were also done with 4F and POPC LUVs in buffer with and without DMSO at 40 °C.

### 3. Lipid binding of Apo A-1 mimetic peptides

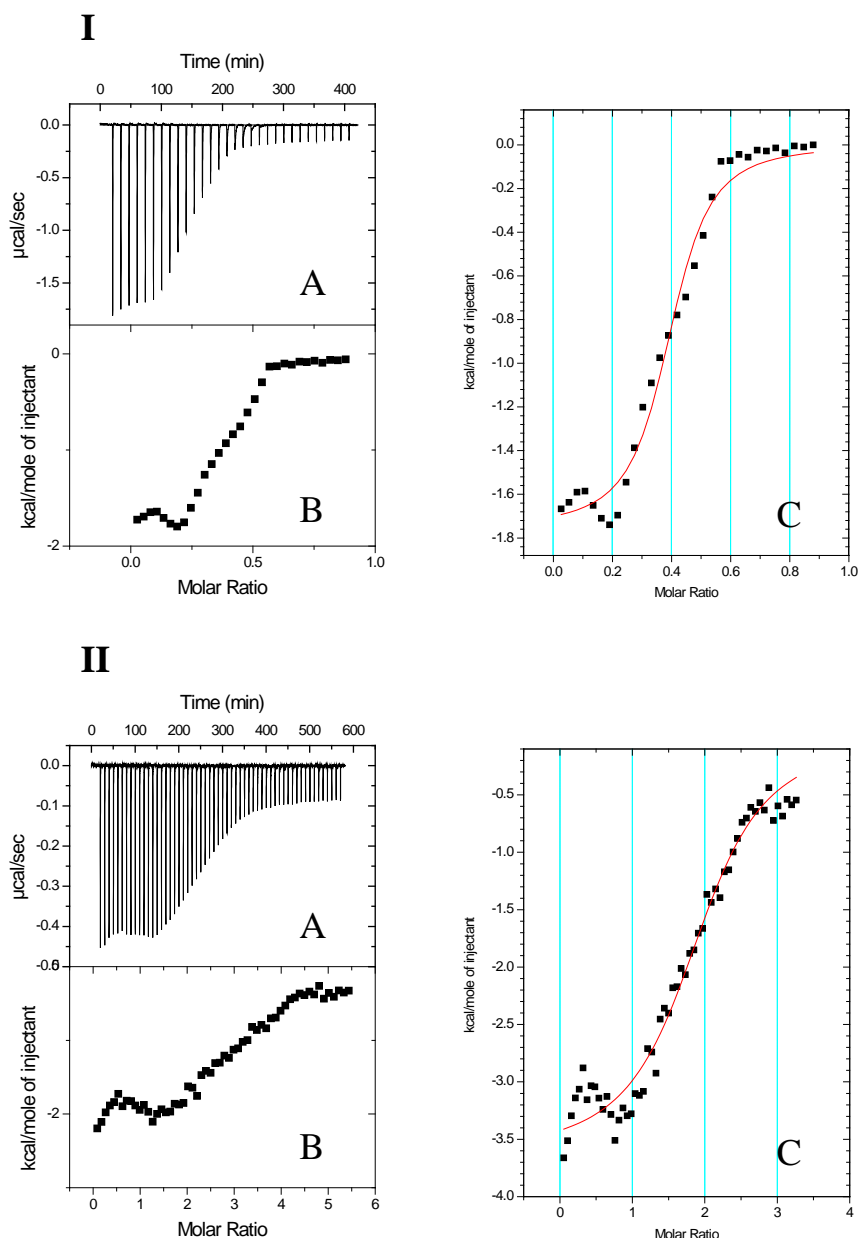


Figure 22: Titration of POPC LUVs and SUVs into peptide P at 40 °C. (A): Calorimetric traces were obtained by titration of POPC LUVs (I: 3 mM) and SUVs (II: 1 mM) into P (I: 80  $\mu$ M, II: 40  $\mu$ M). Each heat peak corresponds to injection of 10  $\mu$ L (I) and 5  $\mu$ L (II) lipids into the microcalorimeter cell. (B): Heats of reaction were obtained by integration of heat peaks and were plotted as a function of the peptide-to-lipid ratio. This experimentally obtained binding isotherm was fitted with a multisite-binding model (I:  $\Delta H = -1.75$  kcal/mol,  $K = 9.87 \cdot 10^4$ ,  $n = 0.4$ ; II:  $\Delta H = -3.62$  kcal/mol,  $K = 2.06 \cdot 10^5$ ,  $n = 2$ ) in (C). Buffer: 10 mM Heps + 10 % DMSO

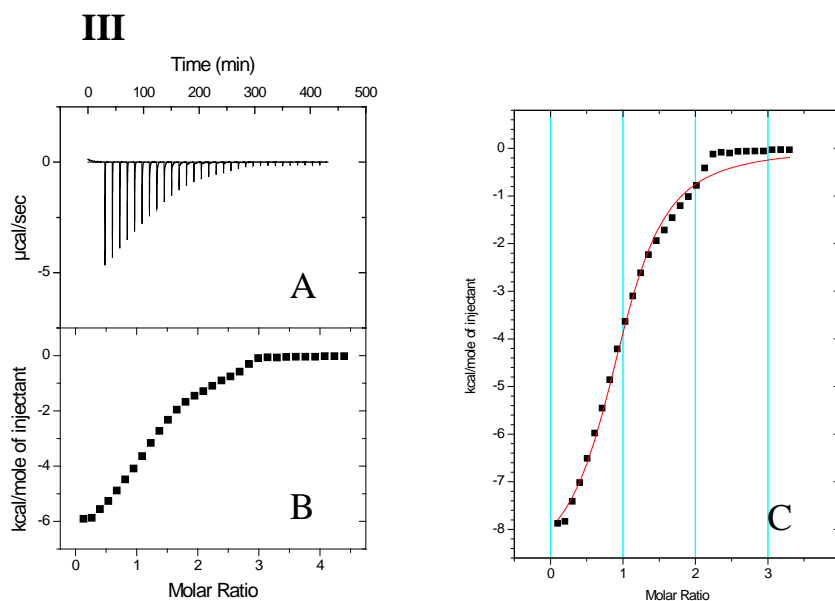


Figure 23: Titration of POPC LUVs into peptide 4F at 40 °C. (A): Calorimetric traces were obtained by titration of POPC LUVs (3 mM) and into 4F (160  $\mu$ M). Each heat peak corresponds to injection of 10  $\mu$ L lipids into the microcalorimeter cell. (B): Heats of reaction were obtained by integration of heat peaks and were plotted as a function of the peptide-to-lipid ratio. This experimentally obtained binding isotherm was fitted with a multisite-binding model ( $\Delta H = -8.93$  kcal/mol,  $K = 4.8 \cdot 10^4$ ,  $n = 1$ ) in (C). Buffer: 10 mM Hepes + 10 % DMSO.

Titration isotherms of 4F in the presence or absence of DMSO were very similar (0 % DMSO:  $K = 7.52 \cdot 10^4$  versus 10 % DMSO:  $K = 4.80 \cdot 10^4$   $M^{-1}$ ) at a stoichiometry of  $n = 1$ . The enthalpy was more exothermic in presence of DMSO in the buffer (-8926 versus -5726 kcal/mol), whereas the reaction entropy was dramatically smaller in the measurement with DMSO and changed sign (-7.09 versus 4.02  $\text{cal mol}^{-1} \text{K}^{-1}$ ).

Comparison of the same ITC experiments with SUVs and LUVs in buffer with 10 % DMSO injected into a solution of 4F at 40 °C yielded similar binding constants (SUVs:

### 3. Lipid binding of Apo A-1 mimetic peptides

$K = 3.84 \cdot 10^4$  vs. LUVs:  $K = 7.52 \cdot 10^4 \text{ M}^{-1}$ ) but quite different entropy and enthalpy values, consistent with earlier observations [34]. These results are similar to those obtained with the peptide P (SUVs:  $K = 2.06 \cdot 10^5$  vs. LUVs:  $K = 9.87 \cdot 10^4 \text{ M}^{-1}$ ). Nevertheless, more experiments are required before conclusive decisions can be made.

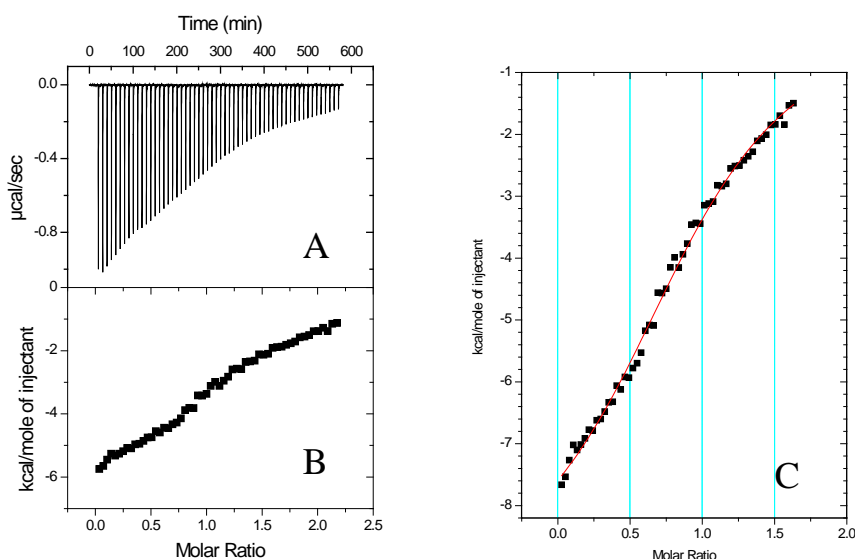


Figure 24: Titration of POPC SUVs into peptide 4F at 40 °C. (A): Calorimetric traces were obtained by titration of POPC SUVs (1 mM) into 4F (100  $\mu\text{M}$ ). Each heat peak corresponds to injection of 5  $\mu\text{L}$  lipids into the microcalorimeter cell. (B): Heats of reaction were obtained by integration of heat peaks and were plotted as a function of the peptide-to-lipid ratio. This experimentally obtained binding isotherm was fitted with a multisite-binding model ( $\Delta H = -9.52 \text{ kcal/mol}$ ,  $K = 3.84 \cdot 10^4$ ,  $n = 1$ ) in (C). Buffer: 10 mM HEPES + 10 mM DMSO.

### 3. Lipid binding of Apo A-1 mimetic peptides

Table 3: Summary of different ITC measurements with 4F and P together with POPC lipids at different reaction conditions. The thermodynamic parameters are listed on the right hand side of the table. Thermograms having a bad quality in terms of a sigmoidal binding isotherm are labeled by a star in the last column, but are listed anyway for the sake of completeness.

peptide	c(peptide) <i>μM</i>	c(POPC(+Chol)) <i>mM</i>	c(Chol) %	T °C	buffer	DMSO %	vesicles	ΔH <i>cal/mol</i>	n	Lipid %	K	ΔS <i>cal/mol/K</i>
4F	200	5	0	40	PBS	0	LUV	-5726	1	70	7.52E+04	4.02
4F	200	5	5	40	PBS	0	LUV	-4064	1	80	6.40E+04	9.01
4F	200	5	10	40	PBS	0	LUV	-3530	1	100	4.20E+04	9.88
4F	200	5	20	40	PBS	0	LUV	-2672	1	100	1.49E+04	10.6
4F	200	5	0	5	PBS	0	LUV	-423	1	70	1.51E+05	22.2
4F	200	5	0	15	PBS	0	LUV	-1776	1	65	3.65E+04	14.7
4F	200	5	0	25	PBS	0	LUV	-3138	1	90	1.99E+04	9.15
4F	200	5	0	35	PBS	0	LUV	-4506	1	80	2.98E+04	5.85
4F	200	5	0	45	PBS	0	LUV	-5559	1	90	7.49E+04	4.82
4F	100	1	0	40	HEPES	10	SUV	-9518	1	75	3.84E+04	9.41*
P	40	1	0	40	HEPES	10	SUV	-3624	2	65	2.06E+05	12.7
4F	160	3	0	40	HEPES	10	LUV	-8926	1	75	4.80E+04	-7.09
P	80	3	0	40	HEPES	10	LUV	-1751	0.4	100	9.87E+04	17.3

## 1. Discussion

### *Self-association*

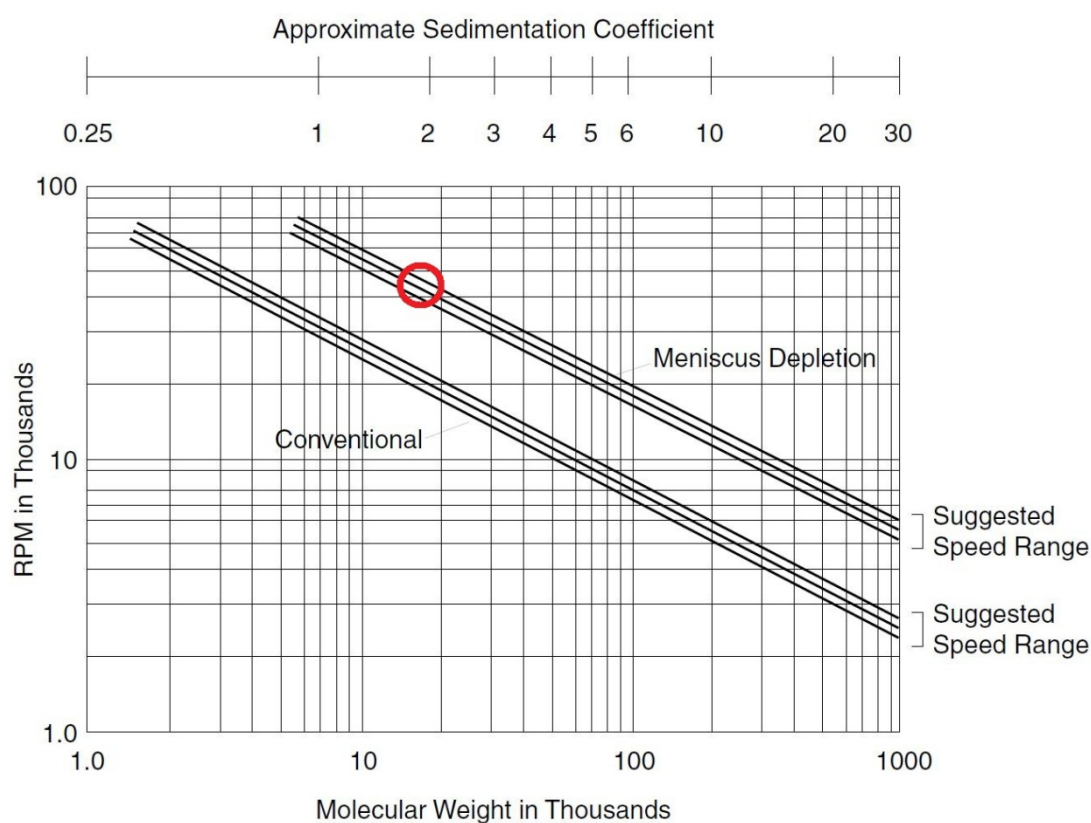


Figure 25: Illustration of suitable velocities regarding analytical ultracentrifuge measurements seen in the manual of the Beckman centrifuge. The red circle shows the conditions used in the experiment shown in Figure 6.

4F dissolved in 10 mM HEPES buffer without salt does not aggregate up to a concentration of 200  $\mu$ M. The same holds true for the peptide dissolved in PBS buffer as evidenced by the DLS and AUC measurements. However, as depicted in Figure 25 by the red circle at 42 krpm, sedimentation would not occur up to a molecular mass of

approximately 18 kDa. Thus peptide associates up to the size of octamers could still be present. This agrees with results obtained by DLS which excludes associates larger than hexamers. There are two possible types of self-associates. Firstly it could be reversible association equilibrium between monomers and oligomers depending on concentration and secondly, it could be an irreversible aggregation of peptide molecules. By diluting a reversible self-associate in a high sensitivity microcalorimeter, heat release of the dissociation reaction can be detected, like it has been described for self-associated Apo A-1 proteins (Chapter 3). Since most lipid binding experiments with ITC were performed at 40 °C, where no dissociation reaction could be detected this could not have biased our lipid binding results obtained by ITC.

#### *Lipid binding*

The binding of peptides 4F and P to POPC lipid vesicles was demonstrated by different types of experiments. The blueshift of the tryptophan fluorescence, the circular dichroism data as well as the ITC binding isotherms indicate consistently binding of the peptides to lipid membranes. Binding constants are of the order of  $10^4 \text{ M}^{-1}$  for the peptide 4F and  $\approx 10^5 \text{ M}^{-1}$  for peptide P.

The thermodynamic parameters of the two peptides 4F and P were derived under slightly different conditions, due to the presence of DMSO in P-solutions. However, for 4F binding to POPC LUVs the binding isotherms and derived binding constants were similar with or without DMSO in buffer (Table 3). In contrast, the reaction enthalpy and entropy differed clearly. The thermodynamic parameter of peptide binding to LUVs and SUVs were also different. This might be due to the less monodisperse characteristics of our POPC SUVs (PDI about 0.3) compared to the LUV preparations (PDI about 0.025).

### 3. Lipid binding of Apo A-1 mimetic peptides

---

4F Experiments done in the same buffer with the same temperature showed slightly smaller binding constants with lipids arranged in SUVs compared to those with LUVs.

The binding constants of 4F to LUVs decreased with the percentage of cholesterol, while the reaction enthalpy was less exothermic (Figure 21). This is surprising since Apo A-1 and mimetic peptides are involved in cholesterol transport and –turnover. However, binding studies with cholesterol incorporated into cyclodextrin cavities, suggested binding of the peptide to cholesterol (Figure 19). A possible explanation would be that the affinity of the peptides to POPC lipids is strong to build HDL like particles, which bind weakly to cholesterol *in vivo*. Weak binding could be necessary to get rid of excess cholesterol for example at the liver to fulfill the function as a carrier through the blood stream.

#### Thermodynamic interpretation

The measured overall enthalpy as derived from ITC measurements with 4F and POPC LUVs is about -5.7 kcal/mol. Three different effects contribute to this measured value.

1. A random coil/ $\beta$ -sheet&turn to  $\alpha$ -helical transition, 2. hydrophobic interactions and 3. solvation of lipid vesicles. In the following each of these processes will be considered energetically.

The results obtained by circular dichroism spectroscopy suggest a transition of random coil/ $\beta$ -sheet&turn segments to  $\alpha$ -helical segments as driving force of lipid binding, like it is known from other peptides (penetratin [35], melittin [36]). Thermodynamically, we assume  $\beta$ -sheet and  $\beta$ -turn structure to be the same. The random coil to  $\alpha$ -helix transition was investigated by Meier et al. and is known to be exothermic with approximately -800 cal/mol-residue. The  $\beta$ -sheet to random coil transition releases



between 0 - -600 cal/mol-residue, depending on the length of the segments [37, 38]. Multiplication of the changed fraction of secondary structural elements ( $\alpha$ -helix  $\rightarrow$  random coil;  $\beta$ -sheet  $\rightarrow$  random coil) with the total residue number yields the number of changed segments ( $n = 5.22$ ). Together with the above mentioned enthalpies this results in a transition enthalpy between -1.9 - -4.0 kcal/mol. The less exothermic the  $\beta$ -sheet to random coil transition enthalpy is assumed the more exothermic is the sum of the transition enthalpies.

The ITC-results of the temperature dependence of reaction enthalpy showed clearly a negative change of heat capacity, meaning hydrophobic interactions are part of the driving force leading to lipid binding.

The third process contributing to the measured reaction enthalpy is the micellization of lipid vesicles as proven by static light scattering. In case of POPC LUVs the process is endothermic with about 1.85 kcal/mol as investigated by Heerklotz et al. [39]. Subtracting this micellisation enthalpy of the measured reaction enthalpy remains -7.55 kcal/mol for the enthalpy of hydrophobic interactions and the secondary structural transition enthalpy. Subtraction of the transition enthalpy resulted in -3.55 - -5.65 kcal/mol accounting for hydrophobic interactions.

The transition of random-coil and  $\beta$ -sheet to  $\alpha$ -helical secondary structural elements and hydrophobic interactions could clearly be addressed as driving force of 4F's lipid binding. Yet balancing the percentage of each process was not achieved.

## References

1. Tall AR: **An overview of reverse cholesterol transport.** *Eur Heart J* 1998, **19 Suppl A**:A31-35.
2. Segrest JP, Garber DW, Brouillette CG, Harvey SC, Anantharamaiah GM: **The amphipathic alpha helix: a multifunctional structural motif in plasma apolipoproteins.** *Adv Protein Chem* 1994, **45**:303-369.
3. Segrest JP, Jackson RL, Morrisett JD, Gotto AM, Jr.: **A molecular theory of lipid-protein interactions in the plasma lipoproteins.** *FEBS Lett* 1974, **38(3)**:247-258.
4. Mendez AJ, Anantharamaiah GM, Segrest JP, Oram JF: **Synthetic amphipathic helical peptides that mimic apolipoprotein A-I in clearing cellular cholesterol.** *J Clin Invest* 1994, **94(4)**:1698-1705.
5. Venkatachalapathi YV, Phillips MC, Epanand RM, Epanand RF, Tytler EM, Segrest JP, Anantharamaiah GM: **Effect of end group blockage on the properties of a class A amphipathic helical peptide.** *Proteins* 1993, **15(4)**:349-359.
6. Datta G, Chaddha M, Hama S, Navab M, Fogelman AM, Garber DW, Mishra VK, Epanand RM, Epanand RF, Lund-Katz S *et al*: **Effects of increasing hydrophobicity on the physical-chemical and biological properties of a class A amphipathic helical peptide.** *J Lipid Res* 2001, **42(7)**:1096-1104.
7. Sherman CB, Peterson SJ, Frishman WH: **Apolipoprotein A-I mimetic peptides: a potential new therapy for the prevention of atherosclerosis.** *Cardiol Rev* 2010, **18(3)**:141-147.

8. Chung BH, Anantharamaiah GM, Brouillette CG, Nishida T, Segrest JP: **Studies of synthetic peptide analogs of the amphipathic helix. Correlation of structure with function.** *J Biol Chem* 1985, **260**(18):10256-10262.
9. Yancey PG, Bielicki JK, Johnson WJ, Lund-Katz S, Palgunachari MN, Anantharamaiah GM, Segrest JP, Phillips MC, Rothblat GH: **Efflux of cellular cholesterol and phospholipid to lipid-free apolipoproteins and class A amphipathic peptides.** *Biochemistry* 1995, **34**(24):7955-7965.
10. Wool GD, Vaisar T, Reardon CA, Getz GS: **An apoA-I mimetic peptide containing a proline residue has greater in vivo HDL binding and anti-inflammatory ability than the 4F peptide.** *J Lipid Res* 2009, **50**(9):1889-1900.
11. Nissen SE, Tsunoda T, Tuzcu EM, Schoenhagen P, Cooper CJ, Yasin M, Eaton GM, Lauer MA, Sheldon WS, Grines CL *et al*: **Effect of recombinant ApoA-I Milano on coronary atherosclerosis in patients with acute coronary syndromes: a randomized controlled trial.** *Jama* 2003, **290**(17):2292-2300.
12. Ou J, Ou Z, Jones DW, Holzhauser S, Hatoum OA, Ackerman AW, Weihrauch DW, Gutterman DD, Guice K, Oldham KT *et al*: **L-4F, an apolipoprotein A-1 mimetic, dramatically improves vasodilation in hypercholesterolemia and sickle cell disease.** *Circulation* 2003, **107**(18):2337-2341.
13. Peterson SJ, Husney D, Kruger AL, Olszanecki R, Ricci F, Rodella LF, Stacchiotti A, Rezzani R, McClung JA, Aronow WS *et al*: **Long-term treatment with the apolipoprotein A1 mimetic peptide increases antioxidants and vascular repair in type I diabetic rats.** *J Pharmacol Exp Ther* 2007, **322**(2):514-520.
14. Peterson SJ, Kim DH, Li M, Positano V, Vanella L, Rodella LF, Piccolomini F, Puri N, Gastaldelli A, Kusmic C *et al*: **The L-4F mimetic peptide prevents**

### 3. Lipid binding of Apo A-1 mimetic peptides

---

- insulin resistance through increased levels of HO-1, pAMPK, and pAKT in obese mice.** *J Lipid Res* 2009, **50**(7):1293-1304.
15. Peterson SJ, Drummond G, Kim DH, Li M, Kruger AL, Ikehara S, Abraham NG: **L-4F treatment reduces adiposity, increases adiponectin levels, and improves insulin sensitivity in obese mice.** *J Lipid Res* 2008, **49**(8):1658-1669.
16. Bloedon LT, Dunbar R, Duffy D, Pinell-Salles P, Norris R, DeGroot BJ, Movva R, Navab M, Fogelman AM, Rader DJ: **Safety, pharmacokinetics, and pharmacodynamics of oral apoA-I mimetic peptide D-4F in high-risk cardiovascular patients.** *J Lipid Res* 2008, **49**(6):1344-1352.
17. Watson CE, Weissbach N, Kjems L, Ayalasomayajula S, Zhang Y, Chang I, Navab M, Hama S, Hough G, Reddy ST *et al*: **Treatment of patients with cardiovascular disease with L-4F, an apo-A1 mimetic, did not improve select biomarkers of HDL function.** *J Lipid Res* 2011, **52**(2):361-373.
18. Ziegler A, Seelig J: **Contributions of glycosaminoglycan binding and clustering to the biological uptake of the nonamphipathic cell-penetrating peptide WR9.** *Biochemistry* 2011, **50**(21):4650-4664.
19. Ziegler A, Seelig J: **Binding and clustering of glycosaminoglycans: a common property of mono- and multivalent cell-penetrating compounds.** *Biophys J* 2008, **94**(6):2142-2149.
20. Klocek G, Seelig J: **Melittin interaction with sulfated cell surface sugars.** *Biochemistry* 2008, **47**(9):2841-2849.
21. Sreerama N, Woody RW: **Estimation of protein secondary structure from circular dichroism spectra: comparison of CONTIN, SELCON, and CDSSTR methods with an expanded reference set.** *Anal Biochem* 2000, **287**(2):252-260.

- 
22. Jayaraman S, Abe-Dohmae S, Yokoyama S, Cavigliolo G: **Impact of self-association on function of apolipoprotein A-I.** *J Biol Chem* 2011, **286**(41):35610-35623.
  23. Vitello LB, Scanu AM: **Studies on human serum high density lipoproteins. Self-association of apolipoprotein A-I in aqueous solutions.** *J Biol Chem* 1976, **251**(4):1131-1136.
  24. Swaney JB, O'Brien K: **Cross-linking studies of the self-association properties of apo-A-I and apo-A-II from human high density lipoprotein.** *J Biol Chem* 1978, **253**(19):7069-7077.
  25. Gianazza E, Calabresi L, Santi O, Sirtori CR, Franceschini G: **Denaturation and self-association of apolipoprotein A-I investigated by electrophoretic techniques.** *Biochemistry* 1997, **36**(25):7898-7905.
  26. Beck A, Li-Blatter X, Seelig A, Seelig J: **On the interaction of ionic detergents with lipid membranes. Thermodynamic comparison of n-alkyl-+N(CH) and n-alkyl-SO.** *J Phys Chem B* 2010, **114**(48):15862-15871.
  27. Lakowicz JR: **Principles of fluorescence spectroscopy**, 3rd edn. New York: Springer; 2006.
  28. Ladokhin AS, Jayasinghe S, White SH: **How to measure and analyze tryptophan fluorescence in membranes properly, and why bother?** *Anal Biochem* 2000, **285**(2):235-245.
  29. Ziegler A, Blatter XL, Seelig A, Seelig J: **Protein transduction domains of HIV-1 and SIV TAT interact with charged lipid vesicles. Binding mechanism and thermodynamic analysis.** *Biochemistry* 2003, **42**(30):9185-9194.

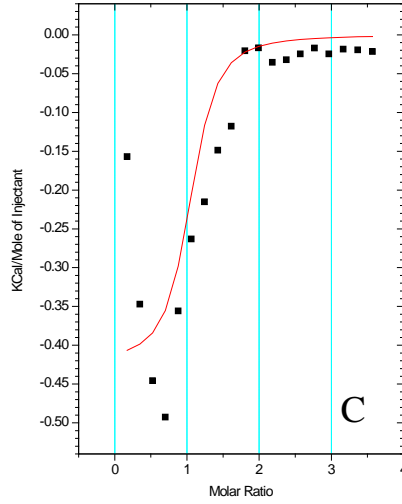
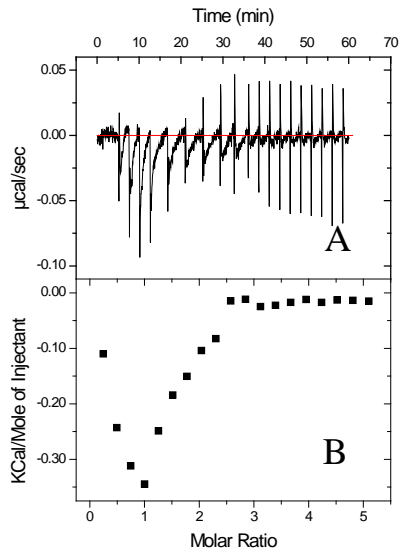
### 3. Lipid binding of Apo A-1 mimetic peptides

---

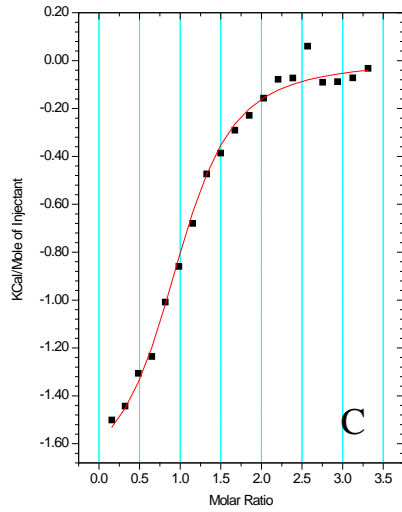
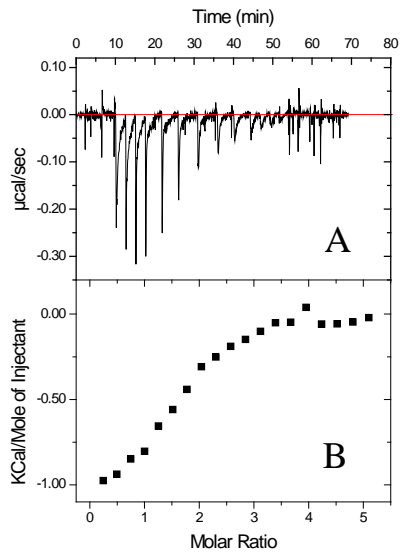
30. Murphy KP, Privalov PL, Gill SJ: **Common features of protein unfolding and dissolution of hydrophobic compounds.** *Science* 1990, **247**(4942):559-561.
31. Connelly PR, Thomson JA: **Heat capacity changes and hydrophobic interactions in the binding of FK506 and rapamycin to the FK506 binding protein.** *Proc Natl Acad Sci U S A* 1992, **89**(11):4781-4785.
32. Tsamaloukas A, Szadkowska H, Slotte PJ, Heerklotz H: **Interactions of cholesterol with lipid membranes and cyclodextrin characterized by calorimetry.** *Biophys J* 2005, **89**(2):1109-1119.
33. Heerklotz H, Szadkowska H, Anderson T, Seelig J: **The sensitivity of lipid domains to small perturbations demonstrated by the effect of Triton.** *J Mol Biol* 2003, **329**(4):793-799.
34. Seelig J: **Thermodynamics of lipid-peptide interactions.** *Biochim Biophys Acta* 2004, **1666**(1-2):40-50.
35. Persson D, Thoren PE, Lincoln P, Norden B: **Vesicle membrane interactions of penetratin analogues.** *Biochemistry* 2004, **43**(34):11045-11055.
36. Vogel H: **Incorporation of melittin into phosphatidylcholine bilayers. Study of binding and conformational changes.** *FEBS Lett* 1981, **134**(1):37-42.
37. Meier M, Seelig J: **Length dependence of the coil <--> beta-sheet transition in a membrane environment.** *J Am Chem Soc* 2008, **130**(3):1017-1024.
38. Meier M, Seelig J: **Thermodynamics of the coil <==> beta-sheet transition in a membrane environment.** *J Mol Biol* 2007, **369**(1):277-289.
39. Heerklotz H, Seelig J: **Titration calorimetry of surfactant-membrane partitioning and membrane solubilization.** *Biochim Biophys Acta* 2000, **1508**(1-2):69-85.

Appendix

**I**



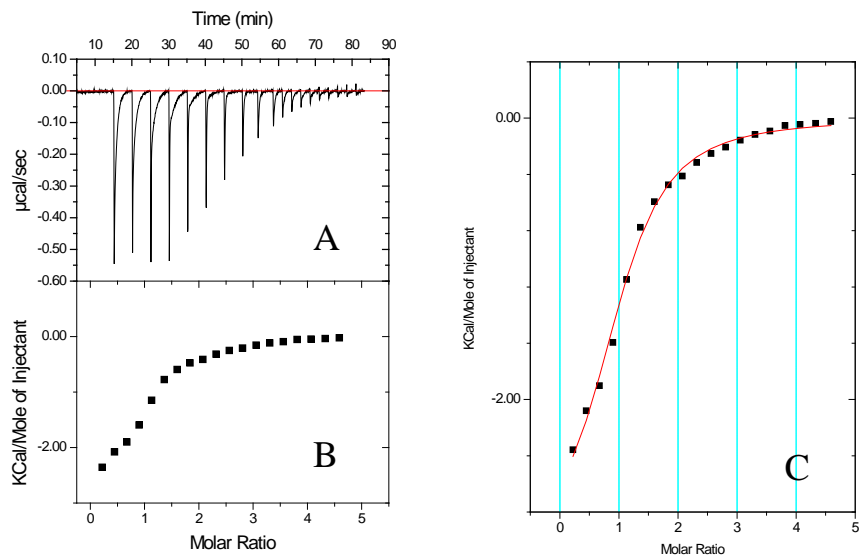
**II**



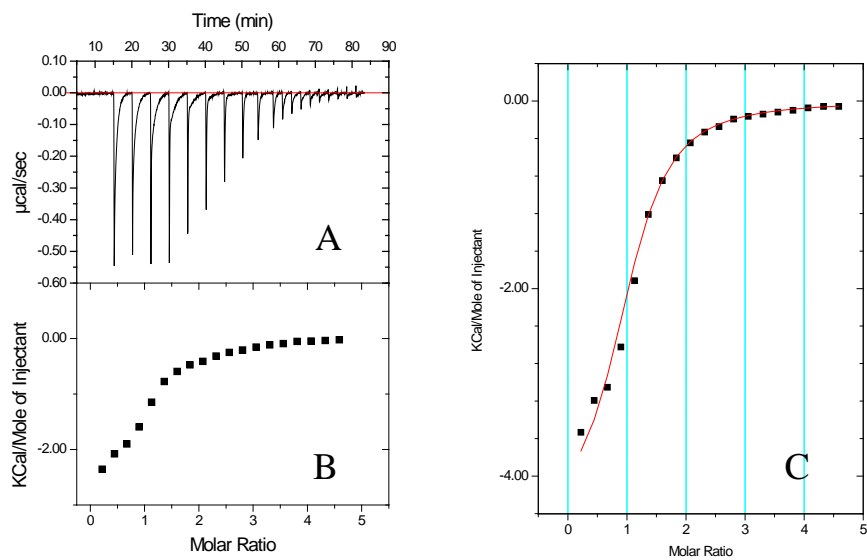
### 3. Lipid binding of Apo A-1 mimetic peptides

---

#### III



#### IV





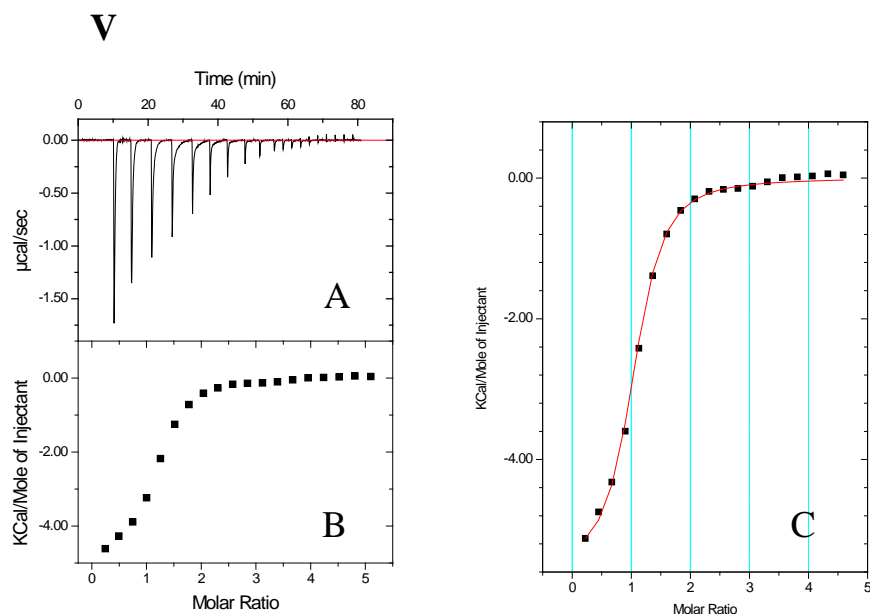
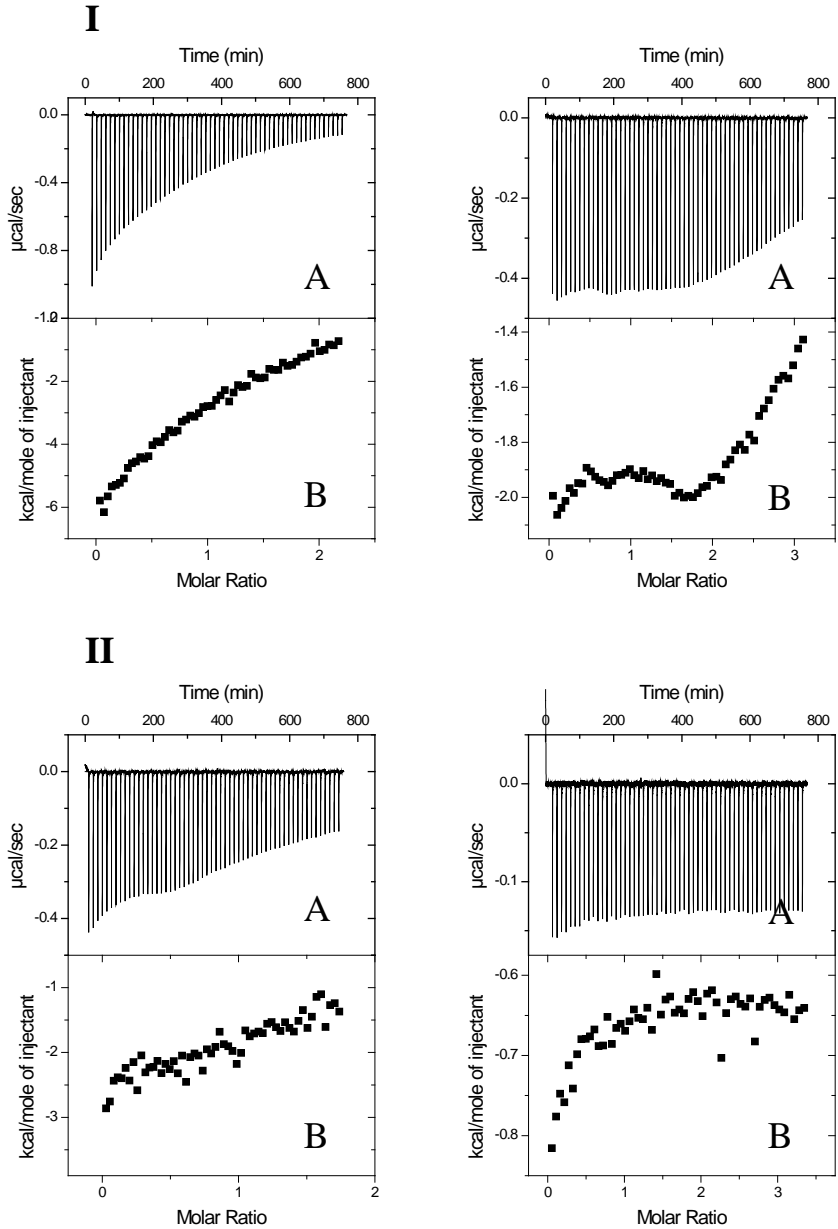


Figure 1: Titration of POPC LUVs into peptide 4F at 5 °C (I), 15 °C (II), 25 °C (III), 35 °C (IV) and 45 °C (V). (A): Calorimetric traces were obtained by titration of POPC LUVs (5 mM) into 4F (200 µM). Each heat peak corresponds to injection of 2 µL lipids into the microcalorimeter cell. (B): Heats of reaction were obtained by integration of heat peaks and were plotted as a function of the peptide-to-lipid ratio. This experimentally obtained binding isotherm was fitted with a multisite-binding model (I:  $\Delta H = -0.42$  kcal/mol,  $K = 3.81 \cdot 10^4$ ,  $n = 1$ ; II:  $\Delta H = -1.78$  kcal/mol,  $K = 3.90 \cdot 10^4$ ,  $n = 1$ ; III:  $\Delta H = -3.14$  kcal/mol,  $K = 4.05 \cdot 10^4$ ,  $n = 1$ ; IV:  $\Delta H = -4.51$  kcal/mol,  $K = 4.28 \cdot 10^4$ ,  $n = 1$ ; V:  $\Delta H = -5.56$  kcal/mol,  $K = 4.59 \cdot 10^4$ ,  $n = 1$ ) in (C). Buffer: PBS + 0.02 % NaN<sub>3</sub>

3. Lipid binding of Apo A-1 mimetic peptides



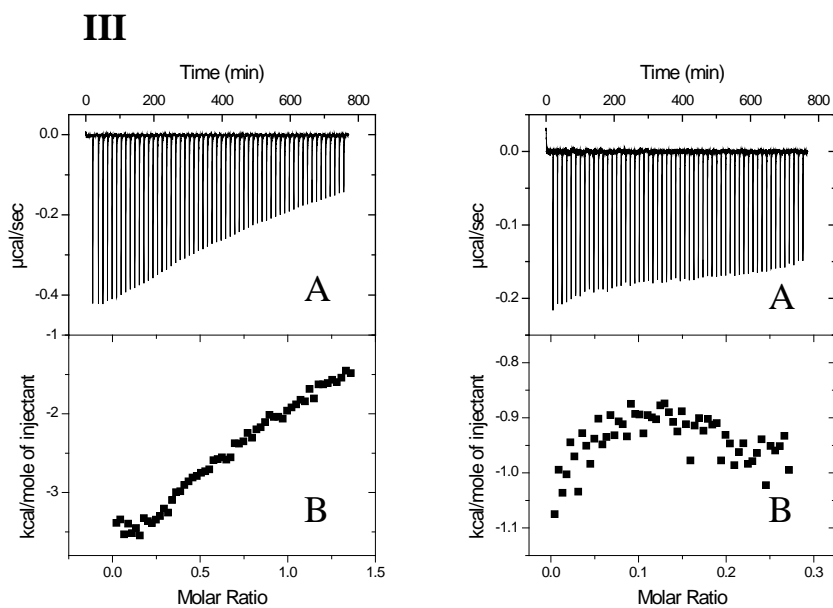


Figure 2: Titration of POPC SUVs into peptide 4F and P at 40 °C. (A) Calorimetric traces were obtained by titration of POPC SUVs (1 mM) into 4F (I: 100  $\mu$ M, III: 125  $\mu$ M, V: 160  $\mu$ M) and P (II: 70  $\mu$ M, IV: 65  $\mu$ M, VI: 80  $\mu$ M). Each heat peak corresponds to injection of 5  $\mu$ L lipids into the microcalorimeter cell. (B) Heats of reaction were obtained by integration of heat peaks and were plotted as a function of the peptide-to-lipid ratio. Buffer: 10 mM Hepes + 10 % DMSO.



## **4. Towards understanding of the allocrite specificity of the lipid floppase ABCA1**

Biozentrum, University of Basel, Div. of Biophysical Chemistry, Klingelbergstrasse  
50/70, CH-4056 Basel, Switzerland

## **Preliminary manuscript**

### **Abstract**

ATP binding cassette transporter A1 (ABCA1) plays a key role in reverse cholesterol transport (RCT). Disorders of the RCT are affecting a large number of patients in form of atherosclerosis. ABCA1 flopps cholesterol from the inner to the outer membrane leaflet, where it is accepted by apolipoprotein A 1 (Apo A-1) and thus controls cholesterol homeostasis. Furthermore the transporter was reported to transport phosphocholines and vitamin E. This was mainly investigated in animal models and cell culture experiments. To further explore the ABCA1/allocrite interaction, the ATPase activity of inside-out vesicles obtained from ABCA1 transfected HEK293 cells was measured by means of a quantitative phosphate release assay. The specificity of the transporter was investigated by titration with putative allocrits of different chemical classes. Amphipatic compounds that carried a polyethyleneglycol (PEG) chain, a heterocyclic group and a hydrocarbon tail such as Tween80, Tween40 and the vitamin E derivatives TPGS400 and TPGS1000 showed increased activity of ABCA1. On the other hand, the stilbene derivatives DIDS and resveratrol decreased the activity of ABCA1 in a concentration dependent manner. Basal activity could not be inhibited by vanadate but aluminum fluorides were found to be strong inhibitors of the nucleotide binding sites (NBDs) of ABCA1. The present data shows that the activity of ABCA1 can be enhanced or reduced in a concentration dependent manner with a relatively broad variety of substances.

## Introduction

Atherosclerosis is a syndrome affecting a large number of people worldwide. Since blood high-density lipoprotein (HDL) levels are inversely correlated to cardiovascular disease, factors associated with HDL metabolism are atheroprotective. One of these factors is the ATP-binding cassette transporter A1 (ABCA1). It is a 220 kDa integral membrane protein consisting of two transmembrane domains (TMDs) and two nucleotide-binding domains (NBDs). The catalytic cycle is assumed to be driven by ATP binding and hydrolysis. ABCA1 plays an essential role in the handling of cellular lipids. By promoting the transport of membrane phospholipids and cholesterol to lipid poor apolipoprotein acceptors, ABCA1 controls the formation of HDL and thus the whole process of cholesterol transport [1-3]. Cholesterol is an essential component of eukaryotic cells, at the same time however, hyper-accumulation of cholesterol is harmful. ABCA1 is mainly located on the plasma membrane but due to endocytosis and resecretion (retroendocytosis) of Apolipoprotein A-1 (Apo A-1) the transporter might also play a role in cellular lipid handling [4] and forming of HDL by pumping lipids into the vesicular lumen in which Apo A-1 is captured [5].

Naturally occurring mutations in the *ABCA1* gene cause Tangier disease, an autosomal recessive disorder of lipid metabolism and familial HDL deficiency [1]. The latter is mainly differentiated to Tangier disease by transmission as a dominant trait [1, 6-9].

Regulation of the transporter takes place on transcriptional and posttranscriptional levels. The ABCA1 protein has a rapid turnover with a half-life of ABCA1 that was reported to be less than one hour in murine macrophage cells [10]. So far ABCA1 is mainly known to control lipid homeostasis by tight regulation of its protein level [11].

#### 4. Towards understanding of the allocrite specificity of the lipid floppase ABCA1

---

In detail, induction of *ABCA1* occurs by overloading cells with cholesterol through activation of the nuclear receptors liver X receptor (LXR) and retinoid X receptor (RXR) [11]. ABCA1 protein levels also seem to be controlled by a degradation process [12-14]. As many proteins with a short life time ABCA1 is characterized by PEST sequences. The PEST motif features a proline (P), glutamate (E), serine (S), and threonine (T) sequence, and is usually flanked by lysine (K), arginine (R), or histidine (H) residues. A calpain protease seems to degrade the transporter via recognition of the PEST motifs. However, ABCA1 protein seems to be stabilized by ligands such as Apolipoprotein A-1 (Apo A-1). Apo A-1 binds directly to the transporter yielding increased ABCA1 protein levels but not mRNA levels [15].

ABCA1 is expressed ubiquitously. However, cholesterol accumulation principally takes place in macrophages in the case of ABCA1 dysfunction [1]. Macrophages having accumulated plenty of cholesterol are called foam cells. Atheroma development and foam cell formation are significantly influenced by the expression level of ABCA1 in macrophages but largely independent of circulating HDL levels [1, 16, 17].

A large number of studies were performed with ABCA1 either in cell culture or in clinical and animal trials. Nevertheless, detailed knowledge of the molecular function of ABCA1 as a membrane floppase is still lacking. The knowledge on molecules likely to be handled by the transporter was derived from experiments with polarized Caco-2 and various other cell monolayers, respectively. In most studies merely transport of cholesterol, phospholipids and vitamin E was investigated. The transport of phospholipids and cholesterol by ABCA1 was either assessed by transport assays with radioactively labeled compounds, detected in the extracellular medium or in acceptor particles like Apolipoprotein A-1/HDL [1, 18-19]. Transport of vitamin E and A was measured in bi-directional transport assays [1, 20]. While transport assays reveal the



#### 4. Towards understanding of the allocrite specificity of the lipid floppase ABCA1

---

apparent or net transport ATPase measurements reflect the effective transport (flopping rate) of ABCA1 [21]. Takahashi et al. present the only study of ABCA1 produced in insect cells and reconstituted in model membranes [22]. The transporter showed ATPase activity reconstituted in vesicles composed of different lipids and lipid mixtures (e.g. PC, PS and PG) as well as in a detergent-soluble form. The effect of other sterol compounds as well as cholesterol was tested by reconstituting ABCA1 in liposomes with a single concentration of the sterol compounds (20 %) as membrane constituent. A mild inhibitory effect was observed for all investigated sterols.

Here, we investigated ABCA1 in inside-out plasma membrane vesicles of *ABCA1*-transfected HEK293 cells using a spectroscopic phosphate assay. The advantage of plasma membranes is that the protein remains embedded in its natural environment, in the proper orientation and conformation. In order to get more insight into the allocrite specificity of the transporter we chose a variety of different structures. The selected molecules have either structural similarities to well-known ABCA1 substrates such as cholesterol and phosphocholines (lyso-phosphocholines, phosphocholines, vitamin E, TPGS, estradiol) or are allocrites of other ABC transporters like P-glycoprotein (detergents). In some cases substances belong to both categories. In contrast to previous studies we also used compounds of other chemical groups such as detergents. Furthermore, all compounds were measured over a broad concentration range.

## Materials and methods

### Cell lines and cell culture

The human embryo kidney cells Flp In HEK293 (HEK293-WT) transfected with the human *ABCA1* gene (HEK293-ABCA1) were generously provided by Matthew Wright from F. Hoffmann-La Roche Ltd., Basel. The mRNA level of the ABCA1 transporter was 21000 fold higher in transfected than in untransfected cells, in which the transporter is essentially undetected. An ABCA1 protein level of transfected cells was estimated by Wright et al. on basis of a cholesterol efflux activity assay. The pump rate was approximated by one molecule cholesterol per transporter per second. The result is a protein level of  $10^5$  ABCA1 transporters per cell.

Cells were maintained in monolayer culture in sterile culture flasks (Costar, 25–75 cm<sup>2</sup>) at 37 °C in an air atmosphere containing CO<sub>2</sub> (5 %) and featuring a humidity saturation of 100 %. DMEM medium was supplemented with fetal bovine serum (10 % v/v), penicillin (100 units/ml), streptomycin (100 ug/ml) and L-glutamine (146 mg/L). The transfected cells were grown in presence of the selection antibiotic Hygromycin B (100 ug/ml). Both cell lines were passaged every 3-4 days. Cell counting was performed with a hemocytometer.

### **Plasma Membrane Vesicle Preparation**

Cells were washed with PBS buffer and scraped in ice-cold PBS, charged with protease inhibitors (1 tablet/50 ml buffer). For lysis the cells were washed with hypotonic lysis buffer (10 mM Tris-HCl, pH 7.5, 10 mM NaCl, 1 mM MgCl<sub>2</sub>, 1 protease inhibitor cocktail tablet/50 mL) and were centrifuged at 2100 g<sub>max</sub> for 10 min at 4 °C. The pellet was resuspended in lysis buffer (1.25 ml per each 15 cm dish). Cell disruption was performed at 400 bar in a “One Shot” cell disrupter (Constant Systems Ltd., Warwickshire, U.K.). The cell lysate was then diluted 1:1 with ice-cold isotonic buffer (10 mM Tris-HCl, pH 7.4, 250 mM sucrose, 50 mM N-methyl-D-glucamine, NMDG, 1 protease inhibitor cocktail tablet/50 mL buffer). Unbroken cells and the nuclei were precipitated by centrifugation at 800 g<sub>max</sub> for 10 min at 4 °C. Afterwards mitochondria were removed by centrifugation at 6000 g<sub>max</sub> for 10 min at 4 °C. The crude membranes were pelleted with the last centrifugation step at 100000 g<sub>max</sub> for 1 hour at 4 °C. The pellet was resuspended with the isotonic buffer and homogenized by aspiration and dispersion cycles with a 23-gauge syringe. The preparation was frozen rapidly in liquid nitrogen and stored at -80 °C. The overall protein content of the membranes was determined to be  $8.6 \pm 2.7$  mg/ml (average of different preparations) by a BCA protein assay with bovine serum albumin as standard.

### **Linearity of the ATP-hydrolysis**

The linearity of the ATP hydrolysis was checked by a slightly modified phosphate release assay. Three samples of each 4.5 ml phosphate release mixtures were placed in a water bath at 37 °C and aliquots of 100 uL were removed at different times. The

#### 4. Towards understanding of the allocrite specificity of the lipid floppase ABCA1

---

reaction of those aliquots was immediately quenched by cooling in an ice-bath and addition of 333  $\mu\text{L}$  stop solution. After subsequent incubation at room temperature at 37  $^{\circ}\text{C}$  for 30 min and transfer of 260  $\mu\text{L}$  to a 96-well microtiter plate (Nunc F96 MicroWell plate, nontreated) the formed phosphate molybdate complex was measured at 820 nm in a Spectramax M2 (Molecular Device, Sunnyvale, CA).

#### **Phosphate release assay**

The inorganic phosphate release of the ABCA1 ATPase was measured according to Litman et al. (1997) and Äänisma et al. (2008) [23-25] in 96-well microtiter plates (Nunc F96 MicroWell plate, nontreated, wells at the border were not considered for analysis) with small modifications. The crude membranes were thawed and diluted to 0.1 mg/ml protein concentration in ice-cold phosphate release assay buffer (25 mM Tris-HCl including 50 mM KCl, 3 mM ATP, 2.5 mM  $\text{MgSO}_4$ , 3 mM DTT, 0.5 mM EGTA, 2 mM ouabain, and 3 mM sodium azide, pH 7.0). The total assay volume was 60  $\mu\text{L}$ /well, containing 5  $\mu\text{g}$ /well of protein. The reaction with and without possible allocrites was started by transferring the plate into a water bath kept at 37  $^{\circ}\text{C}$  for 1 hour and was quenched by rapidly cooling the plate on ice and the addition of an ice-cold stopping solution (200  $\mu\text{L}$ /well, ammonium molybdate (0.2% (w/v)), sulfuric acid (1.43% (v/v)), freshly prepared ascorbic acid (1% (w/v)), and SDS (0.9% (w/v))). The concentration of inorganic phosphate ( $\text{P}_i$ ), resulting from the hydrolysis of ATP was determined by colorimetric quantification after 30 min incubation at room temperature. The formed phosphate molybdate complex was quantified at  $\lambda = 820 \text{ nm}$  in a Spectramax M2 (Molecular Device, Sunnyvale, CA). To inhibit the ABCA1 ATPase selectively, samples were incubated either with aluminum fluorides (1.7 mM

#### 4. Towards understanding of the allocrite specificity of the lipid floppase ABCA1

---

[ADP·Al·F]; prepared from aqueous solutions of 1 mM NaF, 100 mM AlCl<sub>3</sub> and 91.1 mM ADP mixed in this order to gain 20.66 mM of the complex) or vanadate (0.5 mM) to subtract from the measurements. As vanadate inhibited only partially control samples without compounds were kept on ice and were subtracted from the measurements. The colorimetric result was calibrated using reference phosphate standards included in each microtiter plate. Compounds tested were obtained from Avanti lipids or Sigma-Aldrich.

#### **Modified phosphate release assay**

The inhibition assay is based on the phosphate release assay with some simplifications. The mixtures were prepared in parallel on a 96-well microtiter plate (Nunc F96 MicroWell plate, nontreated). Crude membranes were thawed and diluted to 0.1 mg/ml protein concentration in ice-cold phosphate release assay buffer (25 mM Tris-HCl including 50 mM KCl, 3 mM ATP, 2.5 mM MgSO<sub>4</sub>, 3 mM DTT, 0.5 mM EGTA, 2 mM ouabain, and 3 mM sodium azide, pH 7.0). The total assay volume was 60 µL/well, featuring 5 µg/well of protein. The absorbance of the molybdate complex was determined at eight different concentrations of the inhibitor in presence and as a control in absence of crude membranes. The reaction with and without possible allocrites was started by transferring the plate into a water bath kept at 37 °C for 1 hour and was quenched by rapidly cooling the plate on ice and the addition of an ice-cold stopping solution (200 uL/well, ammonium molybdate (0.2% (w/v)), sulfuric acid (1.43% (v/v)), freshly prepared ascorbic acid (1% (w/v)), and SDS (0.9% (w/v))). The absorbance of the inorganic phosphate Pi, resulting from the hydrolysis of ATP was determined by a colorimetric quantification after 30 min incubation at room temperature. The phosphate molybdate complex formed was quantified at 820 nm in a Spectramax M2 (Molecular

#### 4. Towards understanding of the allocrite specificity of the lipid floppase ABCA1

---

Device, Sunnyvale, CA). An absorbance value of samples with ATP, compound and crude membranes at different concentrations was measured. The pH value of sample solutions were checked and adjusted if necessary. Samples without membranes were incubated in parallel in order to correct for unspecific ATP hydrolysis in all measurements. Measurements were performed in duplicate on the microtiter plate. The absorbance of the basal activity was calculated as an average of four samples with crude membranes and ATP.

## Results

### Linearity of the ATP-hydrolysis

The linearity of ATP hydrolysis of inside-out plasma membrane vesicles (HEK293-ABCA1) over time was tested in order to optimize the reaction time of the phosphate release assay. Experiments were performed in phosphate release assay buffer at 37°C without any compounds. The basal activity was measured up to two hours. In Figure 1 the absorbance of the molybdate phosphate complex at  $\lambda = 820$  nm is shown as a function of time. The absorbance increased linearly from  $\sim 0.1$  to  $\sim 0.9$ . The linear fit to the absorbance versus time data is within the limit of error, proving the linearity of the ATP hydrolysis.

Figure 1

### Phosphate release assay

The compounds investigated can be divided into four main classes. (I) short chain phosphocholines (PC) and lyso-phosphocholines (lyso-PC), (II) detergents, which interact with Pgp [26, 27], (III) vitamin E [20] and its derivatives TPGS400 and TPGS1000, and (IV) the stilbenes resveratrol, DIDS and estradiol. HEK-ABCA1-inside-out vesicles were titrated at 37°C. The results for all experiments performed are summarized in Table 1 and the fold of activation as a function of the putative allocrite concentration is shown in the Appendix. Lyso-PC and PC lipids, the steroid hormone

#### 4. Towards understanding of the allocrite specificity of the lipid floppase ABCA1

---

and vitamin E were tested below the critical micellar(/aggregation) concentration (CMC) and showed no reproducible effects in the phosphate release assay. Repetition of the assay with identical putative allocrites revealed significant deviating data ( $\leq 50\%$ ) in some cases.

Table 1

Effects on the ATPase activity were observed with compounds classified as detergents, vitamin E derivatives and stilbenes.

Several detergents were used below and also above the CMC as shown in Table 1 and in the appendix. Note that the CMC could change under different conditions. At the CMC a small increase of activation ( $\leq 5\%$ ) was observed occasionally (n-decyl- $\beta$ -D-glucopyranosid, CHAPS, C<sub>12</sub>EO<sub>8</sub>). The small increase in activity arises due to vesicle lysis above the CMC and the concomitant exposure of originally occluded NBDs [28]. N-decyl- $\beta$ -D-glucopyranosid showed contradicting effects (activation/inhibition) in different assays at higher concentrations and was not further evaluated.

Further effects are grouped into compounds that caused (i) decreased activity below the CMC, (ii) decreased activity above the CMC and (iii) increased activity above the CMC in the phosphate release assay. Increased activity below the CMC was not observed with any tested compound.

(i) Stilbenes tested (resveratrol and DIDS (4,4'-Diisothiocyano-2,2'-stilbenedisulfonic acid)) decreased the activity in the phosphate release assay and in its modified version, respectively (Figure 2, Table 1 and Appendix). DIDS decreased the activity to about 10 % of basal activity, whereas resveratrol inhibited only to about 75 %. In Figure 3 the absorbance of the inhibition assay with DIDS is shown as a function of the



#### 4. Towards understanding of the allocrite specificity of the lipid floppase ABCA1

---

concentration. While the absorbance of samples with membranes decreased, samples without membranes did not show any decrease of absorbance with increasing DIDS concentrations. Hence, an artifact due to interaction of the phosphate molybdate complex with the compound could be ruled out. The absorbance of the samples without membranes is due to the color complex, which was formed by traces of phosphate in the ATP preparation.

Figure 2

Figure 3

(ii) The detergents CHAPS, Triton X-100 and C<sub>12</sub>EO<sub>8</sub> showed decreasing activity above their CMC in the phosphate release assay (Table 1 and Appendix). CHAPS decreased the activity strongly down to ~ 10 %, whereas Triton X-100 and C<sub>12</sub>EO<sub>8</sub> indicated slightly decreased activity (~ 80 %). Inhibitory effects of detergents above the CMC are generally assumed to be unspecific. However, the strong inhibiting effect of CHAPS compared to other tested detergents above the CMC could be a hint of specific interaction with ABCA1. A specific effect is confirmed by repetition of the experiment (CHAPS and C<sub>12</sub>EO<sub>8</sub>) with inside-out-vesicles prepared from HEK293-WT cells that did not show any effect.

(iii) The detergents Tween80 and Tween40 and the vitamin E derivatives TPGS400 and TPGS1000 showed increased activity above its CMC in the phosphate release assay (Table 1, Figure 4 and Appendix). The increased ATPase activity of the transfected inside-out vesicles was ~ 140 % with Tween80, ~ 130 % with TPGS1000, ~ 140 % with Tween40 and ~ 115 % with TPGS400. These compounds are all characterized by an

#### 4. Towards understanding of the allocrite specificity of the lipid floppase ABCA1

---

amphiphilic structure composed of a hydrophilic polyethylene glycol (PEG) chain, a heterocyclic group and a relatively long hydrophobic aliphatic hydrocarbon chain. Activation above the CMC could be a sign of very low affinity of these allocrits to the transporter, analogous to the ABC transporter SAV1866 (Andreas Beck, Päivi Äänismaa and Anna Seelig; unpublished). Low affinity requires a high concentration of the allocrite in the membrane, as it occurs above an allocrite's CMC.

Figure 4

#### **Modified phosphate release assay**

Putative inhibitors of the NBDs of HEK293-ABCA1 cells were tested by means of a modified phosphate release assay. Generally, vanadate and aluminum fluoride complexes are inhibitors of nucleotide binding domains (NBDs) due to its chemical analogy to phosphate. The result of the inhibition assay is illustrated in Figure 2. The basal activity of the transfected inside-out vesicles is plotted against the logarithm of the inhibitor concentration and shows a linear dependence. Therefore inhibition followed an exponential rule. Vanadate, which is a capable inhibitor of the ATPase of P-glycoprotein [30] did not fully inhibit ABCA1 ATPase activity (35 %). In contrast, aluminum fluorides and DIDS showed inhibition to less than 10 %. Until now it is unclear whether DIDS is interacting with the NBDs, whereas aluminum fluorides and vanadate are known to inhibit the NBDs [31].

## Discussion and conclusions

The copy number of ABCA1 proteins per HEK293-ABCA1 cell is estimated to be  $10^5$ . This is ten times lower than in *MDR1* transfected mouse embryo fibroblasts NIH-MDR1-G185. Therefore, relatively small increasing effects on the activity were measured in the phosphate release assay.

The small activating effect of less than 5 % after lysis of the inside-out vesicles at the CMC of several detergents indicates a high percentage of inside-out vesicles compared to right-side-out vesicles.

The endogenous allocrits PCs and vitamin E as well as Lyso-PCs did not show any effect. This could either mean that these compounds are not transported or that they are transported with basal activity.

DIDS and resveratrol, both carry a stilbene group. The compounds affected decreased activity in the phosphate release assay and in its modified version, the inhibition assay, respectively. The effect of resveratrol was also found for Pgp in inside-out vesicles made of NIH cells transfected with *Pgp* (NIH-MDR1-G185). But the effect was not observed with inside-out vesicles made of *wildtype* NIH cells (NIH-3T3) (PGP and *wiltype*: Xiachun Li-Blatter and Anna Seelig; unpublished results) suggesting a specific effect on ABCA1. Since the concentrations of half-maximum activation,  $K_1$ , for the two transporters Pgp and ABCA1 were virtually identical and DIDS ( $pK_a$ : -3.21, -1.43, -0.37, 0.23) does not insert into the lipid bilayer an interaction with the NBDs is more likely than an interaction with the TMDs.

The activity of ABCA1 was decreased by many detergents near or above the CMC. This is generally assumed to be an unspecific effect. Nevertheless, a specific effect cannot be

#### 4. Towards understanding of the allocrite specificity of the lipid floppase ABCA1

---

excluded since detergents very often stabilize membrane proteins and have specific effects to ABC transporters [26].

Tween and TPGS are amphiphilic compounds that are featured by a PEG chain, a heterocyclic group and a hydrocarbon chain as common structural elements and showed activation in the phosphate release assay with ABCA1 above the CMC. In contrast, these substances inhibited Pgp activity below the CMC [26, 32]. Activation above the CMC could be a sign of low affinity of the transporter to TPGS and Tween as eluded above (chapter: results). Low affinity of ABCA1 to allocrits could be a general feature of these interactions. Regarding the high concentrations of phospholipids and cholesterol in lipid membranes, a low affinity of ABCA1 to these allocrits is probably physiologically necessary to fulfill its function as efflux transporter. High affinity and high concentrations would yield inhibition of the transporter [25]. Furthermore it is in agreement with the study of Takahashi et al. [22] who measured compounds in mixed vesicles at high concentrations (e.g. steroids at 20 % w/w). On the other hand, activation above the CMC could also be an effect due to changed membrane parameters. However, Tween80 yields a lower, whereas TPGS leads to higher packing density of the membrane [33] but both compounds increased the activity in the phosphate release assay suggesting a specific interaction with the transporter. The assumption of a specific effect is also supported by the fact that all tested detergents changed membrane parameters but most of them showed decreasing activity.

Compared to Pgp, which interacts with a lot of different molecules via hydrogen bond formation [34, 35] ABCA1 seems to be more specific to its allocrits.

Aluminum fluorides and vanadate are typical inhibitors of NBDs due to their phosphate mimicking characteristics. Several ABC transporters and other nucleotide triphosphate hydrolysing proteins are known to be inhibited by aluminum fluorides (AtABCD1,

#### 4. Towards understanding of the allocrite specificity of the lipid floppase ABCA1

---

MRP1, G-proteins) [30, 36, 37]. Vanadate is commonly used in the phosphate release assay with Pgp overexpressing cells at a concentration of 0.5 mM in order to inhibit Pgp ATPase activity almost completely. At this concentration ABCA1 was only inhibited to ~ 55 % by vanadate. This is in agreement with investigations of Takahashi et al. [22]. The lack of vandate sensitivity observed in our assays proves a specific measurement of the ABCA1 ATPase. Vanadate and aluminum fluorides are both inhibitors arresting the enzyme in similar ATP hydrolysis transition states [30]. Even though, different vanadate sensitivity may mean that the NBDs of Pgp hydrolyze ATP on a different mechanism than ABCA1.

## Legends to the figures

*Figure 1:* ATP hydrolysis of HEK-ABCA1 inside-out vesicles measured by quantification of inorganic phosphate released. The absorbance of the molybdate-phosphate complex was measured at 820 nm and is plotted against the time of hydrolysis.

*Figure 2:* The graphs show inhibition of the basal activity of HEK293-ABCA1 inside-out plasma membrane vesicles in a phosphate release assay as a function of the tested compound concentration. Tested compounds were vanadate (A), aluminum fluorides (B) and DIDS. The activity decreased linearly with the concentration for all three substances in a semi logarithmic plot. However, vanadate decreased to about 30 %, whereas aluminum fluorides and DIDS decreased the activity to less than 10 % in the concentration range measured.

*Figure 3:* The absorbance of the molybdate-phosphate complex formed is shown in dependence of the concentration of DIDS. The samples without inside-out vesicles (blue points) show approximately constant absorbance values, whereas the difference of absorbance of samples with ATP and without (see materials and methods) is decreasing linearly in this semi logarithmic plot.

*Figure 4:* TPGS400 (A) and TPGS1000 (B) were measured with the phosphate release assay. The normalized activity of one measurement is plotted as a function of the compound concentration. The error bars represent the differences of duplicates. The

#### 4. Towards understanding of the allocrite specificity of the lipid floppase ABCA1

---

CMC of both compounds lies at a concentration of.  $\sim 10 \mu\text{M}$ . Both compounds showed slight activation at concentrations above the CMC.

*Table 1:* Summary of putative allocrites tested in phosphate release assays with inside-out vesicles of ABCA1 transfected HEK293 cells. Ice samples were subtracted in experiments in which vanadate was used to inhibit the ATPase. Critical micellar concentrations (CMC) or critical aggregation concentrations were obtained from Li-Blatter et al. [26] (#), Stafford et al. [29] (\*) and the Avanti lipid homepage ([http://avantilipids.com/index.php?option=com\\_content&view=article&id=1703&Itemid=422](http://avantilipids.com/index.php?option=com_content&view=article&id=1703&Itemid=422)) (+). The remaining CMCs are from unpublished results generously provided by Xiachun Li-Blatter and Anna Seelig. Concentrations above the CMC are colored in red.

## Literature

1. Zarubica A, Trompier D, Chimini G: **ABCA1, from pathology to membrane function.** *Pflugers Arch* 2007, **453**(5):569-579.
2. Van Eck M, Pennings M, Hoekstra M, Out R, Van Berkel TJ: **Scavenger receptor BI and ATP-binding cassette transporter A1 in reverse cholesterol transport and atherosclerosis.** *Curr Opin Lipidol* 2005, **16**(3):307-315.
3. Lee JY, Parks JS: **ATP-binding cassette transporter AI and its role in HDL formation.** *Curr Opin Lipidol* 2005, **16**(1):19-25.
4. Takahashi Y, Smith JD: **Cholesterol efflux to apolipoprotein AI involves endocytosis and resecretion in a calcium-dependent pathway.** *Proc Natl Acad Sci U S A* 1999, **96**(20):11358-11363.
5. Boadu E, Francis GA: **The role of vesicular transport in ABCA1-dependent lipid efflux and its connection with NPC pathways.** *J Mol Med (Berl)* 2006, **84**(4):266-275.
6. Brooks-Wilson A, Marcil M, Clee SM, Zhang LH, Roomp K, van Dam M, Yu L, Brewer C, Collins JA, Molhuizen HO *et al*: **Mutations in ABC1 in Tangier disease and familial high-density lipoprotein deficiency.** *Nat Genet* 1999, **22**(4):336-345.
7. Lawn RM, Wade DP, Garvin MR, Wang X, Schwartz K, Porter JG, Seilhamer JJ, Vaughan AM, Oram JF: **The Tangier disease gene product ABC1 controls the cellular apolipoprotein-mediated lipid removal pathway.** *J Clin Invest* 1999, **104**(8):R25-31.



4. Towards understanding of the allocrite specificity of the lipid floppase ABCA1

---

8. Rust S, Rosier M, Funke H, Real J, Amoura Z, Piette JC, Deleuze JF, Brewer HB, Duverger N, Deneffe P *et al*: **Tangier disease is caused by mutations in the gene encoding ATP-binding cassette transporter 1.** *Nat Genet* 1999, **22**(4):352-355.
9. Rust S, Walter M, Funke H, von Eckardstein A, Cullen P, Kroes HY, Hordijk R, Geisel J, Kastelein J, Molhuizen HO *et al*: **Assignment of Tangier disease to chromosome 9q31 by a graphical linkage exclusion strategy.** *Nat Genet* 1998, **20**(1):96-98.
10. Oram JF, Lawn RM, Garvin MR, Wade DP: **ABCA1 is the cAMP-inducible apolipoprotein receptor that mediates cholesterol secretion from macrophages.** *J Biol Chem* 2000, **275**(44):34508-34511.
11. Oram JF, Heinecke JW: **ATP-binding cassette transporter A1: a cell cholesterol exporter that protects against cardiovascular disease.** *Physiol Rev* 2005, **85**(4):1343-1372.
12. Schmitz G, Langmann T: **Transcriptional regulatory networks in lipid metabolism control ABCA1 expression.** *Biochim Biophys Acta* 2005, **1735**(1):1-19.
13. Wellington CL, Walker EK, Suarez A, Kwok A, Bissada N, Singaraja R, Yang YZ, Zhang LH, James E, Wilson JE *et al*: **ABCA1 mRNA and protein distribution patterns predict multiple different roles and levels of regulation.** *Lab Invest* 2002, **82**(3):273-283.
14. Wang N, Tall AR: **Regulation and mechanisms of ATP-binding cassette transporter A1-mediated cellular cholesterol efflux.** *Arterioscler Thromb Vasc Biol* 2003, **23**(7):1178-1184.

#### 4. Towards understanding of the allocrite specificity of the lipid floppase ABCA1

---

15. Wang N, Chen W, Linsel-Nitschke P, Martinez LO, Agerholm-Larsen B, Silver DL, Tall AR: **A PEST sequence in ABCA1 regulates degradation by calpain protease and stabilization of ABCA1 by apoA-I.** *J Clin Invest* 2003, **111**(1):99-107.
16. Aiello RJ, Brees D, Francone OL: **ABCA1-deficient mice: insights into the role of monocyte lipid efflux in HDL formation and inflammation.** *Arterioscler Thromb Vasc Biol* 2003, **23**(6):972-980.
17. Aiello RJ, Brees D, Bourassa PA, Royer L, Lindsey S, Coskran T, Haghpassand M, Francone OL: **Increased atherosclerosis in hyperlipidemic mice with inactivation of ABCA1 in macrophages.** *Arterioscler Thromb Vasc Biol* 2002, **22**(4):630-637.
18. Liu L, Bortnick AE, Nickel M, Dhanasekaran P, Subbaiah PV, Lund-Katz S, Rothblat GH, Phillips MC: **Effects of apolipoprotein A-I on ATP-binding cassette transporter A1-mediated efflux of macrophage phospholipid and cholesterol: formation of nascent high density lipoprotein particles.** *J Biol Chem* 2003, **278**(44):42976-42984.
19. Fielding PE, Nagao K, Hakamata H, Chimini G, Fielding CJ: **A two-step mechanism for free cholesterol and phospholipid efflux from human vascular cells to apolipoprotein A-1.** *Biochemistry* 2000, **39**(46):14113-14120.
20. Reboul E, Tromprier D, Moussa M, Klein A, Landrier JF, Chimini G, Borel P: **ATP-binding cassette transporter A1 is significantly involved in the intestinal absorption of alpha- and gamma-tocopherol but not in that of retinyl palmitate in mice.** *Am J Clin Nutr* 2009, **89**(1):177-184.
21. Seelig A: **The role of size and charge for blood-brain barrier permeation of drugs and fatty acids.** *J Mol Neurosci* 2007, **33**(1):32-41.

4. Towards understanding of the allocrite specificity of the lipid floppase ABCA1

---

22. Takahashi K, Kimura Y, Kioka N, Matsuo M, Ueda K: **Purification and ATPase activity of human ABCA1.** *J Biol Chem* 2006, **281**(16):10760-10768.
23. Litman T, Zeuthen T, Skovsgaard T, Stein WD: **Competitive, non-competitive and cooperative interactions between substrates of P-glycoprotein as measured by its ATPase activity.** *Biochim Biophys Acta* 1997, **1361**(2):169-176.
24. Litman T, Zeuthen T, Skovsgaard T, Stein WD: **Structure-activity relationships of P-glycoprotein interacting drugs: kinetic characterization of their effects on ATPase activity.** *Biochim Biophys Acta* 1997, **1361**(2):159-168.
25. Aanismaa P, Gatlik-Landwojtowicz E, Seelig A: **P-glycoprotein senses its substrates and the lateral membrane packing density: consequences for the catalytic cycle.** *Biochemistry* 2008, **47**(38):10197-10207.
26. Li-Blatter X, Nervi P, Seelig A: **Detergents as intrinsic P-glycoprotein substrates and inhibitors.** *Biochim Biophys Acta* 2009, **1788**(10):2335-2344.
27. Seelig A, Gerebtzoff G: **Enhancement of drug absorption by noncharged detergents through membrane and P-glycoprotein binding.** *Expert Opin Drug Metab Toxicol* 2006, **2**(5):733-752.
28. Lu P, Liu R, Sharom FJ: **Drug transport by reconstituted P-glycoprotein in proteoliposomes. Effect of substrates and modulators, and dependence on bilayer phase state.** *Eur J Biochem* 2001, **268**(6):1687-1697.
29. Stafford RE, Fanni T, Dennis EA: **Interfacial properties and critical micelle concentration of lysophospholipids.** *Biochemistry* 1989, **28**(12):5113-5120.

#### 4. Towards understanding of the allocrite specificity of the lipid floppase ABCA1

---

30. Kern A, Felfoldi F, Sarkadi B, Varadi A: **Expression and characterization of the N- and C-terminal ATP-binding domains of MRP1.** *Biochem Biophys Res Commun* 2000, **273**(3):913-919.
31. Chabre M: **Aluminofluoride and beryllorfluoride complexes: a new phosphate analogs in enzymology.** *Trends Biochem Sci* 1990, **15**(1):6-10.
32. Werle M: **Natural and synthetic polymers as inhibitors of drug efflux pumps.** *Pharm Res* 2008, **25**(3):500-511.
33. Rege BD, Kao JP, Polli JE: **Effects of nonionic surfactants on membrane transporters in Caco-2 cell monolayers.** *Eur J Pharm Sci* 2002, **16**(4-5):237-246.
34. Seelig A: **A general pattern for substrate recognition by P-glycoprotein.** *Eur J Biochem* 1998, **251**(1-2):252-261.
35. Seelig A: **How does P-glycoprotein recognize its substrates?** *Int J Clin Pharmacol Ther* 1998, **36**(1):50-54.
36. Nyathi Y, De Marcos Lousa C, van Roermund CW, Wanders RJ, Johnson B, Baldwin SA, Theodoulou FL, Baker A: **The Arabidopsis peroxisomal ABC transporter, comatose, complements the Saccharomyces cerevisiae pxa1 pxa2Delta mutant for metabolism of long-chain fatty acids and exhibits fatty acyl-CoA-stimulated ATPase activity.** *J Biol Chem* 2010, **285**(39):29892-29902.
37. Strunecka A, Strunecky O, Patocka J: **Fluoride plus aluminum: useful tools in laboratory investigations, but messengers of false information.** *Physiol Res* 2002, **51**(6):557-564.

## Figures and Tables

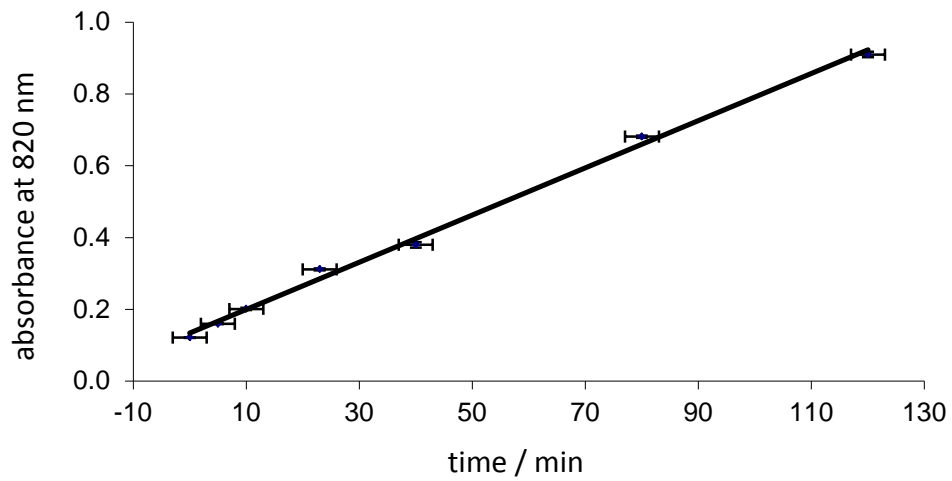


Figure 1

#### 4. Towards understanding of the allocrite specificity of the lipid floppase ABCA1

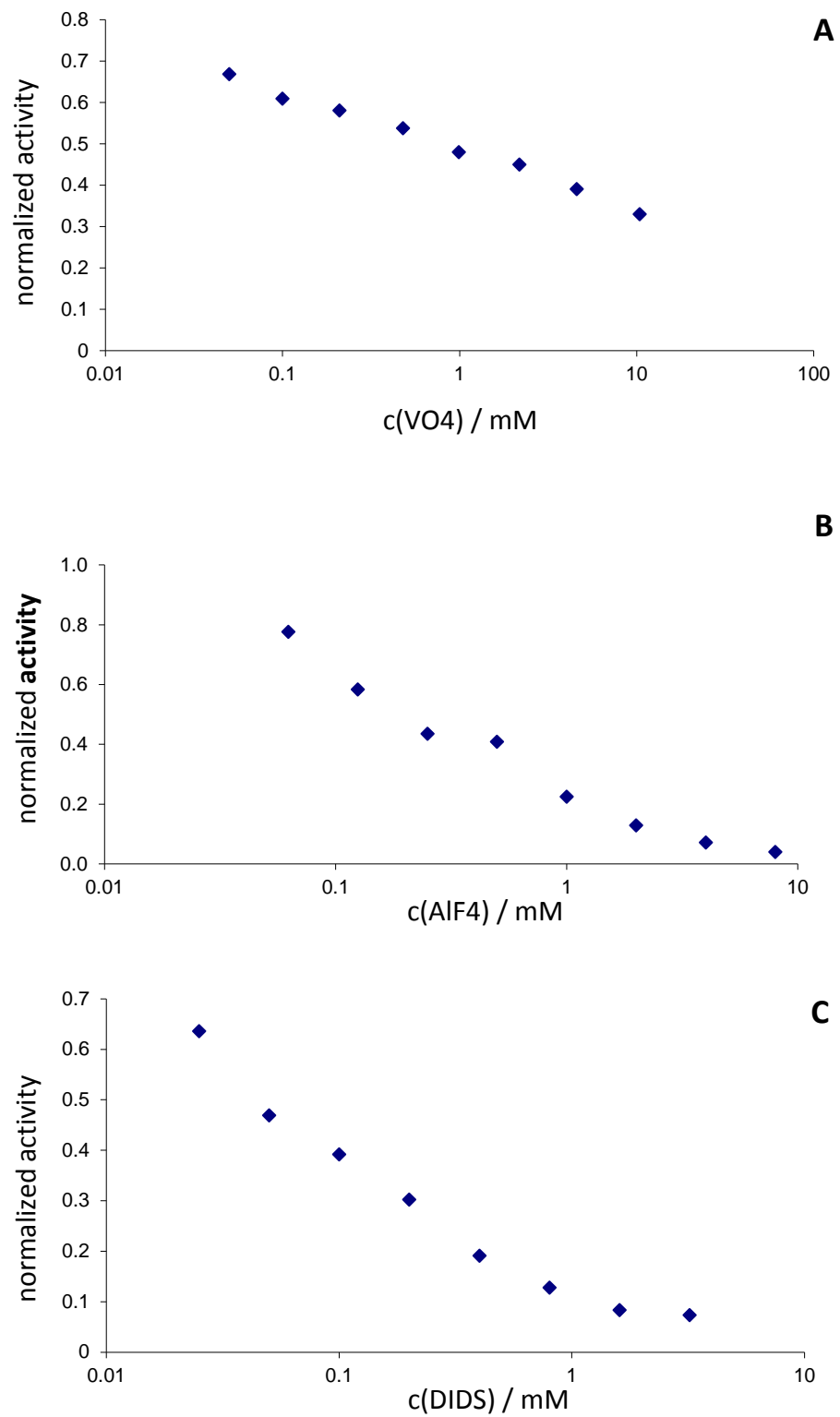


Figure 2

#### 4. Towards understanding of the allocrite specificity of the lipid floppase ABCA1

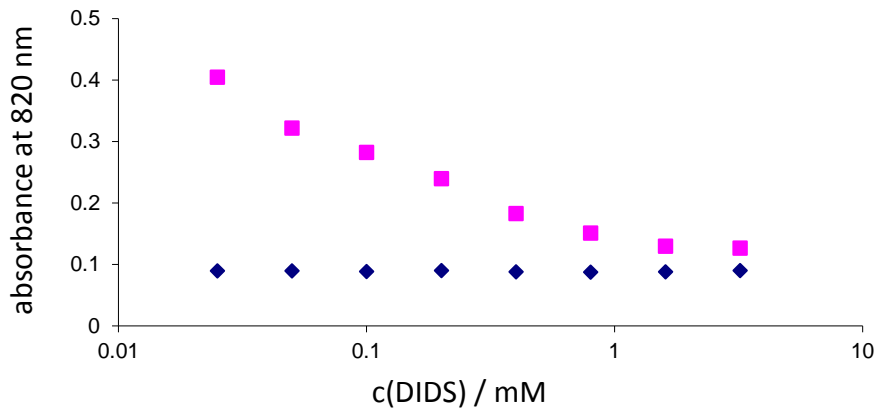


Figure 3

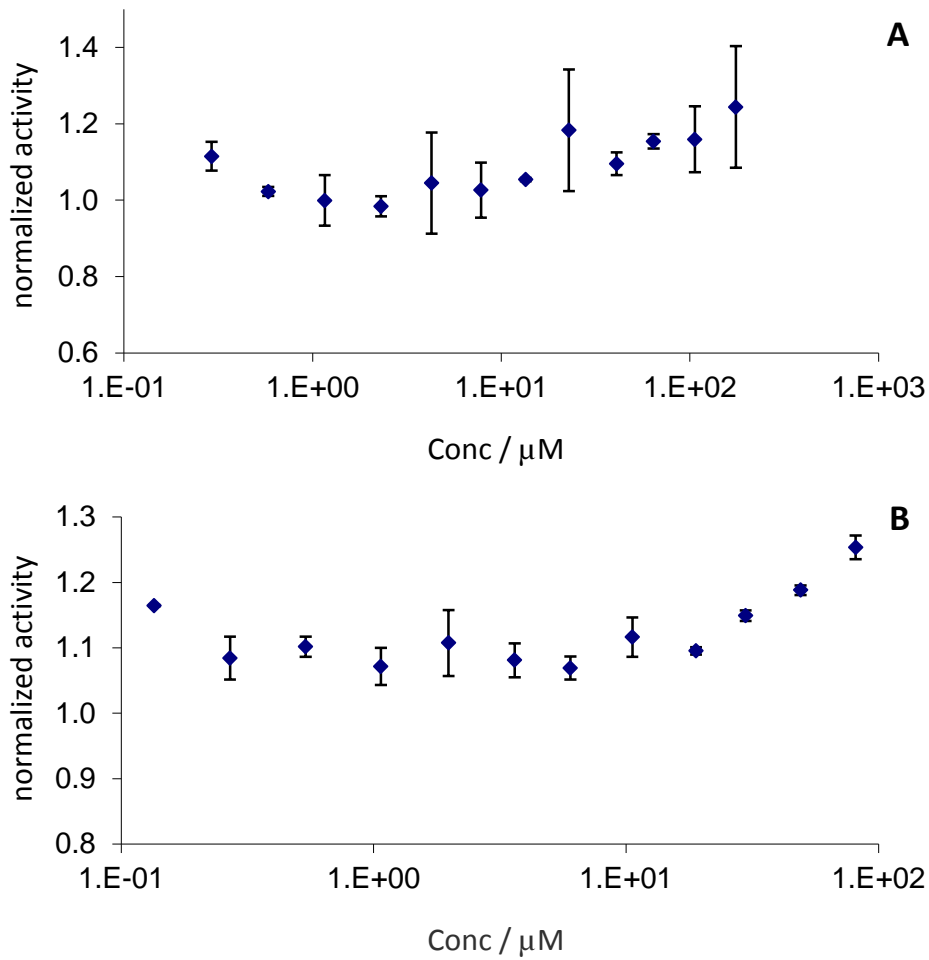


Figure 4

#### 4. Towards understanding of the allocrite specificity of the lipid floppase ABCA1

Table 1

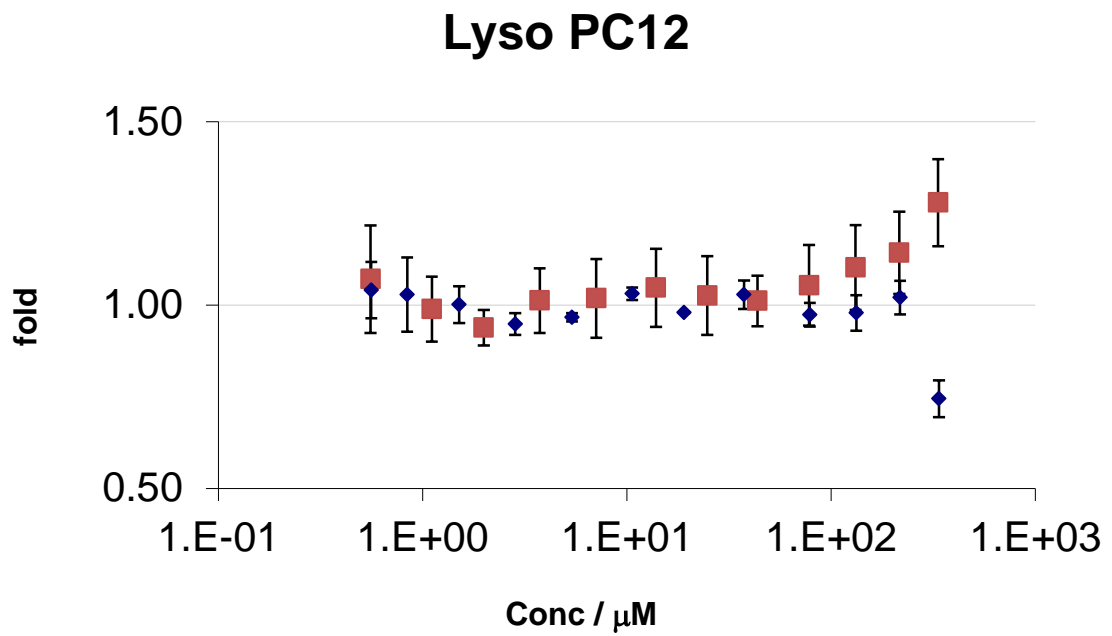
group	compound	kinase inhibit.	approx.. max. activation / %	approx. max. inhibition / %	conc. range / $\mu\text{M}$	CMC / $\mu\text{M}$
<b>Lyso PCs</b>	8	Vanadate	-	-	5-5335	60000 <sup>+</sup>
	8	Vanadate	-	-	5-5335	60000 <sup>+</sup>
	10	Vanadate	-	-	7.3-2912	7000 <sup>*</sup>
	10	Vanadate	-	-	1.4-564	7000 <sup>*</sup>
	12	Vanadate	+	-	0.6-337	700 <sup>*</sup>
	12	Vanadate	-	-	0.6-334	700 <sup>*</sup>
<b>PCs</b>	8	Vanadate	-	-	0.6-380	270 <sup>+</sup>
	8	Vanadate	-	-	0.6-381	270 <sup>+</sup>
	8	Vanadate	-	-	0.6-382	270 <sup>+</sup>
	8 in DMSO	Vanadate	-	-	2.1-4168	
	8 in DMSO	Vanadate	-	-	2.1-4169	
	8	Vanadate	-	-	0.4-251	270 <sup>+</sup>
	8	Vanadate	-	-	0.4-251	270 <sup>+</sup>
	8	Vanadate	-	-	0.6-387	270 <sup>+</sup>
	9	Vanadate	-	-	0.1-58	29 <sup>+</sup>
	9	Vanadate	-	-	0.1-58	29 <sup>+</sup>
<b>Detergents</b>	C12EO8	Al·F <sup>-</sup>	$\Delta \leq 5$ at CMC	80	0.7-747	90 <sup>#</sup>
	C12EO8	Al·F <sup>-</sup>	$\Delta \leq 5$ at CMC	80	0.7-747	90 <sup>#</sup>
	C12EO8	Vanadate	$\Delta \leq 5$ at CMC	80	0.7-747	90 <sup>#</sup>
	C12EO8	Vanadate	$\Delta \leq 5$ at CMC	90	0.7-747	90 <sup>#</sup>
	CHAPS low	Vanadate	-	-	2.8-5529	10000 <sup>#</sup>
	CHAPS low	Vanadate	-	-	2.8-5530	10000 <sup>#</sup>
	CHAPS high	Vanadate	$\Delta \leq 5$ at CMC	20	39-78823	10000 <sup>#</sup>
	CHAPS high	Vanadate	$\Delta \leq 5$ at CMC	5	39-78823	10000 <sup>#</sup>
	CHAPS high	Al·F <sup>-</sup>	$\Delta \leq 5$ at CMC	20	39-78823	10000 <sup>#</sup>
	n-decyl- $\beta$ -gylcopyranosid	Vanadate	$\Delta \leq 5$ at CMC	75	6.3-2542	2200 <sup>#</sup>
	n-decyl- $\beta$ -gylcopyranosid	Vanadate	110 and $\leq 5$ at CMC	-	6.3-2543	2200 <sup>#</sup>
	Triton X-100	Vanadate	-	80	2.2-886	300 <sup>#</sup>
	Triton X-100	Vanadate	-	80	2.2-887	300 <sup>#</sup>
	Tween40	Vanadate	120	-	0.3-105	27 <sup>#</sup>
	Tween 80	Vanadate	105	-	0.03-11.9	12 <sup>#</sup>
	Tween 80	Vanadate	105	-	0.03-11.10	12 <sup>#</sup>
Tween 80	Vanadate	140	-	0.14-56	12 <sup>#</sup>	
<b>Vitamin E – (derivatives)</b>	Vitamin E	Vanadate	-	-	0.1-77	
	Vitamin E	Vanadate	-	-	0.1-78	
	TPGS 1000	Vanadate	140	-	0.1-81	~ 10
	TPGS 1000	Vanadate	125	-	0.1-81	~ 10
	TPGS 400	Vanadate	115	-	0.4-172	~ 10
	TPGS 400	Vanadate	115	-	0.4-172	~ 10
<b>Steroids</b>	Estradiol	Vanadate	-	-	1.7-2000	~ 1400
	Estradiol	Vanadate	-	-	4.6-5512	~ 1400
<b>Stilbenes</b>	Resveratrol	Vanadate	-	60	0.5-616	~ 680
	Resveratrol	Vanadate	-	70	0.5-610	~ 680
	DIDS	modified assay	-	10	25-3210	

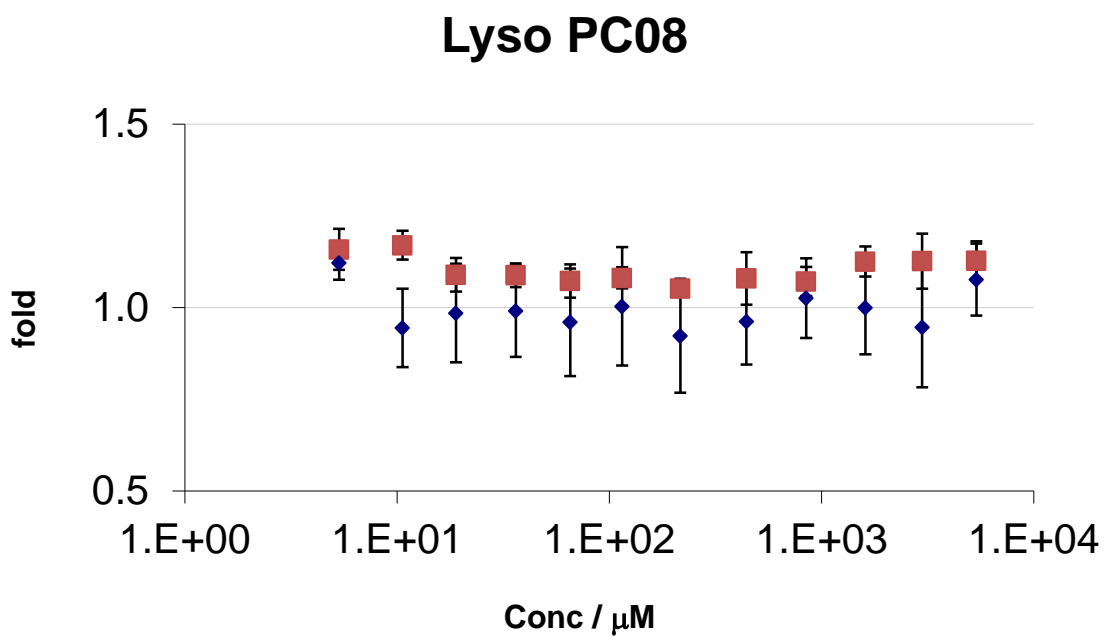
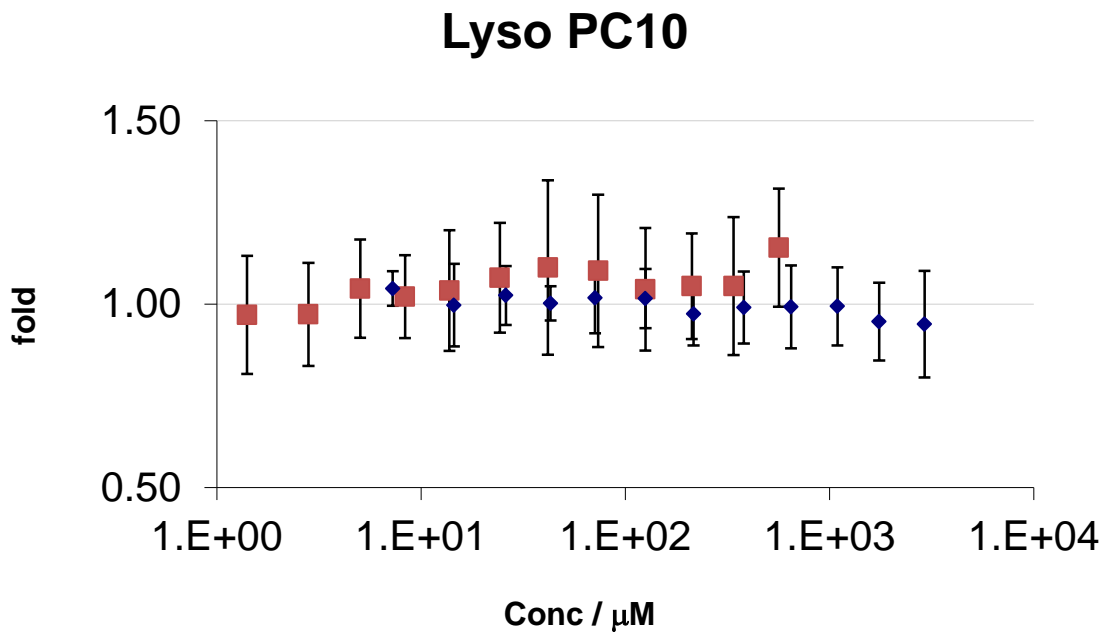


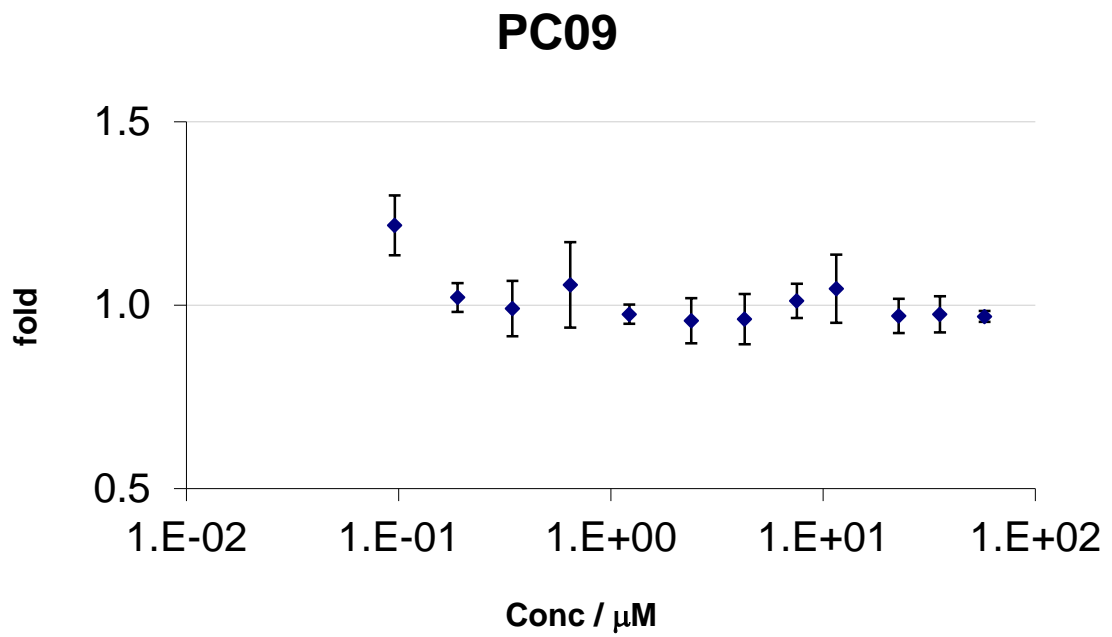
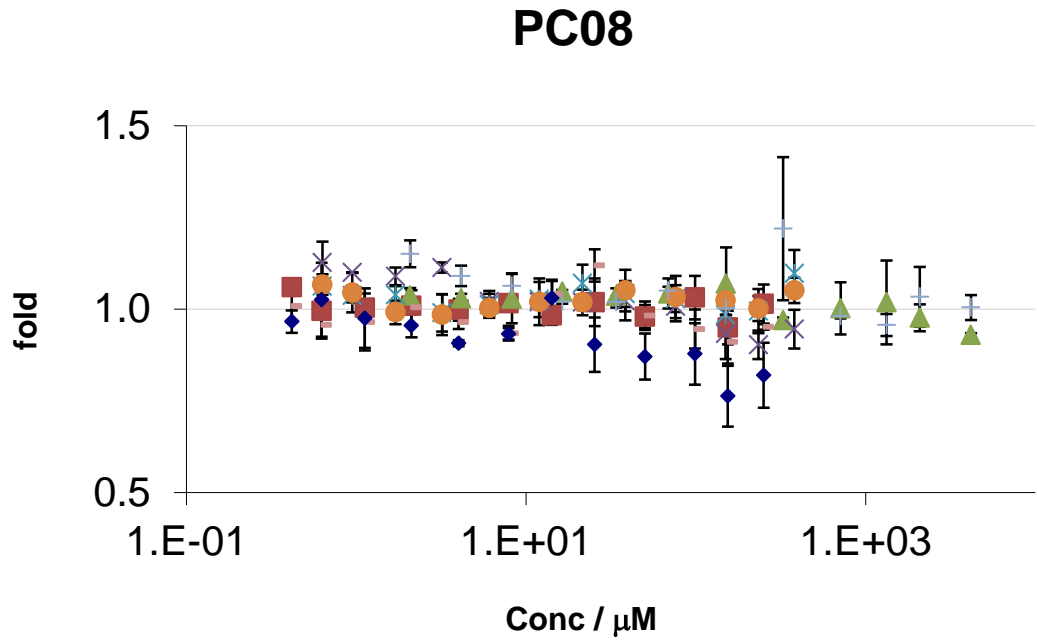
---

## Appendix

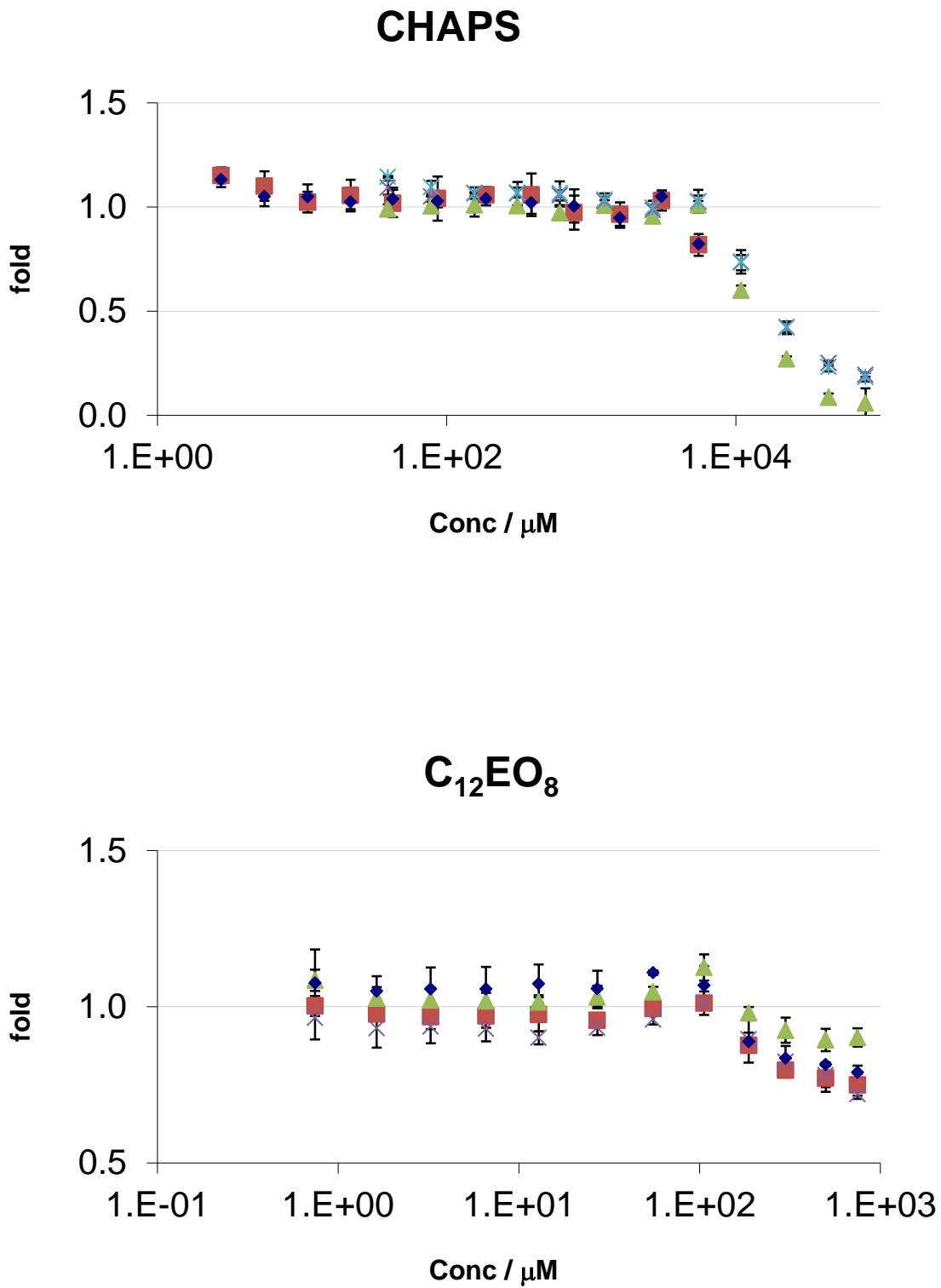
Fold vs. concentration plots of all measured compounds in the phosphate release assay. Measurements of the lowest and the highest concentration should not be taken into account as they are from wells at the edge of the 96-well plates.



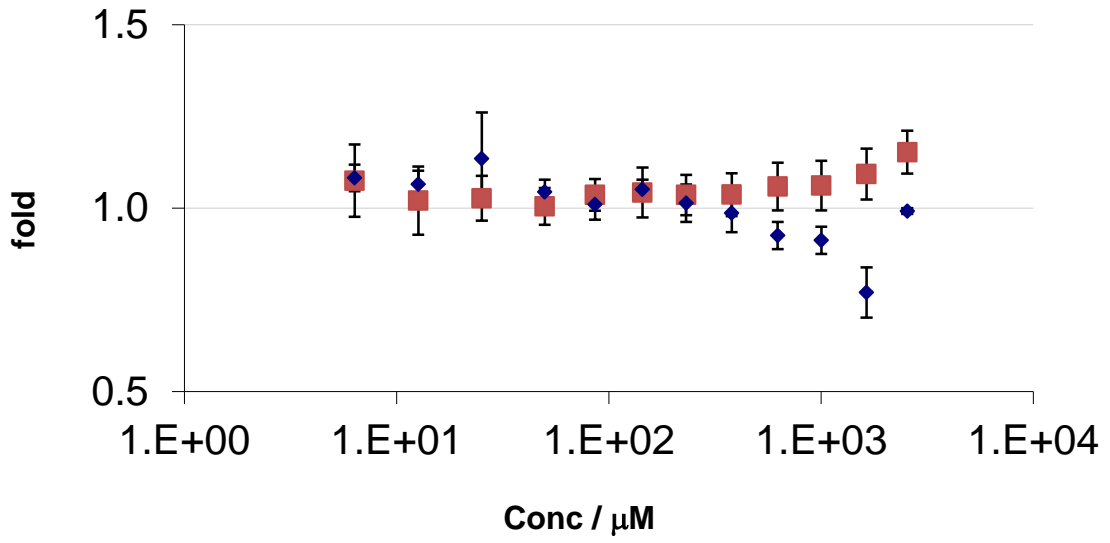




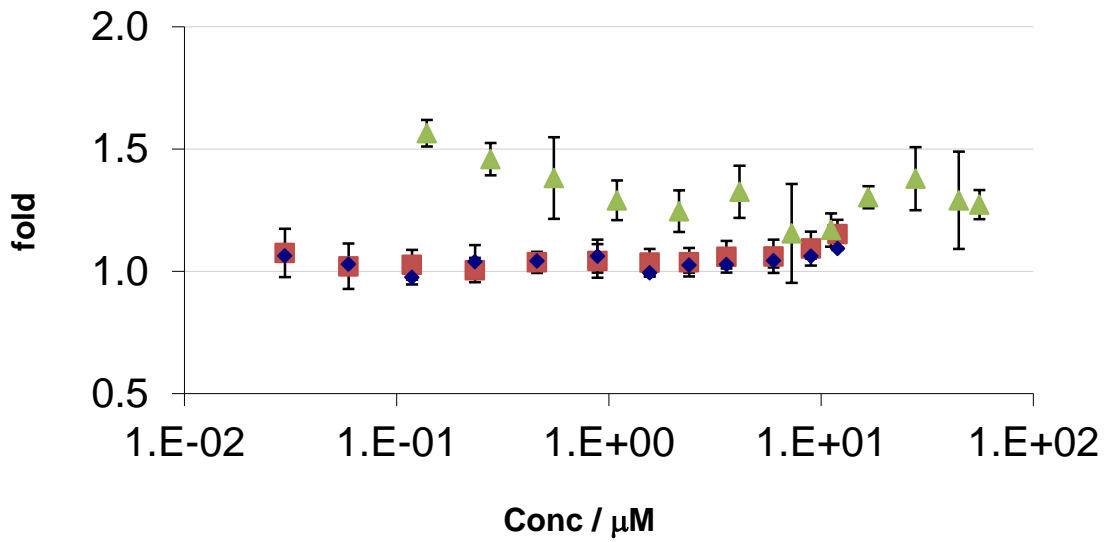
#### 4. Towards understanding of the allocrite specificity of the lipid floppase ABCA1

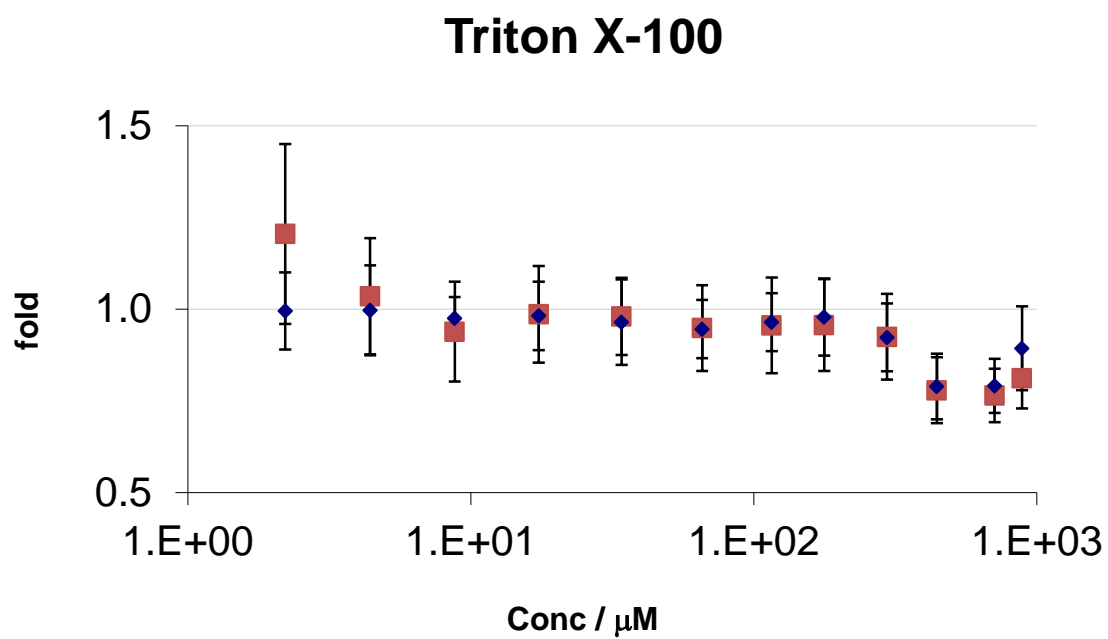
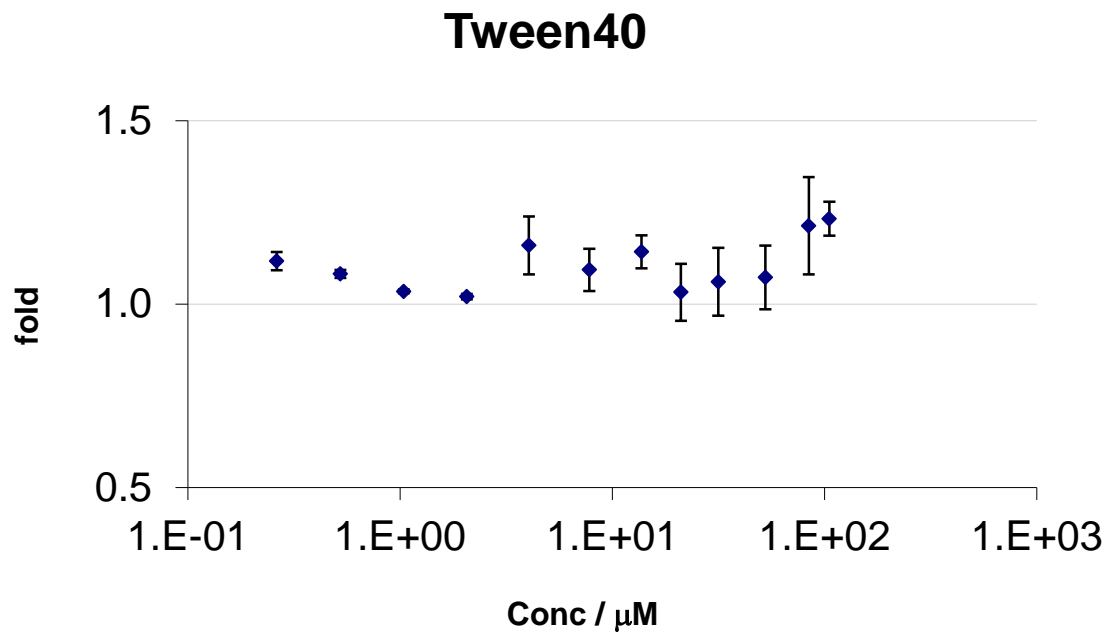


### n-Deyl-beta-D-glucopyranoside

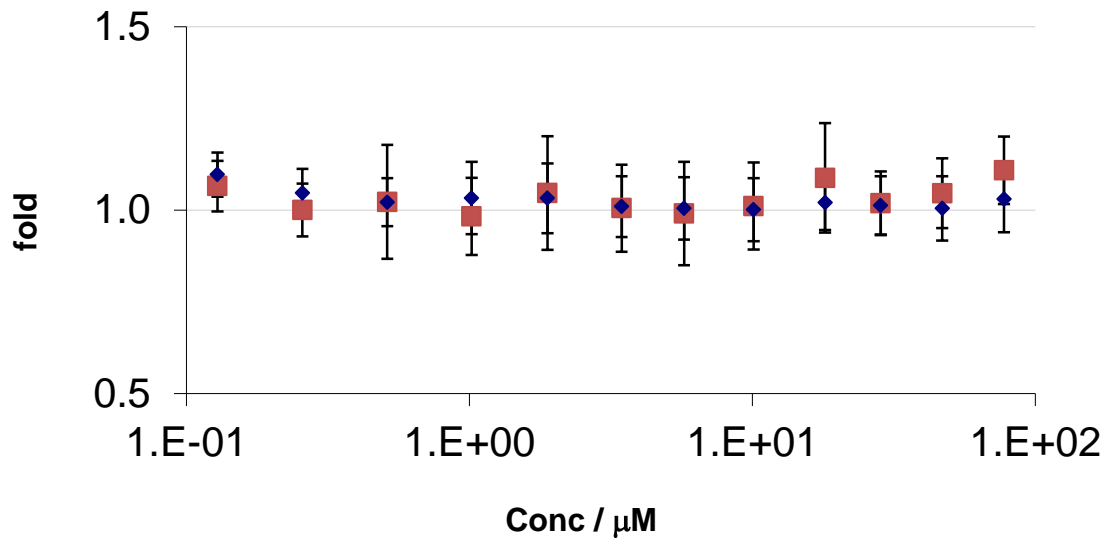


### Tween80

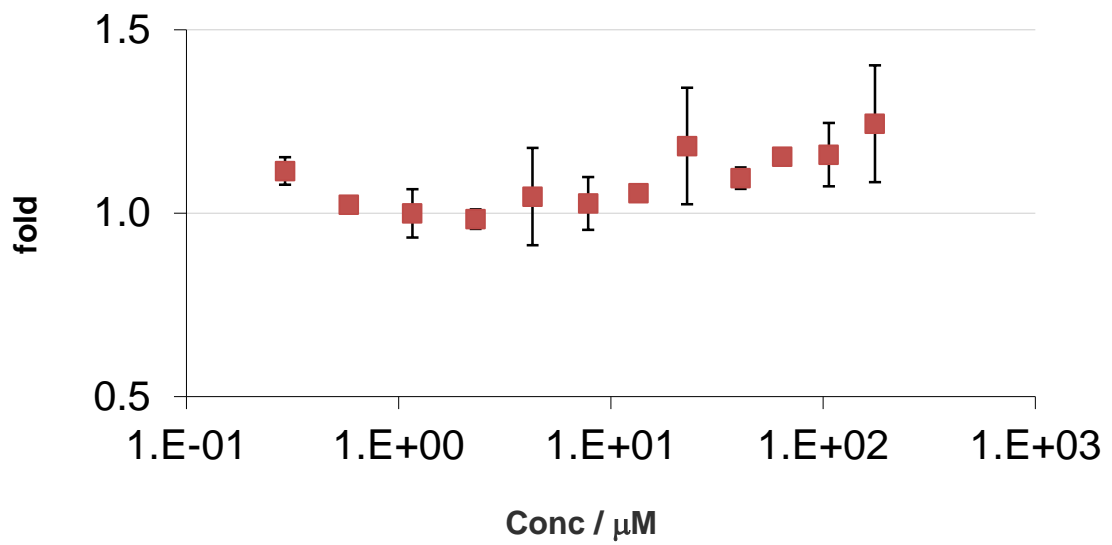




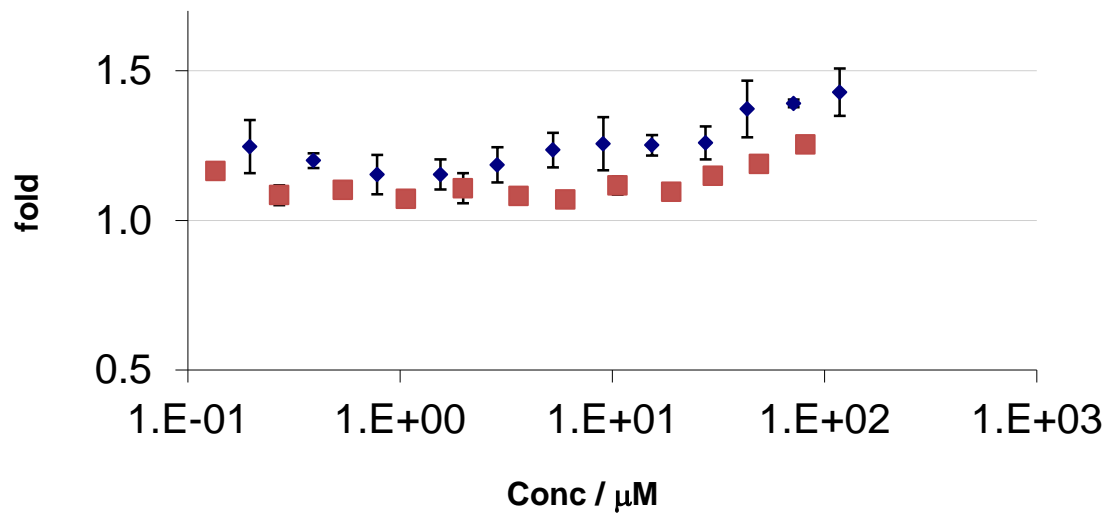
### Vitamin E



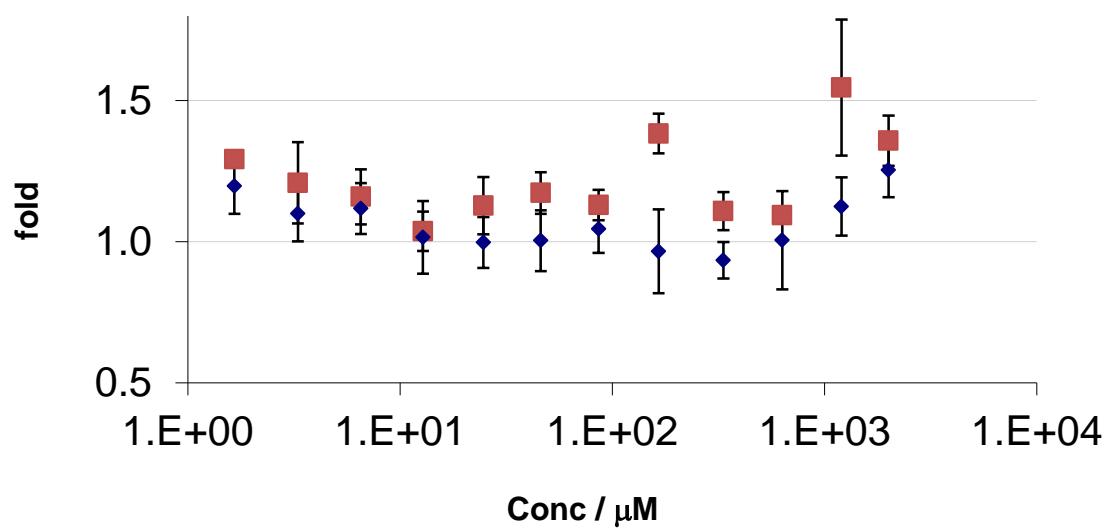
### TPGS400



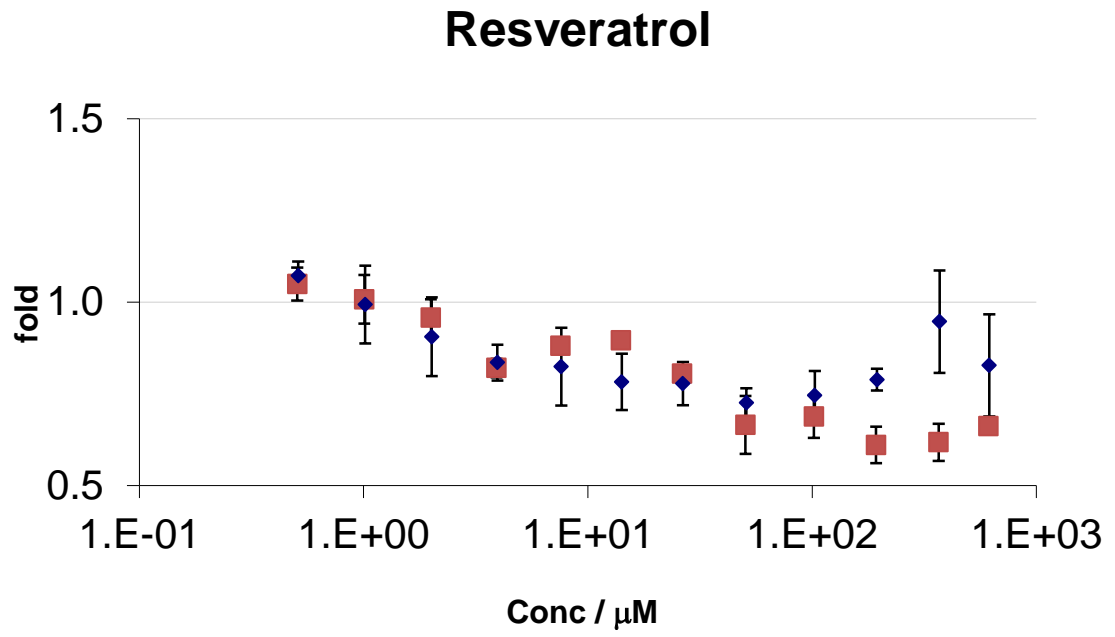
### TPGS1000



### Estradiol









## 5. Acknowledgements

This work was carried out from October 2008 until February 2012 in the laboratories of Prof. Dr. Joachim Seelig and Prof. Dr. Anna Seelig in the Department of Biophysical Chemistry at the Biozentrum of the University of Basel.

First of all I would like to express my sincere gratitude to my supervisor, Professor Joachim Seelig. His wide knowledge and his efficient modus operandi were of great value to me. I am further grateful for the freedom I experienced in doing research and choosing interesting projects.

I also want to thank Professor Anna Seelig for supervising me in my project about ABC transporters. I learned a lot in inspiring discussions about research at the edge of biophysics and pharmaceutical science. Her guidance in the beginning of my thesis was a great help.

Thanks to Dr. Hans-Joachim Schönfeld for generously supplying us with plenty of highly purified Apo A-1 and Dr. Matthew Wright for the transfected HEK293 cell lines.

I wish to express my thanks to Dr. André Ziegler for his support, competent advice and time for discussion. He introduced me to most of the experimental methods I have learned.

Also, I appreciate the work of Professor Jörg Huwyler as referee of this thesis.

Special thanks go to Therese Schulthess, whose experience, preciseness and helpfulness in the lab made my lab-life easier. Analogous, Xiaochun Li-Blatter helped me with important last-minute measurements.

## 5. Acknowledgement

---

Thanks to Dr. Andreas Beck, Christian Müller, Reto Sauder and Xiaochun Li-Blatter for nice hours in the Mensa and discussions about interesting topics that went far beyond the world of research.

Many thanks to present and former lab and floor mates for support and the friendly working environment, in particular (if not already mentioned) Dr. Päivi Äänismaa, Estefania Egido, Dr. Cinzia Esposito, Dr. Thomas Etzerodt, Dr. Sarah Güte, Dr. Michael Hayley, Dr. Gabriela Klocek, Dr. Caroline Loew, Dr. Koiji Mochizuki, Rita Müller, Susanna Notz, Dr. Samantha Persicace, Joseph Zolnerciks and Matthias Zwick. Furthermore I experienced great support from Leo Faletti and Simon Sarner of the technical workshop.

I owe my loving thanks to my family and friends.

## 6. Curriculum vitae

Fabian Zehender  
Institute of Biophysical Chemistry  
Biozentrum, University of Basel  
Klingelbergstrasse 50-70  
CH-4056 Basel  
Tel +41 612672192  
[fabian.zehender@unibas.ch](mailto:fabian.zehender@unibas.ch)

### **Personal information**

Date of birth: 14.04.1982  
Place of birth: Freiburg, Germany  
Nationality: german

### **Education**

#### **2008/10 – 2012/02**

Graduate (Ph.D.) studies in Biophysics  
Biozentrum, Biophysical Chemistry, University of Basel (CH)  
Thesis supervisor: Prof. Joachim Seelig  
PhD thesis: “Biophysical Characterization of Reactions Associated with Reverse Cholesterol Transport”

#### **2008/01 – 2008/07**

Internship Novartis Pharma, Basel (CH)

#### **10/2002 – 09/2007**

Albert-Ludwigs-University Freiburg (D)  
Diploma studies in chemistry

## 6. Curriculum vitae

---

Thesis supervisor: Prof. Peter Gräber

Thesis title: Korekonstitution der H<sup>+</sup>-ATPsynthase aus Chloroplasten mit Bakteriorhodopsin aus *Halobacterium salinarium*.

**2001/06**

Abitur: Richard-Fehrenbach Gewerbeschule Freiburg (D)

### **Publikations**

Fabian Zehender, A. Ziegler, H.-J. Schönfeld, and J. Seelig. **Thermodynamics of Protein Self-Association and Unfolding. The Case of Apolipoprotein A-I.** *Biochem.* Recently accepted manuscript. Publication date (web): 23.01.2012

Zehender F, Labahn A, Koslowski T: **Detecting protein-protein interactions by isotope-edited infrared spectroscopy: a numerical approach.** *J Phys Chem B* 2005, **109**(49):23674-23678.

Koslowski T, Zehender F: **Towards a quantitative understanding of horizontal gene transfer: a kinetic model.** *J Theor Biol* 2005, **237**(1):23-29.

## 7. Declaration

I declare that I have written this thesis “Biophysical Characterization of Reactions Associated with Reverse Cholesterol Transport” with the help indicated and that I have only submitted it to the Faculty of Science of the University of Basel and to no other faculty or university.

Basel, 07.02.2012

---

Fabian Zehender